

304

INFRARED MULTIPHOTON INDUCED REACTIONS
OF ORGANIC ESTERS

by

VALENTIN C. RIO

B.S., University of Texas at Austin, 1976

A MASTER'S THESIS

Submitted in partial fulfillment of the
requirements for the degree

MASTER OF SCIENCE

Department of Chemistry

KANSAS STATE UNIVERSITY

Manhattan, Kansas

1980

Approved by:

D.W. Setzer

Major Professor

**THIS BOOK
CONTAINS
NUMEROUS PAGES
WITH THE ORIGINAL
PRINTING BEING
SKEWED
DIFFERENTLY FROM
THE TOP OF THE
PAGE TO THE
BOTTOM.**

**THIS IS AS RECEIVED
FROM THE
CUSTOMER.**

1980 TABLE OF CONTENTS

LIST OF TABLES	R56	page
LIST OF FIGURES	C. 2	
I. INTRODUCTION		1
II. EXPERIMENTAL		5
A. Reagents		5
B. Irradiation Cells		5
C. Analysis		6
D. Infrared Spectra		7
E. CO ₂ Laser		7
F. Laser Pulse Energy Measurement		9
G. Measurement of Laser Pulse Shape		13
H. Laser Tuning		13
I. Measurement of Laser Absorption Cross Sections, σ_L		15
III. EXPERIMENTAL METHODOLOGY		20
A. First Order Kinetics of Laser Induced Reactions		20
B. Definition of Reaction Probability		24
C. Energy Absorption Measurement		26
D. Presentation of Experimental Results		28
E. Optimum Conditions for Studying Laser Induced Reactions		30
1. Extent of Intermolecular Energy Transfer		30
2. Dependence of $P(\emptyset)$ on Parent Pressure		35
3. Dependence of $P(\emptyset)$ and Thermal Effects on Geometry		35
4. Effect of Quencher Bath Gas in the MPIUR of Ethyl Acetate		37
a. Helium, as Bath Gas		37
b. Nitrogen as Bath Gas		40
c. Isopropyl Bromide as Bath Gas		40
IV. EXPERIMENTAL DATA		44
A. Ethyl Acetate		44
1. Reaction Probability Dependence on Fluence		44
2. Measurement of σ_L , \bar{n} and \bar{n}_r		53

B. Ethyl Fluoroacetate	59
1. Reaction Probability Dependence on Fluence	59
2. Measurement of σ_L , \bar{n} and \bar{n}_r	65
C. <u>sec</u> -Butyl Acetate	72
1. Laser and Thermal Initiated Butene Product Distribution	72
2. Reaction Probability Dependence on Fluence	75
3. Measurement of σ_L , \bar{n} and \bar{n}_r	78
D. <u>n</u> -Butyl Acetate	82
1. Reaction Probability Dependence on Fluence	82
2. Measurement of σ_L , \bar{n} and \bar{n}_r	86
E. Ethyl 2-Bromopropionate	90
1. Reaction probability Dependence on Fluence	90
2. Measurement of σ_L , \bar{n} and \bar{n}_r	96
F. Ethyl Acrylate	101
1. Reaction Probability Dependence on Fluence	101
2. Measurement of σ_L , \bar{n} and \bar{n}_r	104
V. DISCUSSION	107
A. Literature Review	107
1. Effect of Pressure in the MPIUR and MPA Processes	107
2. Yield <u>vs</u> Fluence Behavior	109
3. Fluence <u>vs</u> Power as the Critical Parameter for Yield	110
B. Discussion of Experimental Results of the Acetates	111
1. Effect of Pressure on the MPIUR of Ethyl Acetate	111
2. Yield Dependence on Power	112
3. Yield <u>vs</u> Fluence for Esters	114
4. Dependence of the Yield on Frequency	123
5. σ_L Dependence on Fluence	123
C. A Simple Model for MPIUR	128
D. Deficiencies of Model for Neat Samples	137
VI. CONCLUSIONS	143
VII. APPENDIX	152
ACKNOWLEDGEMENTS	163
LITERATURE CITED	164

LIST OF TABLES

1. Reaction Yield Dependence on Number of Pulses
2. Ratio of Rate Constants for the Elimination Reactions of Ethyl Acetate and Isopropyl Bromide, and of sec-Butyl Acetate and tert-Butyl Chloride vs Temperature
- 3a. Irradiation of 40% Isopropyl Bromide and 60% Ethyl Acetate Mixture with P(20) at $\phi = 9 \text{ J/cm}^2$
- 3b. Irradiation of 50% tert-Butyl Chloride and 50% sec-Butyl Acetate Mixture at P(38)
4. Irradiation of 3% Isopropyl Bromide and 97% Ethyl Acetate Mixture for Various Conditions
5. $P(\phi)_{\text{EA}}$ Dependence on Pressure for a 3% Isopropyl Bromide, 97% Ethyl Acetate Mixture
6. $P(\phi)_{\text{EA}}$ Dependence on Geometry for a 3% Isopropyl Bromide, 97% Ethyl Acetate Mixture
7. Stern-Volmer plots for Ethyl Acetate using He as Bath Gas
8. Stern-Volmer plot for Ethyl Acetate using N_2 as Bath Gas
9. Stern-Volmer plot for Ethyl Acetate using Isopropyl Bromide as Bath Gas, $\phi = 2.0 \text{ J/cm}^2$
10. Stern-Volmer plot for Ethyl Acetate using Isopropyl Bromide as Bath Gas, $\phi = 3.6 \text{ J/cm}^2$
11. Ethyl Acetate Irradiated with P(12), 1053.9 cm^{-1}
12. Ethyl Acetate Irradiated with P(16), 1050.4 cm^{-1}
13. Ethyl Acetate Irradiated with P(18), 1048.66 cm^{-1}
14. Ethyl Acetate Irradiated with P(20), 1046.85 cm^{-1} (long pulse)
15. Ethyl Acetate Irradiated with P(20), 1046.85 cm^{-1} (short pulse)
16. Ethyl Acetate Irradiated with P(38), 1029.43 cm^{-1}
17. Measurement of σ_{L} for Ethyl Acetate at P(20)
18. Measurement of σ_{L} for Ethyl Acetate at P(38)
19. \bar{n} and \bar{n}_{r} for Ethyl Acetate Irradiated with P(20)
20. \bar{n} and \bar{n}_{r} for Ethyl Acetate Irradiated with P(38)
21. Ethyl Fluoroacetate Irradiated with R(20), 1078.58 cm^{-1}

22. Ethyl Fluoroacetate irradiated with R(12),
1073.27 cm^{-1}
23. Ethyl Fluoroacetate irradiated with P(10),
1055.27 cm^{-1}
24. Ethyl Fluoroacetate irradiated with R(8),
1070.46 cm^{-1}
25. σ_L of Ethyl Fluoroacetate at R(12)
26. σ_L of Ethyl Fluoroacetate at P(10)
27. \bar{n} and \bar{n}_r values for Ethyl Acetate at R(12)
28. \bar{n} and \bar{n}_r values for Ethyl Fluoroacetate at P(10)
29. Butene Product Distribution of sec-Butyl Acetate
30. sec-Butyl Acetate irradiated with P(38), 1029.43 cm^{-1}
31. Measurement of σ_L for sec-Butyl Acetate at P(38)
32. \bar{n} and \bar{n}_r for sec-Butyl Acetate at P(38)
33. Reaction Probability vs Fluence for n-Butyl
Acetate irradiated at R(8), 1070.46 cm^{-1} and
P(26), 1041.27 cm^{-1}
34. σ_L of n-Butyl Acetate at R(8) and P(26)
35. \bar{n} and \bar{n}_r values for n-Butyl Acetate at P(26)
36. Ratio of Products vs Fluence for MPIUR and
Thermal Excitation of Ethyl 2-Bromopropionate
37. Ethyl 2-Bromopropionate irradiated with R(14),
1074.64 cm^{-1}
38. σ_L of Ethyl 2-Bromopropionate at R(12)
39. σ_L of Ethyl 2-Bromopropionate in a 96% He,
4% Ester Mixture
40. \bar{n} and \bar{n}_r values for Ethyl 2-Bromopropionate
at R(12)
41. Ethyl Acrylate irradiated with R(10), 1071.88 cm^{-1}
42. Measurement of σ_L for Ethyl Acrylate at R(10)
43. \bar{n} and \bar{n}_r for Ethyl Acrylate at R(10)
44. Summary of P(\emptyset), \emptyset , E_0 , n , \bar{n} and \bar{n}_r for the MPIUR
of Esters
45. Laser Absorption Cross Sections

46. $k_{\infty}(T)$, T and $\langle E \rangle$ values for Ethyl Acetate and Butyl Acetate
47. Fraction of Reaction Predicted by Model Compared to Fraction of Reaction During the Laser Pulse
48. T_i^V , T_f , $\langle E \rangle$ and $\langle E_{vib}^f \rangle$ for Collisionless and Equilibrium Conditions for Ethyl Acetate and n-Butyl Acetate.
49. Δt Estimates at Different T
50. Values of Constants used in Calculating k_E
51. Frequencies of Ester Molecules and Activated Complexes

LIST OF FIGURES

1. CO₂ Laser Gain Curve
2. Laser Beam Profile
3. Laser Pulse Shape
4. Arrangement for Measuring σ_L at High Fluence
5. Arrangement for Measuring σ_L at Lower Fluence
6. Yield vs Number of Pulses for Ethyl 2-Bromopropionate
7. Yield vs Number of Pulses for Ethyl Acetate and sec-Butyl Acetate
8. Stern-Volmer Plots for He Added to Ethyl Acetate
9. Stern-Volmer Plots for N₂ and Isopropyl Bromide Added to Ethyl Acetate
10. Infrared Spectrum of Ethyl Acetate
11. Log P(\emptyset) vs log \emptyset for Ethyl Acetate
12. Log Transmittance vs Ethyl Acetate Pressure
13. σ_L vs \emptyset for Ethyl acetate
14. Infrared Spectrum of Ethyl Fluoroacetate
15. Log P(\emptyset) vs log \emptyset for Ethyl Fluoroacetate
16. Log Transmittance vs Ethyl Fluoroacetate Pressure at R(12)
17. Log Transmittance vs Ethyl Fluoroacetate Pressure at P(10)
18. σ_L vs \emptyset for Ethyl fluoroacetate
19. Infrared Spectrum of sec-Butyl Acetate
20. Log P(\emptyset) vs log \emptyset for sec-Butyl Acetate
21. Log Transmittance vs sec-Butyl Acetate Pressure
22. σ_L vs \emptyset for sec-Butyl Acetate
23. Infrared Spectrum of n-Butyl Acetate
24. Log P(\emptyset) vs log \emptyset for n-Butyl Acetate
25. Log Transmittance vs n-Butyl Acetate Pressure
26. σ_L vs \emptyset for n-Butyl Acetate
27. Infrared Spectrum of Ethyl 2-Bromopropionate and Ethyl Acrylate
28. Log P(\emptyset) vs log \emptyset for Ethyl 2-Bromopropionate
29. Log Transmittance vs Ethyl 2-Bromopropionate Pressure
30. σ_L vs \emptyset for Ethyl 2-Bromopropionate and Ethyl Acrylate

31. Log $P(\emptyset)$ vs $\log \emptyset$ for Ethyl Acrylate
32. Log Transmittance vs Ethyl Acrylate Pressure
33. $P(\emptyset)$ Dependence on Power
34. Log $P(\emptyset)$ vs \emptyset for Ethyl Acetate
35. Log $P(\emptyset)$ vs \emptyset for Ethyl Fluoroacetate
36. Log $P(\emptyset)$ vs \emptyset for sec-Butyl Acetate
37. Log $P(\emptyset)$ vs \emptyset for Ethyl Acrylate
38. Infrared Spectrum and σ_L vs \emptyset Plot of Methyl Acetate
39. Boltzmann Distributions for Ethyl Acetate
40. Boltzmann Distributions for n-Butyl Acetate
41. Model Calculated Curves for Ethyl Acetate
42. Model Calculated Curves for n-Butyl Acetate
43. $P(\emptyset)$ vs $\bar{n} + E_{\text{vib}}(\text{thermal})$ for the Esters
44. \bar{n}_r vs $P(\emptyset)$ for the Esters
45. $\log [1.0 - P(\emptyset)]^{-1}$ vs \emptyset for Ethyl Acetate and Ethyl Acrylate
46. k_E , sec^{-1} (RRKM) vs E kcal/mole for Ethyl Acetate and Ethyl Fluoroacetate
47. k_E , sec^{-1} (RRKM) vs E kcal/mole for sec-Butyl Acetate and n-Butyl Acetate
48. k_E , sec^{-1} (RRKM) vs E kcal/mole for the two Reaction Channels of Ethyl 2-Bromopropionate

I INTRODUCTION

The multiple photon absorption (MPA) and multiple photon induced unimolecular reaction (MPIUR) processes have been actively studied recently¹. The fact that unimolecular reactions can be induced by highly intense, monochromatic radiation made available by lasers has aroused great interest in developing a new approach to chemical synthesis which would differ from the traditional thermal excitation in which energy is supplied in Boltzmann form by heating of the reaction components. Other interests in this new phenomenon are the basic nature of the MPA process, the resulting energy distribution, the mechanism of the MPIUR processes and isotope separation.

All polyatomic molecules show absorption bands in the infrared and consequently absorb infrared photons. In principle these polyatomic molecules could be irradiated with photons of frequencies matching those of the absorption bands, and they could display MPA or MPIUR. At the present time, only a limited range of frequencies in the infrared is available from lasers with enough power to cause MPA or MPIUR. The most commonly used laser is the CO₂ laser, although work has been done with HF and other special lasers.

The principal reason for the synthetic interest is the difference in the conditions under which infrared laser induced reactions and those of the usual thermal equilibrium conditions are thought to occur. In the latter case the internal (vibrational) and external (translational, rotational) degrees of freedom are in mutual equilibrium. In the case of laser induced reactions, the energy required to activate the molecule is deposited exclusively as vibrational energy (providing no collisions take place) with the rotational and translational degrees of freedom being essentially unaffected. It has been established that pulsed infrared radiation can lead to a completely different pathway of reaction from that followed by thermal heating for some chemical systems². High energy reaction pathways can even be made to predominate over the low energy pathway³. This, however, is not the usual case.

For small polyatomic molecules, of which SF_6 and the freons are the most thoroughly studied cases, the MPA process is explained by the following scheme. The first few discrete levels are assumed to be pumped coherently ⁴. Anharmonic splitting of excited vibrational states ⁵ or rotational compensation ⁶ is supposed to overcome the anharmonicity of the polyatomic molecule in the region of these discrete levels. The initial excitation over the discrete levels depends not only on the frequency of the radiation and the power of the laser, but also on the rotational quantum states and the excitation of hot bands ⁷. This region is mainly responsible for the high selectivity of the MPA process which leads to isotope separation. For the higher energy levels, the density is sufficiently high to be treated as a quasicontinuum ⁸. There is no clearly definable boundary between the discrete levels and the quasicontinuum regions. Further excitation of the molecule in this quasicontinuum, which is thought to be an incoherent process, leads to dissociation of the molecule. In the quasicontinuum, laser fluence rather than laser power was shown to be responsible for driving the molecules up the energy ladder and to determine the yield of the reaction. Under collision free conditions, the irradiated molecules migrate up the vibrational levels under pumping from the laser pulse. The pumped molecules continue climbing the ladder until, at a certain energy above the threshold energy for reaction, the unimolecular rate competes with the pumping rate resulting in the formation of products. For small polyatomic molecules, the power of the laser and the rate of unimolecular reaction determines the average level of excitation. Some aspects of this view may need modification for MPIUR of large polyatomic molecules.

For several small molecules, careful experiments on dissociation dynamics, such as measurement of the fragment products, translational energy and the internal energy distributions of the excited reactant ^{9,10} have been performed. These measurements have demonstrated that the energy is completely randomized before dissociation. This implies that energy randomization among vibrational modes is faster than the rate of

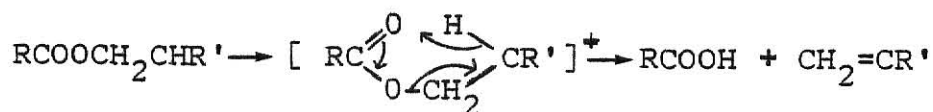
excitation near dissociation. Energy randomization makes possible the use of statistical theory of unimolecular reactions, such as RRKM¹¹, to treat the unimolecular dynamics of laser induced reactions. This is as expected since the time scale for energy deposition is of the order of microseconds while the energy randomization proceeds at rates of picoseconds¹².

In this work, The laser MPA and MPIUR of organic esters containing 14 to 20 atoms are investigated. The size of these polyatomic molecules is significantly greater than that of SF₆ or the freons which have been most carefully studied. The main difference between large and small polyatomic molecules is the greater density of states of the former. This greater density of states affects several things:

- (i) The quasicontinuum region will occur at a much lower energy.
- (ii) The magnitude of the rate constants at the threshold energy is much lower.
- (iii) The Boltzmann thermal distribution extends to much higher vibrational energies.
- (iv) The small rotational constants lead to a high density of rotational states for each vibrational band.

Another feature of polyatomic molecules is that several unimolecular reaction pathways generally exist.

The purpose of this thesis is to characterize the MPA and MPIUR processes of organic esters. The characteristic unimolecular reaction of esters is the six-centered rearrangement reaction with a threshold energy of 45 - 48 kcal mole⁻¹.



Where R, R' could be H or some other atom or group. The esters are a convenient series because the absorption is relatively strong and because systematic changes can be made in the molecular structure. The laser absorption occurs mainly in the O-CH₂ stretching motion of the ester molecule.

The dependence of the laser induced reaction probability on laser fluence, laser power, irradiation frequency, pressure of ester and addition of bath gas was studied in this work. Also reported are the product distributions of MPIUR when there is more than one channel of dissociation. Laser absorption measurements were made in order to define the efficiency of the MPIUR processes. The dependence of the average number of photons absorbed per molecule on laser fluence, laser frequency and addition of an inert gas to the ester were studied. These data are compared to some predictions of simple models and the overall view of MPIUR for large molecules is discussed.

All experiments were conducted utilizing small static cells at low pressures of reactant. Experiments were performed using uniform fluences in the range of 0.2 to 10 J/cm². For the higher fluences, a long focal length lens, which produced approximately uniform fluence throughout the short cell, was used. Fortunately, the absorption by the organic esters is sufficiently strong that a wide range of reaction probability can be examined at fluences below 10 J/cm² and a high degree of focusing is not required. The use of uniform fluence cells is preferable to any highly focused geometry, which gives a large photon concentration gradient in the cell.

II EXPERIMENTAL

A. Reagents.

The following esters were used in this study: ethyl acetate, ethyl fluoroacetate, ethyl acrylate, *n*-butyl acetate, *sec*-butyl acetate and ethyl 2-bromopropionate. In order to monitor the effect of thermal reactions, the following compounds were used: isopropyl bromide, isopropyl chloride and *tert*-butyl chloride. The products from irradiation of these compounds and esters were: propene, isobutene, ethene, *trans*-2-butene, *cis*-2-butene and 1-butene. No effort was made to follow the acid fragment from the ester decomposition. All these compounds were commercially available. Liquid samples were distilled under vacuum and used without further purification. These samples were checked by gas chromatography and shown to be of satisfactory purity for experimental purposes. All samples were stored in large vessels in the gas phase, which were attached to a vacuum system that was capable of achieving a pressure of 10^{-5} torr. The vessels were fitted with greaseless needle valve teflon stopcocks that regulated the gas flow. When dealing with light-sensitive compounds, the vessels were painted black.

B. Irradiation Cells.

The cells into which the esters were transferred were made of Pyrex tubing of different diameters and lengths to which glass or teflon stopcocks were attached. The total volume was then calculated and polished salt flats were glued to the cell with epoxy. The polishing of the flats was accomplished in three steps: 1) the rough flat was polished with fine silicon carbide sand paper; 2) the flat was polished with 600 grit carborundum powder sprinkled on a clean cloth and using ethanol for lubrication; 3) cerium oxide powder was placed on a clean piece of cotton and polishing was done until the desired finish was obtained. In the last step, it was necessary to use gloves to avoid any clouding of the polished surfaces by water vapor or oil from the skin.

The salt flats were then immediately glued to the Pyrex cells and left to cure for 3 hours. Next, the cells were checked for leaks by evacuating them and testing with a He leak detector. When not in use, the cells were stored in a moisture-free container.

C. Analysis.

The reagents and products from MPIUR were analyzed with a Varian 2700 series gas chromatograph equipped with a flame ionization detector. A 6' long, 1/8" diameter stainless steel column filled with Porapak Q was used to separate the components (except in the case of the product analysis of sec-butyl acetate, where a 30' x 1/4" diameter propylene carbonate column connected to a 5' x 1/8" diameter 10% carbowax 20M on chromasorb W column at 0°C was used).

The standard procedure for sample irradiation and analysis was the following: after a good vacuum was obtained in the vacuum system, the reactant was metered to the irradiation cell and the pressure was carefully measured with an MKS Baratron pressure transducer, type 222AHS-A-B-100 (or 10). The cell was then placed in front of the CO₂ laser and irradiated "i" times with the laser. Next, the contents of the cell were transferred to a trap cooled to 77 K and filled with glass wool. The sample was condensed in the trap; all non-condensable products (77 K) were pumped away. To transfer the sample from the cold trap to the chromatograph injection loop quantitatively, boiling water was applied to the frozen sample (isolated from the rest of the system) and the gauge. injection loop was cooled with liquid nitrogen. After complete vaporization, the stopcock quickly opened to allow the sample to freeze in the injection loop while the transfer is monitored by the pressure gauge. Once the transfer is complete, the injection loop is pressurized with carrier gas, heated with hot water and injected into the G. C. column by simultaneously opening two toggle valves.

All gas chromatography analyses were done isothermally; 200°C for ethyl 2-bromopropionate, ethyl acrylate and n-butyl

acetate, 190°C for sec-butyl acetate, 180°C for ethyl fluoroacetate and 175°C for ethyl acetate. Retention times for the light gases were of the order of 2 to 3 minutes and those of the esters ranged from 5 to 17 minutes, depending on the molecular weight.

The areas of the peaks from G. C. analysis were measured using a planimeter. This method was preferred over peak heights due to the tailing of the peaks from the heavier esters which resulted in asymmetric peak shapes. To check mass balance of reactants and products, absolute calibrations were made using accurately measured amounts of sample; the peak areas were measured to obtain the ratio of the sample size (in units of torr in the given cell volume) to the area of the peak.

D. Infrared Spectra.

The infrared spectra of the reactants and some of the products were taken with a Perkin-Elmer model 180 infrared spectrophotometer. The frequency region of interest was from 1040 cm^{-1} to 1090 cm^{-1} , which corresponds to the R and P branches of the $00^0_1-02^0_0$ CO_2 band of the TEA laser. The "white light" absorption cross section, σ , for each ester was calculated from the ir spectrum at pressures below 2 torr using Beer's law.

E. CO_2 Laser.

A TEA CO_2 laser series 100 made by Lumonics of Canada was used in this work. The TEA laser operates by the method of transverse excitation of a three-gas mixture (CO_2 , He and N_2). The laser was operated on a single line, which means that an intracavity grating selected a given rotational line from the vibrational CO_2 bands. For a given branch of a vibrational band, the pulse energy varied with rotational quantum number J. The laser energy curve is shown in Fig. 1.

Due to the shape of the electrodes in the TEA laser, the full beam has an oval shape with a higher intensity at the center. An iris with a 3/4" diameter was used to reduce the beam size. The laser beam profile for this size was measured

**THIS BOOK
CONTAINS
NUMEROUS PAGES
WITH DIAGRAMS
THAT ARE CROOKED
COMPARED TO THE
REST OF THE
INFORMATION ON
THE PAGE.**

**THIS IS AS
RECEIVED FROM
CUSTOMER.**

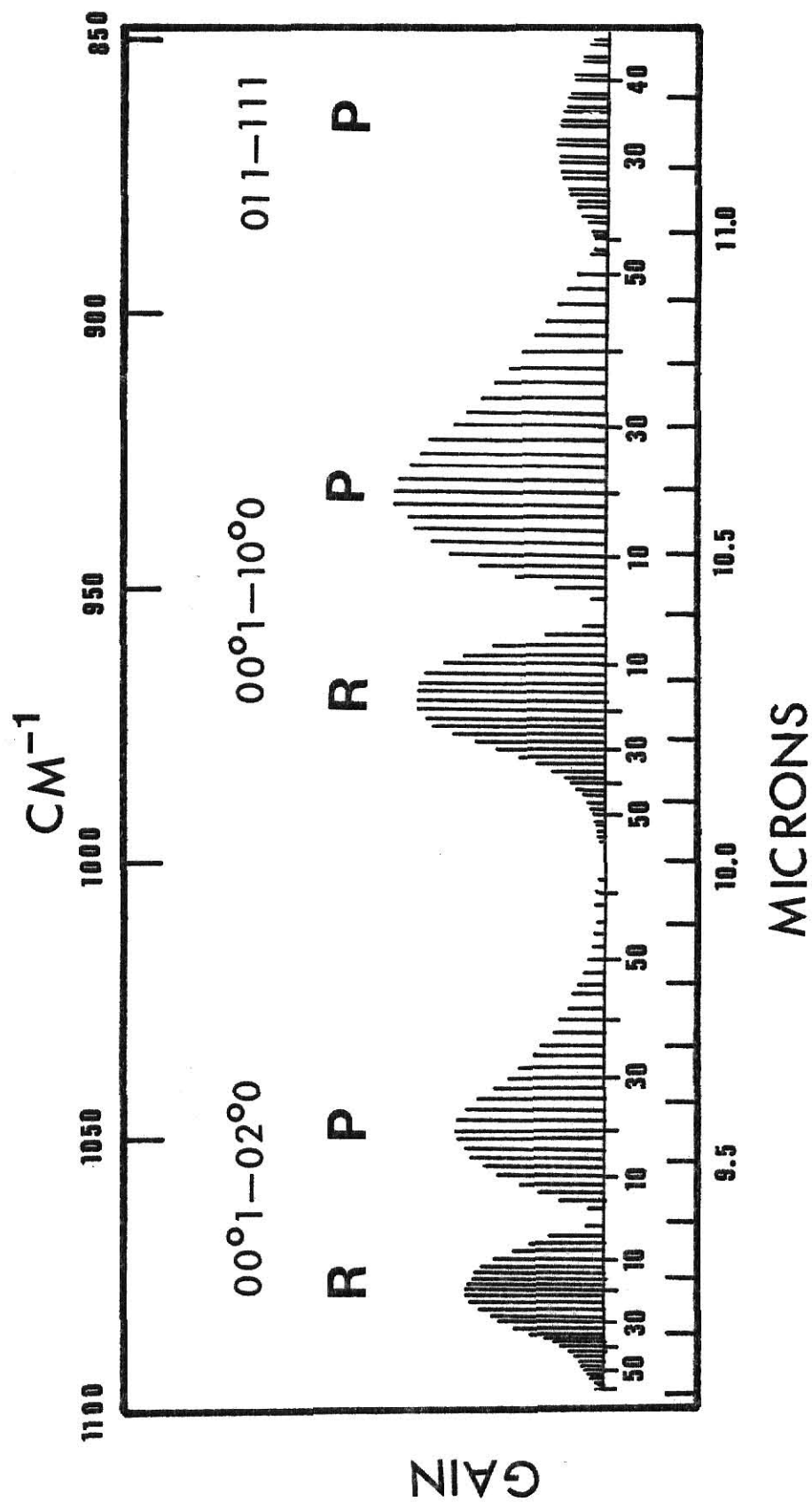


FIG.1 CO₂ LASER GAIN CURVE

using a 1/8" diameter iris placed before the pyroelectric detector. The detector (and iris) was then placed at six different positions across the 3/4" beam and the average fluence was measured for these positions (Fig. 2). The apparent variation in fluence, ~5% across the 3/4" beam was remarkably small.

F. Laser Pulse Energy Measurement.

The energy of the beam was measured using a Lumonics pyroelectric detector model 20D 110 with a responsivity of 1.71 volts per joule. The voltage of the detector was measured with a Hewlett Packard 1710 B oscilloscope; the voltage reading was converted to joules and this value of energy was divided by the cross sectional area of the beam to yield fluence.

Because the detector could not safely take more than 0.3 J/cm^2 , it was necessary to use a Ge flat at 45° from the normal of the beam to reflect a small fraction of the beam energy to the detector. The percent reflected was measured by attenuating the beam to a low fluence. Then the energy reflected by the Ge flat was measured, and by removing the Ge flat, the total energy was also measured. The fraction of energy reflected by the Ge, F_r , was calculated by dividing the measured reflected energy by the total energy. Once F_r is known, the attenuation is removed and high energies can be calculated by dividing their reflected value by F_r .

When higher fluences were required, a long focal length BaF_2 lens was used to decrease the cross sectional area of the beam resulting in higher fluence. For fluences greater than 10 J/cm^2 , damage to the NaCl windows of the cell resulted. In order to decrease the value of fluence in small intervals, successive layers of Handy Wrap (Dow Chem.) plastic were employed to attenuate the beam. This material was especially suitable since it did not deteriorate after long use and the fraction of incident energy lost upon passing through several layers of plastic was proportional to the number of layers. Since the thickness of a layer is

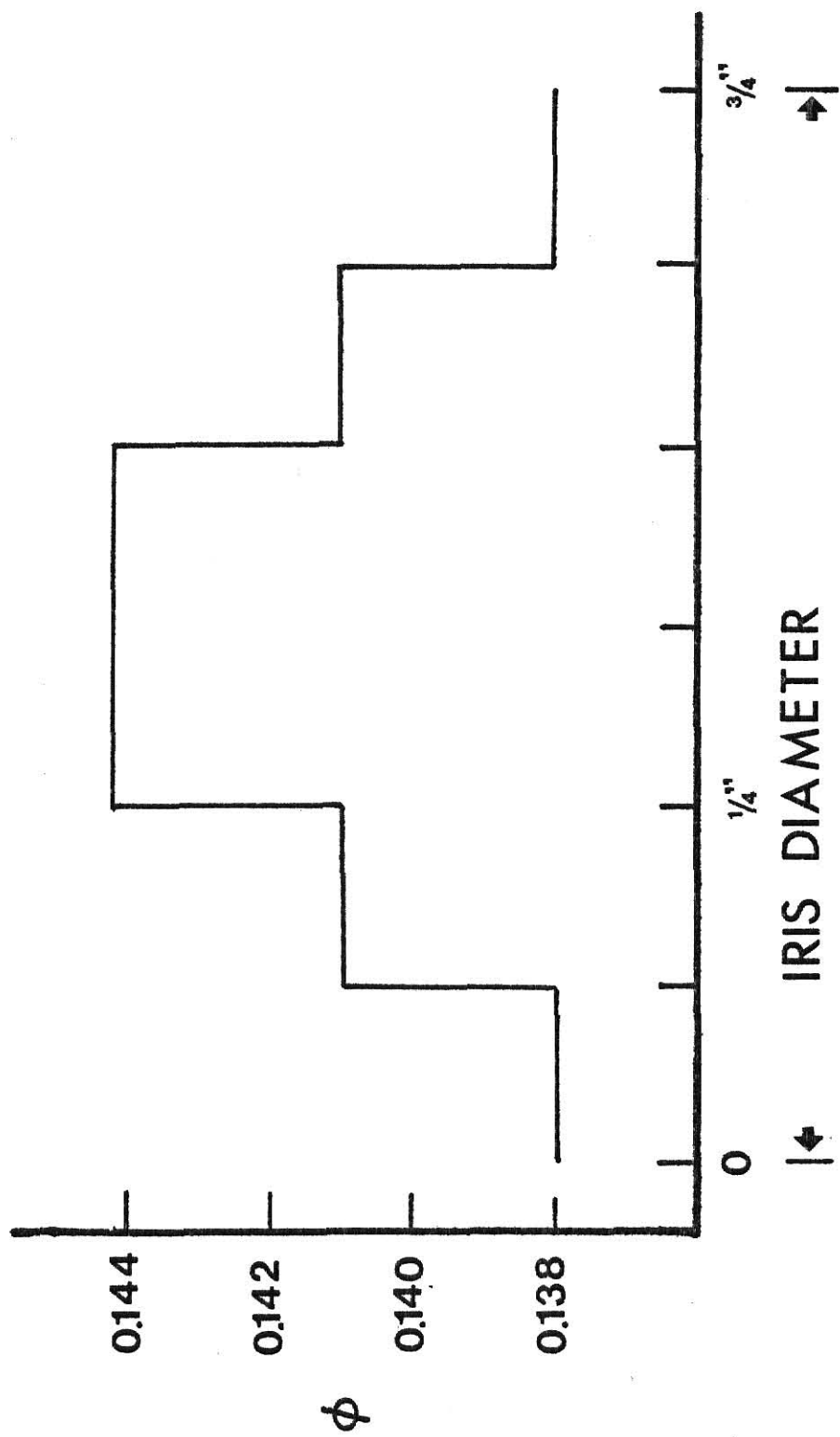
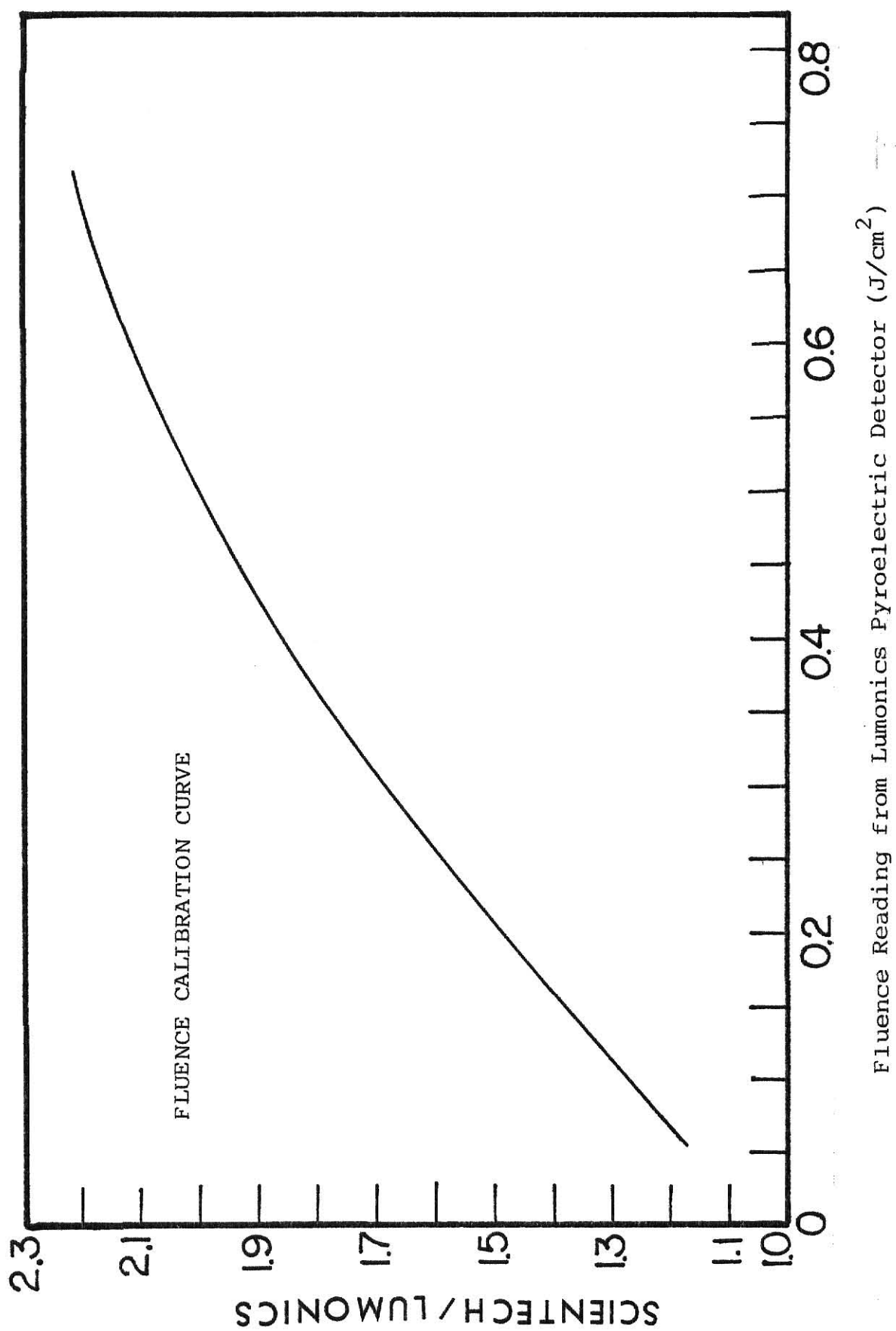


FIG.2 LASER BEAM PROFILE

of the same order of magnitude as the wavelength of the laser photons, the attenuation is mainly caused by multiple reflections rather than by absorption.

After all of the experimental work was completed, a new energy detector was purchased. By comparing the Lumonics pyroelectric detector model 20D used to measure fluence throughout this work, with the calibrated Scientech detector model 38-0102 it was learned that the response of the Lunonics detector was too low. Even more serious, the pyroelectric detector's response was nonlinear; the correction factor increased from 1.25 at 0.10 J/cm^2 to 2.20 at 0.67 J/cm^2 . In order to correct the experimental data to the correct fluence, a calibration curve was constructed. The corrected ϕ was obtained by the following procedure: (1) For ϕ from 0 to 0.4 J/cm^2 the ϕ_{pyro} were multiplied by the corresponding factor from the calibration curve to give the corrected ϕ . (2) For unfocused conditions with ϕ_{pyro} from 0.4 J/cm^2 to the highest unfocused ϕ , the ϕ_{pyro} were measured using a Ge flat. This flat reflects 28% of the energy instead of 38% as was measured using the pyroelectric detector. To obtain the corrected ϕ , the tabulated ϕ_{pyro} were multiplied by 0.38 to obtain the pyroelectric meter reading. The resulting ϕ_{pyro} were then multiplied by the corresponding factor from the calibration curve to give the ϕ_r , which would have been the response of the Scientech detector. These ϕ_r were divided by 0.28 to obtain the corrected ϕ that the sample received. (3) For focused conditions the ϕ_{pyro} were multiplied by the area of the focused beam, then divided by the area of the unfocused beam and these ϕ_{pyro} were multiplied by 0.38 to give the signal observed by the Lumonics detector. The resulting ϕ were then multiplied by the corresponding factor from the calibration curve and the result multiplied by the area of the unfocused beam and then divided by the area of the focused beam to obtain the corrected ϕ . All ϕ values in this thesis have been corrected using the above procedure.



G. Measurement of Laser Pulse Shape.

The laser pulse shapes shown in Fig. 3 were measured using a photon drag detector made by Rofin LTD. of England. The signal from the detector was fed to a Biomation digitizer, where about ten pulses were added and averaged by a computer program that also subtracted the noise produced by the laser. The result was displayed as an intensity vs time curve and the area under this curve was proportional to the total energy of the pulse. The type of pulse used mainly in this work was the long pulse, which was produced by setting the flow controls that regulate the composition of the lasing mixture at 8.0 for helium, 2.0 for CO₂ and 0.8 for nitrogen (the units on the flow meters are SCFH AIR at 70° & 14.7 psia). The pulse consisted of an initial spike of about 130 nanoseconds at FWHM, followed by a lower intensity tail, lasting about 1.2 microseconds. The fraction of the total energy contained in the initial spike was approximately 0.43, the other 0.57 was contained in the tail. The contribution of the tail to the pulse can be reduced by cutting down on the amount of nitrogen. The shortest pulse, 110 nanoseconds at FWHM, was obtained for the limit of zero nitrogen. For the short pulse the flow meter settings were: 10.0 for helium, 5.0 for CO₂ and 0.0 for nitrogen. The voltage used throughout the experiments was 40 kV.

To maximize the energy per pulse, the micrometers which move the output coupler vertically and horizontally were varied until the highest energy was obtained. Finally, the best position of the iris was selected with the help of burn patterns in infrared sensitive paper.

H. Laser Tuning.

Selection of a particular rotational line was achieved by rotating the micrometer located at the back of the laser unit which turned the intracavity grating until the desired line was obtained. Measurement of the wavelength of the rotational line was done with a precalibrated Model 16-A laser spectrum analyzer made by Optical Engineering Inc. Once the

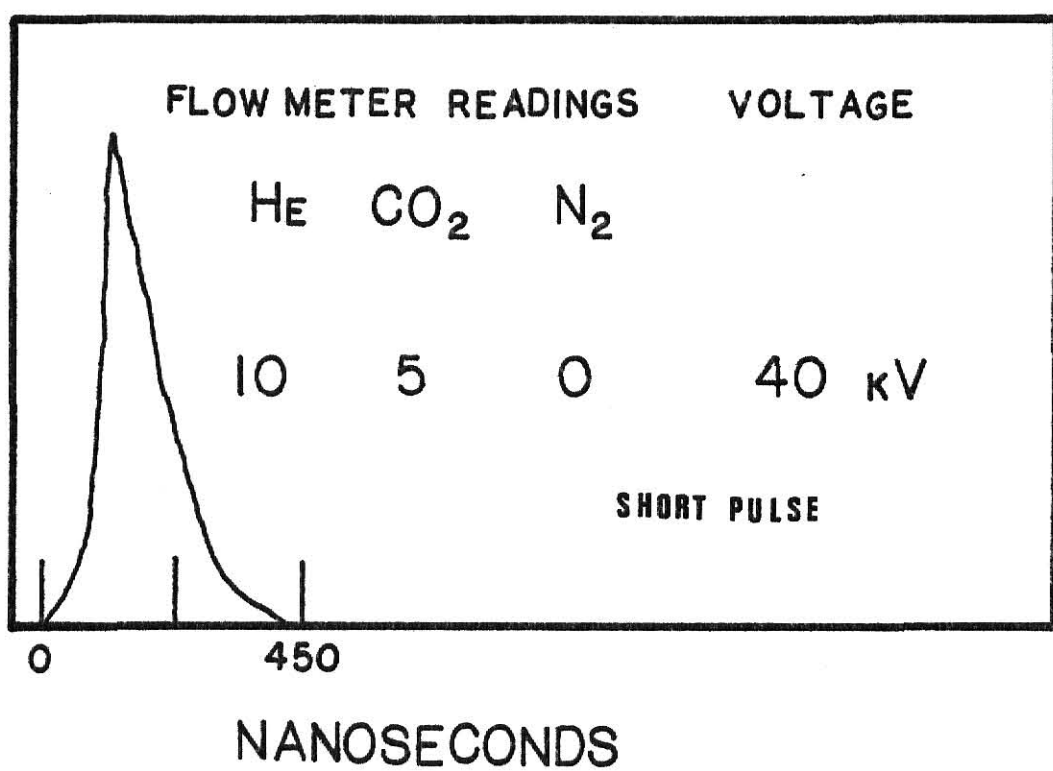
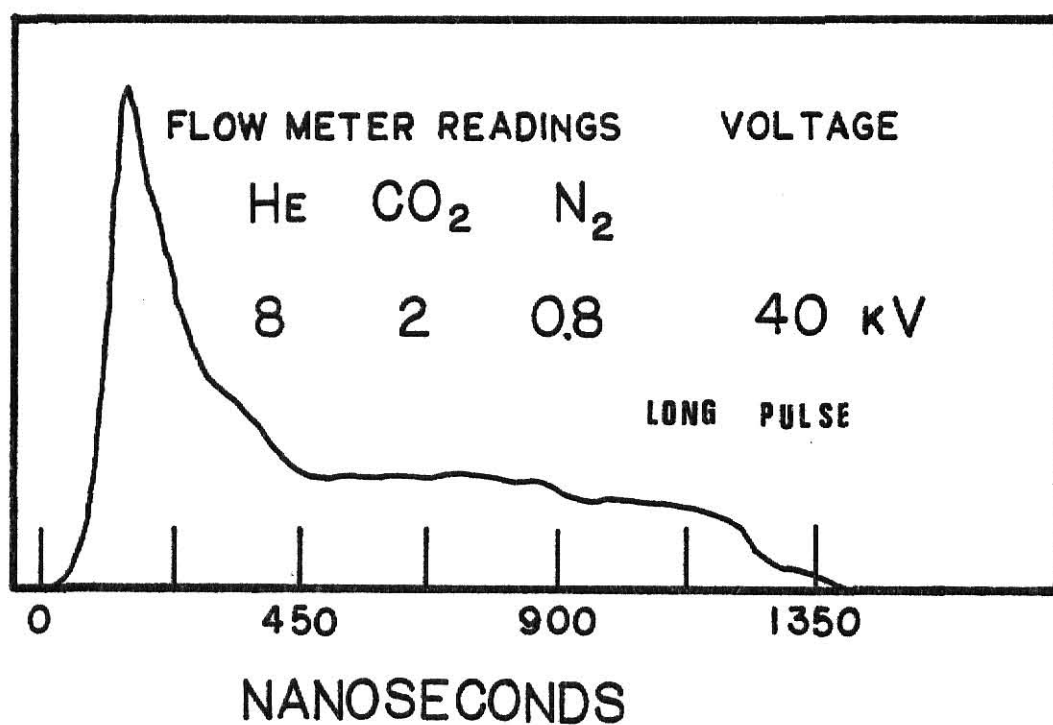


FIG.3 LASER PULSE SHAPE

desired line was observed in the spectrum analyzer, a salt flat was used to reflect a small fraction of the beam into a pyroelectric detector whose signal was displayed on an oscilloscope. In order to maximize the signal, the micrometer setting was varied slightly until a maximum in signal was displayed on the oscilloscope. Due to small variations in the position of the grating with time, a wavelength calibration using micrometer settings that corresponded to given rotational lines was not reliable, and the spectrum analyzer was used each time a new line was selected.

I. Measurement of Laser Absorption Cross Sections, σ_L .

The measurement of the σ_L , which were employed in the calculation of the average number of photons absorbed per molecule, was done using a dual pyroelectric detector arrangement which measured the energy entering and leaving the cell. The arrangements used to measure σ_L at high and low fluences are shown in Figs. 4 and 5, respectively. In arrangement A, a fraction F_r^{NaCl} of the energy E_0 , was reflected by a NaCl flat into DET 1. The rest of the beam then passed through the cell and (assuming there are no losses due to reflection by the windows) a fraction of the transmitted beam $F_r^{\text{Ge}}(1-F_r^{\text{NaCl}})$, was reflected by a Ge flat into DET 2 when the cell was evacuated. In the case of arrangement B, F_r^{Ge} was the fraction of E_0 reflected by the Ge flat into DET 1, and $(1-F_r^{\text{Ge}})$ was the fraction of E_0 received by DET 2 when the cell was evacuated. Multiplying the fractions by E_0 gave the total energy received at each detector.

When the cell was filled with sample at a given pressure, the amount of energy received by DET 2 was decreased. For arrangement A the decrease was $F_r^{\text{Ge}}(1-F_r^{\text{NaCl}}) E_0 F_T$, and for arrangement B the decrease was $(1-F_r^{\text{Ge}}) E_0 F_T$. Where F_T was the fraction transmitted by the gas.

The signals from DET 1 and DET 2 were amplified by PREAMP 1 and PREAMP 2 with adjustable gains α and β , respectively, and transmitted to a PDP 8 computer where they were displayed as peak 1 and peak 2. The amplified signals had energies equal to $\alpha F_r^{\text{NaCl}} E_0$ for peak 1 and

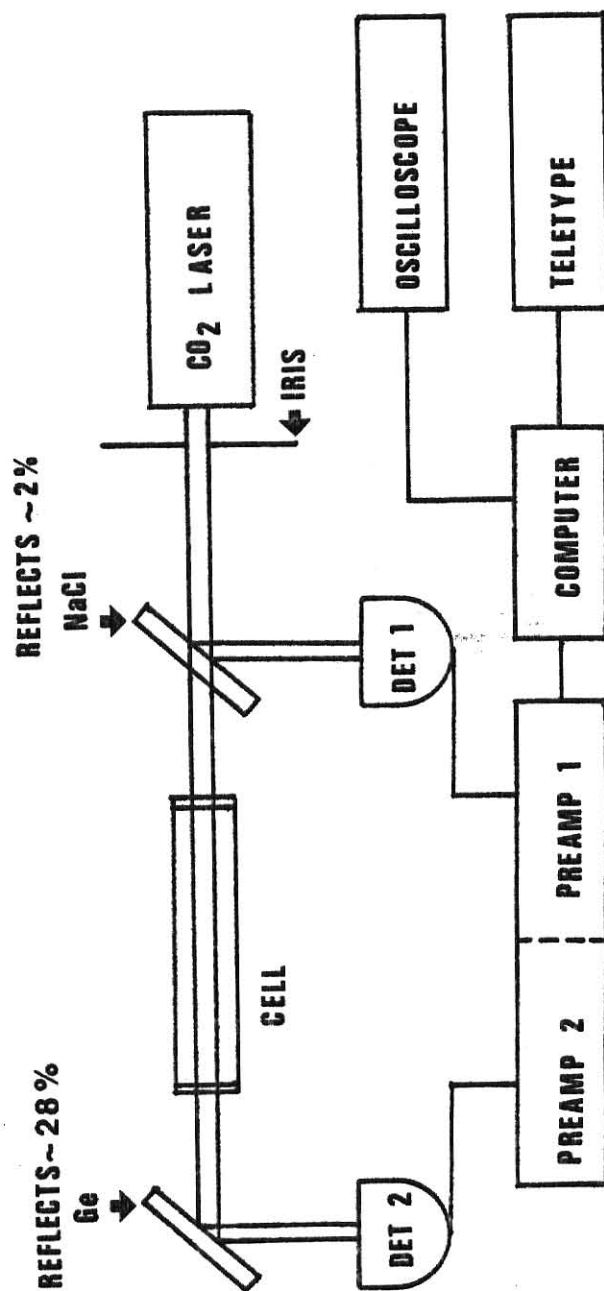


FIG.4 ARRANGEMENT "A" FOR MEASURING σ_L AT HIGH FLUENCE.

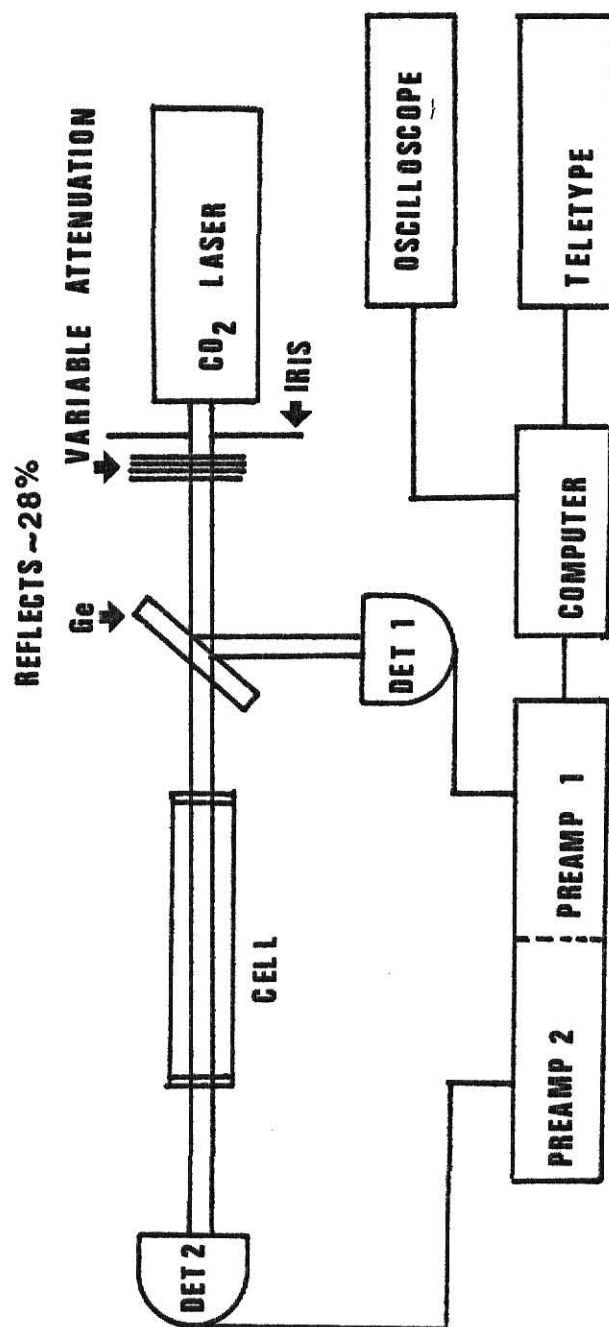


FIG.5 ARRANGEMENT "B" FOR MEASURING σ_L AT LOWER FLUENCE.

$\beta F_r^{\text{Ge}}(1-F_r^{\text{NaCl}}) E_o$ (or $E_o F_T$ when sample was in the cell) for peak 2 for arrangement A; and energies equal to $\alpha F_r^{\text{Ge}}(1-F_r^{\text{Ge}}) E_o$ for peak 1, and $\beta (1-F_r^{\text{Ge}}) E_o$ (or $E_o F_T$ when sample was in the cell) for peak 2 for arrangement B. A teletype then printed the values of peak 1 and peak 2 in millivolts and the ratio of peak 2 to peak 1 was multiplied by 100.

The transmittance for a given pressure was obtained by dividing the ratio of peak 2 to peak 1 when the cell contained sample, by the ratio of peak 2 to peak 1 when the cell was empty. For arrangement A, equation (1) applies:

$$\frac{\beta F_r^{\text{Ge}}(1-F_r^{\text{NaCl}}) E_o F_T / \alpha F_r^{\text{NaCl}} E_o}{\beta F_r^{\text{Ge}}(1-F_r^{\text{NaCl}}) E_o / \alpha F_r^{\text{NaCl}} E_o} = F_T = \text{Transmittance.} \quad (1)$$

For arrangement B, equation (2) results:

$$\frac{\beta (1-F_r^{\text{Ge}}) E_o F_T / \alpha F_r^{\text{Ge}} E_o}{\beta (1-F_r^{\text{Ge}}) E_o / \alpha F_r^{\text{Ge}} E_o} = F_T = \text{Transmittance} \quad (2)$$

For the case where the compound was highly reactive at the fluence used, each pulse dissociated a large fraction of reactant in the irradiated volume; only the transmittance of the first pulse was used in the calculation of F_T .

Somewhat surprisingly, it was found that for the organic esters, a form of Beer's law was obeyed for the 0.01-5 torr pressure range with intensities replaced by fluences. Therefore, the transmittance values (given by ϕ/ϕ_o) obtained from experiments at various pressures were used to calculate σ_L using equation (3),

$$\ln F_T = -\sigma_L DX \quad \text{or} \quad \log F_T = -\sigma_L DX / 2.303 \quad (3)$$

F_T = transmittance

σ_L = laser absorption cross section in $\text{cm}^2/\text{molecule}$

X = length of cell in cm

D = concentration in molecules/ cm^3 .

At room temperature, D can be expressed as a function of pressure by:

$$D = [3.24 \times 10^{16} \text{ molecule}/\text{cm}^3 \text{ torr}] P \text{ torr},$$

this gives equation (4) after converting to base 10 logs

$$\log F_T = -\sigma_L [1.42 \times 10^{16} \frac{\text{molecule}}{\text{cm}^3 \text{ torr}}] P \text{ torr} X \text{ cm} \quad (4)$$

III. EXPERIMENTAL METHODOLOGY

A. First Order Kinetics of Laser Induced Reactions.

Lyman, Rockwood and Freund¹³ have treated the pulsed radiation problem as if the number of pulses was a variable, analogous to time, in normal kinetic studies. The relationship describing the change in concentration of reactant with the number of pulses "i" is given by (5) as

$$\frac{d[\text{ester}]}{di} = -k[\text{ester}], \quad (5)$$

which, when integrated, gives (6).

$$\ln ([\text{ester}]/[\text{ester}]_0) = -k i. \quad (6)$$

In (6), k is the unimolecular rate constant and i is the number of pulses. Bado and Van den Bergh¹⁴ have shown that the concentration of SF₆ declined exponentially with i, and other investigators also have shown this treatment to be valid. In our work (6) was tested for several esters at different pressures and fluences. In each case log ([ester]/[ester]₀) vs i plots were linear and passed through 1.0 at i=0. The linearity of the plots (but not the slope) was invariant to pressure or fluence; however, curved plots were formed if the pulse rate was too high. Such plots showed upward curvature from the linear plots. One plausible explanation is that the deviation is a consequence of the time required between pulses for molecules to diffuse from the irradiated volume to form a homogeneous mixture before the next pulse occurred. A rate of approximately one pulse every ten seconds, was satisfactory. This problem is specially noticeable for esters at high fluence because a high fraction of the molecules in the irradiated volume may react per pulse.

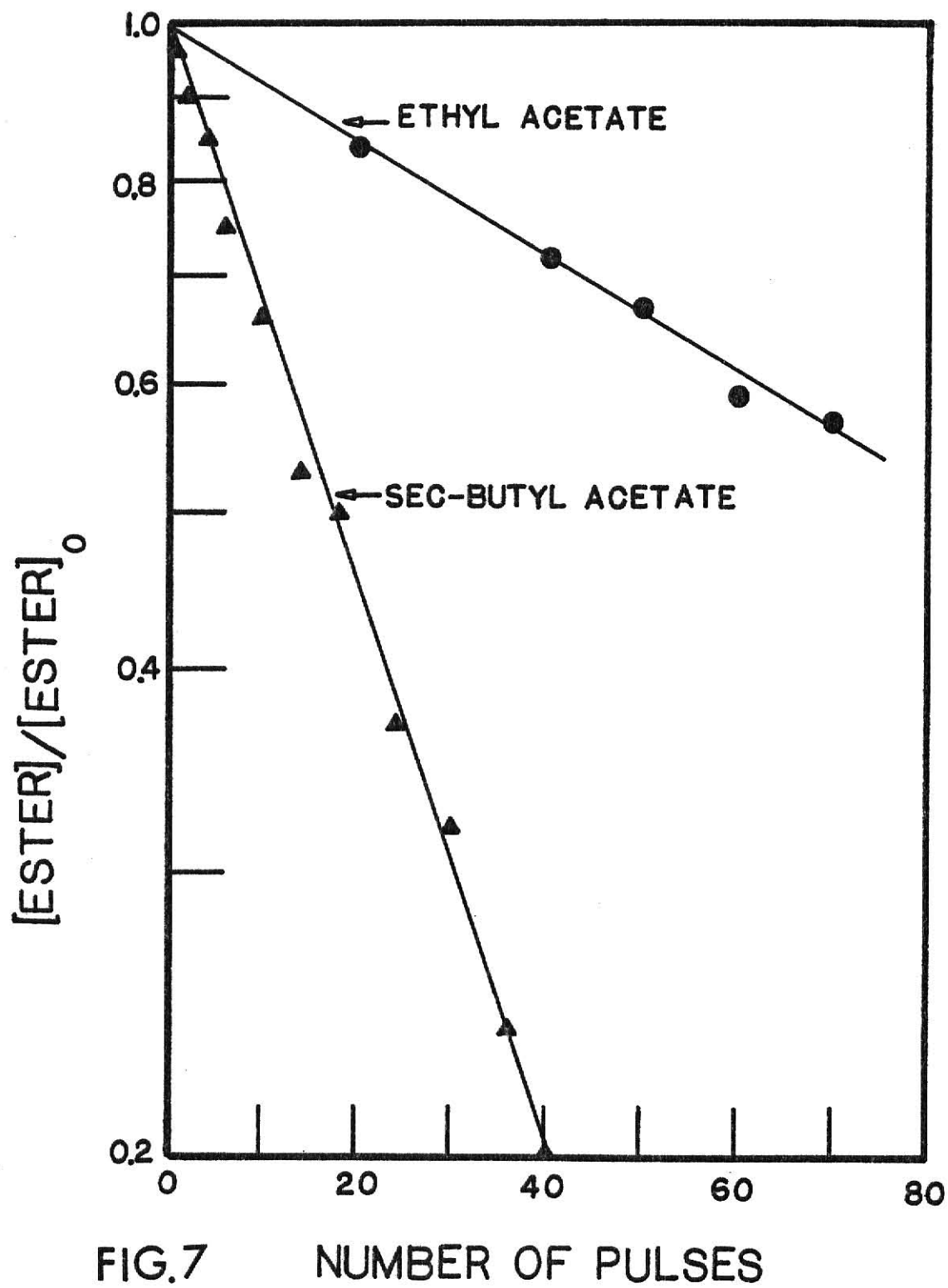
The reaction yield dependence on the number of pulses for ethyl acetate, sec-butyl acetate and ethyl 2-bromopropionate are tabulated in Table 1 and the data are displayed in Figs. 6 and 7.

Table 1. Reaction yield dependence on number of pulses.

Ethyl 2-bromopropionate		Sec-butyl acetate		Ethyl acetate	
i	C_i/C_o	i	C_i/C_o	i	C_i/C_o
1	0.86	1	0.96	20	0.84
2	0.74	2	0.90	40	0.72
3	0.60	4	0.85	50	0.67
4	0.55	6	0.75	60	0.59
6	0.41	10	0.66	70	0.57
		14	0.53		
		18	0.50		
		24	0.37		
		30	0.32		
		36	0.24		
		40	0.20		

Ethyl 2-bromopropionate was irradiated with R(10) at a pressure of 0.1 torr and fluence of 1.0 J/cm^2 in a 21 cm long cell with total volume, $V_o = 79.3 \text{ cm}^3$ and irradiated volume (obtained by multiplying the cross sectional area of the laser beam by the length of the cell), $G_o = 60.17 \text{ cm}^3$. Sec-butyl acetate was irradiated with P(38) at a pressure of 0.1 torr and fluence of 5 J/cm^2 (5 cm from cell was placed at 15 cm from a 40 cm focal length Ge lens) with $V_o = 31 \text{ cm}^3$ and $G_o = 74.5 \text{ cm}^3$. C_i is the concentration of ester remaining after i pulses and C_o is the initial concentration.

Ethyl Acetate was irradiated with the P(22) line at a pressure of 0.05 torr and $\phi = 1 \text{ J/cm}^2$, with $V_o = 186 \text{ cm}^3$ and $G_o = 74.5 \text{ cm}^3$.



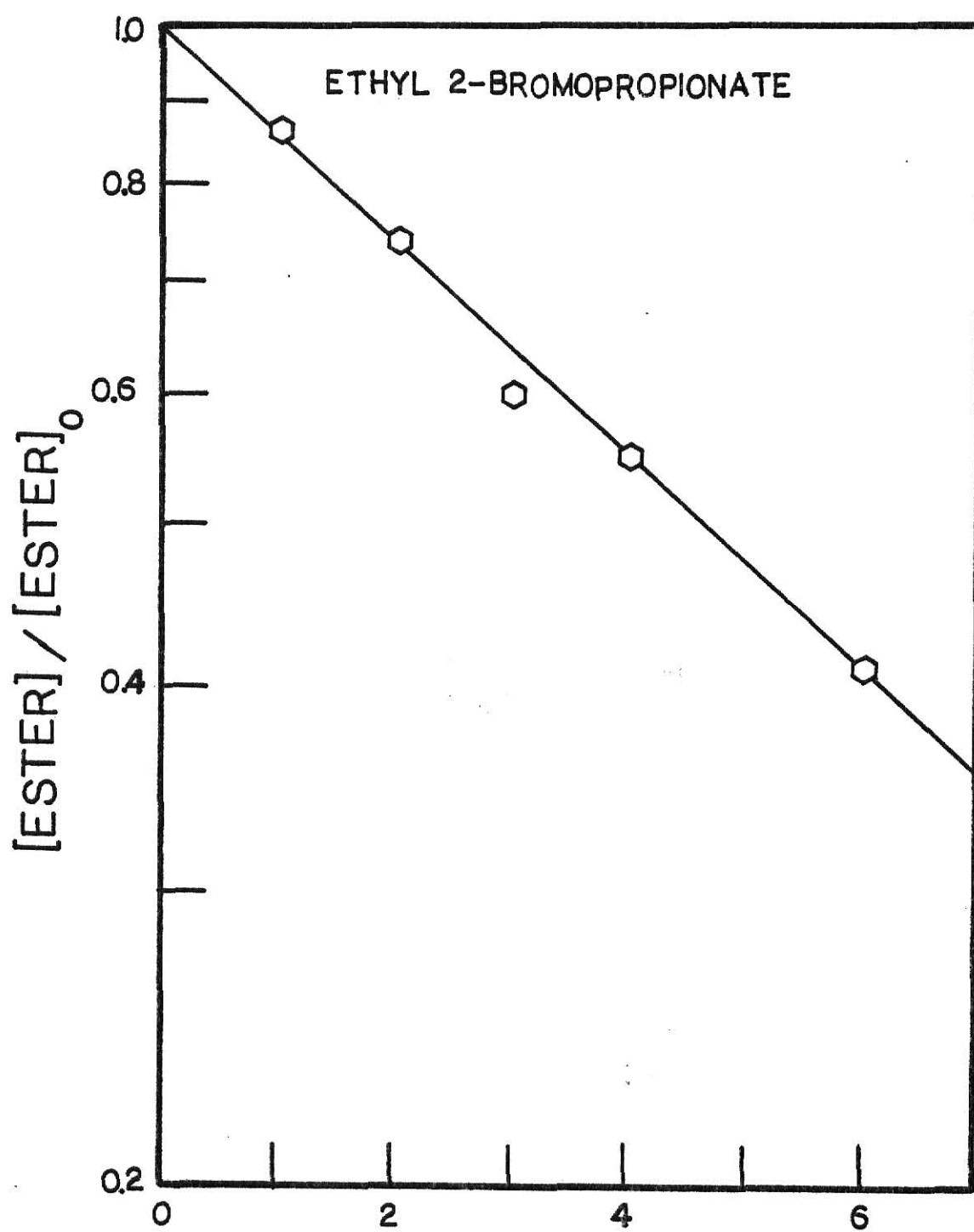


FIG. 6 NUMBER OF PULSES

B. Definition of Reaction Probability.

To calculate the reaction probability (number of molecules that react in the first pulse divided by the number of molecules in the irradiated volume) it was necessary to find the fraction of the total ester concentration that reacted in the first pulse from data of the first order kinetics plots. One begins by assuming that the first order law applies. Then the fraction of reactant remaining after i pulses is

$$C_i/C_o = \exp(-ki) \quad (7)$$

and the fraction reacted is

$$1.0 - \exp(-k i) \quad \text{where } -k = \ln(C_i/C_o)/i.$$

For one pulse the fraction of reaction reduces to

$$1.0 - \exp[\ln(C_1/C_o)] = 1.0 - C_1/C_o. \quad (8)$$

For several pulses, but with only one measurement of C_i , the fraction reacted by one pulse is given by

$$1.0 - \exp[\ln(C_i/C_o)^{1/i}] = 1.0 - (C_i/C_o)^{1/i}. \quad (9)$$

This fraction must be corrected for the ratio of the total volume V_o to the irradiated volume G_o to obtain the reaction probability as

$$P(\emptyset) = V_o/G_o [1 - (C_i/C_o)^{1/i}]. \quad (10)$$

This expression was used for the reaction probability in this work. The most reliable way to determine the reaction probability would be to measure k from the first order plots. However, this requires a large number of experiments. Usually only one point on the plot was measured, but this point was

done in duplicate or triplicate.

The above result for the reaction probability is equivalent to a formulation that assumes a constant fraction, f , of reaction per pulse

$$C_i/C_o = (1.0 - f)^i \quad (11)$$

A plot of $\ln(C_i/C_o)$ vs i is linear with slope $\ln(1.0 - f)$.

If one measures C_i/C_o after i pulses, then f can be calculated as follows

$$\ln(C_i/C_o)^{1/i} = \ln(1.0 - f)$$

Taking the exponential on both sides gives

$$f = 1.0 - (C_i/C_o)^{1/i},$$

which is the same result as equation (9).

Lyman et al.¹³, proposed an analytical form for the reaction probability as a function of fluence that has a power dependence on fluence at low fluence and that approaches unity at high fluence:

$$P(\phi) = 1.0 - \exp[-(\phi/\phi_r)^n] \quad \text{or} \quad C[1.0 - \exp[-(\phi/\phi_r)^n]] \quad (12)$$

$$P(\phi) = (\phi/\phi_r)^n \quad \phi \ll \phi_r$$

$$P(\phi) = 1.0 \quad \phi \gg \phi_r$$

Where ϕ_r is a constant and is the fluence at which $P(\phi)$ is $1.0 - 1/e$ if $C = 1.0$. In their treatment, k from equation (7) becomes V/V_o , where V_o is the total volume of the cell and V is defined as "the equivalent volume of sample reacted per pulse" and is given by equation (13).

$$V = -V_o \ln(C_i/C_o)^{1/i}$$

For unfocused conditions one has:

$$V = G_O P(\emptyset) \quad (14)$$

Solving for $P(\emptyset)$ and using (13) for V results in (15):

$$P(\emptyset) = [-V_O \ln(C_i/C_O)]/G_O i \quad (15)$$

This expression for the reaction probability was not useful for the data obtained at high fluence, because it gives probabilities greater than one. Both (10) and (15) however, become equal at low fluence. This is seen by first changing (15) to

$$P(\emptyset) = [-V_O/G_O] \ln [1 + ((C_i/C_O)^{1/i} - 1)]$$

and employing the series expansion

$$\ln [1+x] = x - x^2/2 + x^3/3 - x^4/4 + \dots$$

which results in (16).

$$P(\emptyset) = [-V_O/G_O] [((C_i/C_O)^{1/i} - 1) - ((C_i/C_O)^{1/i} - 1)^2/2 + \dots] \quad (16)$$

This expression, with only the first term taken into account, is valid for $(C_i/C_O)^{1/i}$ values close to unity.

C. Energy Absorption Measurement

To calculate \bar{n} (average number of photons absorbed per molecule in the irradiated volume, G_O) one needs to know how much energy is absorbed in the sample per pulse and how many molecules occupy the irradiated volume. From (3), the Beer's law relation,

$$F_T = \emptyset/\emptyset_O = \exp [-\sigma_L D X]$$

and the energy absorbed is

$$(\emptyset_O - \emptyset) A_b = \emptyset_O [1.0 - \exp[-\sigma_L D X]] A_b, \quad (17)$$

where A_b is the cross sectional area of the beam. Dividing the energy absorbed (17) by the number of molecules in G_o gives

$$\frac{\phi_o [1 - \exp(-\sigma_L DX)] A_b}{DG_o} = \frac{\phi_o [1 - \exp(-\sigma_L DX)]}{DX} \quad (18)$$

The exponential can be expanded for small absorption,

$$\frac{E_{ab}}{DG_o} = \frac{\phi_o}{DX} \left[1 - \left[1 + \frac{(-\sigma_L DX)^1}{1!} + \frac{(-\sigma_L DX)^2}{2!} + \dots \right] \right] = \phi_o \quad (19)$$

dividing (19) by the photon energy gives the mean number of photons absorbed per molecule in G_o as

$$\bar{n} = \frac{\phi_o \sigma_L}{hc\bar{\nu}} \quad (20)$$

where h is Planck's constant, c is the speed of light and $\bar{\nu}$ is the reciprocal wavelength of the laser photon. The extra terms in (19) are only important at very high pressures of sample or long path length.

Another quantity of interest is the mean number of photons absorbed per reacted molecule, \bar{n}_r . This is just \bar{n} divided by the fraction of molecules that react in G_o per pulse:

$$\bar{n}_r = \frac{\bar{n}}{P(\phi)} \quad (21)$$

To obtain the mean vibrational energy possessed by the ester molecules, it is necessary to add to the \bar{n} values the vibrational thermal energy of the molecules at the temperature of irradiation. This contribution is significant for large polyatomic molecules containing a large number of degrees of freedom (the molecules studied here range from 14 to 20 atoms), and this contribution is:

$$E_{\text{vib}}(\text{thermal}) = \sum_{i=1}^{3N-6} \frac{v_i h}{\exp(hv_i/kT) - 1} \quad (22)$$

The largest contributions come from the low frequency vibrations like torsions and structural bendings. For 300 K $E_{\text{vib}}(\text{thermal})$ will contribute an amount of energy equivalent to one or two CO_2 photons; but, equation (22) obviously depends on temperature and for higher T the mean vibrational energy contained in the molecule would increase significantly.

D. Presentation of Experimental Results

The experimental results collected in this work will be presented separately for each ester. These results are the following: Dependence of reaction probability on fluence, frequency of laser energy, laser power, parent pressure, and effect of bath gas. For the case of sec-butyl acetate and ethyl 2-bromopropionate product distributions resulting from sensitized excitation and MPIUR at different pressures and fluence are also reported. Finally the white light absorption cross sections of the esters and laser absorption cross sections at various fluences are plotted for the different frequencies used to cause MPIUR. These plots are used to calculate \bar{n} and \bar{n}_r using equations (20) and (21).

The uncertainty of the experimental results will be summarized before the data presentation. The uncertainty in the value of $P(\emptyset)$ is related to the accuracy in measuring C_i/C_o , the total volume of the cell, V_o , and the irradiated volume, G_o . The uncertainty in measuring C_i/C_o depends on the calibration of the G. C. and this uncertainty is about 10%. V_o can be accurately measured resulting in no significant contribution to the uncertainty in $P(\emptyset)$. For nonfocused conditions with a totally collimated beam, G_o is accurately given by multiplying the area of the iris times the length of the cell. Conversely, for conditions in which the beam is focused beyond the cell, there is significant uncertainty in the measurement of G_o which is approximated as a cylinder of volume equal to the length of the cell times the area of

the focused beam at the center of the cell. This area was measured directly using a planimeter to trace the burn spot in ir sensitive paper and was also calculated by geometry from the diameter of the iris, the focal length of the BaF_2 lens, and distance from the lens to the middle of the cell.

The area of the beam at the center of the cell was calculated using the focal length of the BaF_2 lens (50 cm), the radius of the unfocused beam (0.955 cm), and the distance from the lens to the center of the cell, L, which gives for the area:

$$\text{Area} = \frac{[(50-L)^2 \cos^2 \theta]}{[1-\cos^2 \theta]} \pi \quad \text{where} \quad \cos^2 \theta = \frac{(0.955)^2}{(0.955^2 + 50^2)}.$$

This formula gave areas 30% smaller at $L = 35$ cm and 13% smaller at $L = 22$ cm than those areas measured with ir sensitive paper. These numbers are a measure of the uncertainty in energy for focused conditions.

The uncertainty in the fluence depends on several factors as well as the measurement of the cross sectional area of the beam. (1) The largest factor is the uncertainty in the absolute calibration of the energy meter, which is used in all fluence measurements. (2) Another factor is the variation in the pulse to pulse energy from the CO_2 laser; but this is only about 3% as measured in our laboratory. (3) The fraction of light scattered from the front window of the cell may depend on fluence. In this work it was assumed that scattering from the windows was negligible. This is approximately true at low fluence, but it may not hold at highly focused conditions. We estimate the relative fluence measurements to be reliable to 10-20% for a given detector. The absolute fluence is probably 20-40% because of the problem with the Lumonics detector.

The uncertainty of the σ_L obtained using equation (4) was taken to be proportional to the correlation coefficients of the Beer's law plots which were around 0.98.

Also important is the absolute fluence since the variation in σ_L vs fluence was needed to calculate \bar{n} . The uncertainty in fluence was given above.

The estimates mentioned above (except for the fluence measurement) are primarily associated with random errors. These estimates also were confirmed in several instances by repeating measurements after intervals of several weeks. We are confident of our estimates, except for the absolute calibration of the energy meter (see section II.F).

E. Optimum Conditions for Studying Laser Induced Reactions.

1. Extent of Intermolecular Energy Transfer.

MPIUR of esters resulted when samples were irradiated with the CO_2 laser. The importance of vibrational energy transfer from laser excited ester molecules to nonabsorbing molecules will be investigated in this section. If the degree of vibrational energy relaxation is sufficient to induce reaction in the nonabsorbing molecule, this component will be termed a thermal component in this thesis. The presence of a significant thermal component can be ascertained by using a thermal monitoring molecule. This should be a compound with an activation energy similar to that of the ester, but one that does not itself absorb CO_2 photons when irradiated with the laser frequency used to excite the ester. Thermal effects will be significant at pressures where the collisional frequency corresponds to the laser pulse length and/or the rate of unimolecular reaction. Excited ester molecules will be deactivated by collisions with monitor molecules or excited ester molecules, but in the former case the thermal monitor molecules can gain enough energy from collisions to react and the extent of this reaction is a measure of the importance of collisions with the unexcited ester molecules. One certainly would expect that the pressure must be sufficiently low so that there are no collisions during the laser pulse in order to avoid thermal effects. The collisional frequency, w , for

two kinds of molecules (in this case excited and cold ester or quencher molecules) is

$$w = \pi d^2 \bar{u} N^* \quad (22)$$

For ethyl acetate at 0.05 torr and 298 K, d is the molecular diameter = 5.2×10^{-8} cm, \bar{u} is the average speed = $[8 k T / \pi \mu]^{1/2} = 3.78 \times 10^4$ cm/sec. and N^* is the molecular density = 1.61×10^{15} molecules/cm³. Using these values in equation (22) gives w equal to 5.18×10^5 collisions/sec. Thus, the time between collisions is 1.93 μ sec, which is a factor of 2 longer than the pulse used in this study.

Thermal effects were investigated for ethyl acetate and sec-butyl acetate using isopropyl bromide and tert-butyl chloride, respectively, as thermal monitors. The ratios of the ester rate constant¹⁵ to the thermal monitor rate constant vs temperature are shown in Table 2.

Table 2. Ratio of Rate constants vs Temperature.

<u>k_{ethyl acetate}</u>	<u>k_{sec-butyl acetate}</u>	Temperature K
<u>k_{isopropyl bromide}</u>	<u>k_{tert-butyl chloride}</u>	
0.069	0.021	300
0.080	0.063	500
0.086	0.116	800
0.088	0.141	1000
0.093	0.211	2000

Results from the thermal monitoring experiments are shown in Tables 3a, 3b and 4. Each Table shows that total pressure has a strong effect on the amount of thermal component. At pressures below 0.1 torr the thermal effect is negligible. In Tables 3a and 4 the propene came only from reaction of isopropyl bromide while ethene resulted from both laser and thermal induced reaction of ethyl acetate.

Table 3a. Irradiation of 40% Isopropyl Bromide and 60% EthylAcetate Mixture with P(20) at $\phi = 9 \text{ J/cm}^2$.

Total Pressure (torr)	[Propene]/[Ethene]
0.35	1.26
0.20	0.99
0.10	0.24
0.05	0.08
0.04	0.00

Table 3b. Irradiation of 50% tert-Butyl Chloride and 50% sec-Butyl Acetate Mixture with P(38).

$\phi = 4 \text{ J/cm}^2$		$\phi = 7 \text{ J/cm}^2$	
P _{total} (torr)	Q	P _{total} (torr)	Q
1.0	0.94	1.0	0.83
0.7	0.73	0.7	0.57
0.4	0.21	0.4	0.26
0.2	0.12	0.2	0.06
0.1	0.00	0.15	0.04

$Q = [\text{Isobutene}]/[\text{1-Butene}] + [\text{trans-2-Butene}] + [\text{cis-2-Butene}]$.
 w for sec-Butyl acetate at 0.1 torr and 298 K is 1.64×10^6 collisions/second; thus the time between collisions is 0.61 μsec .

In Table 3b the isobutene comes only from reaction of the thermal monitor (tert-butyl chloride); whereas, the 1-butene, trans-2-butene and cis-2-butene arise from both laser and thermal induced reaction of sec-butyl acetate. Thermal effects were investigated at 4 and 7 J/cm² and the results show no strong dependence of thermal effects upon fluence for pressures below 0.1 torr. As expected, the thermal contribution is very dependent upon pressure (for constant fluence). Prior work by Danen, Munslow and Setser¹⁶ using a 3:1 ethyl acetate to isopropyl bromide mixture at pressures ranging from 5 to 20 torr demonstrated a decrease of the thermal contribution at higher fluence for constant pressure.

The increase of thermal component with increasing pressure is due to the increase in frequency of collisions; thus, the thermal monitor molecules are heated more quickly. The rate of bulk cooling probably is reduced by higher pressure.

It was later realized that in order to better test the amount of heating, the thermal monitor should only be a small fraction of the mixture to avoid changing the heat capacity of the irradiated volume. For this purpose a 3% isopropyl bromide, 97% ethyl acetate mixture was prepared. For this mixture the fraction of thermal monitor is small enough so that the added monitor molecules can not affect the kinetic and thermodynamic properties of the mixture relative to the pure ester samples. For Table 4 reaction probabilities, rather than yield ratios were calculated. In Tables 3a and 3b the absolute yields were not measured so $P(\emptyset)$ could not be calculated. Experiments showed that the $P(\emptyset)$ of isopropyl bromide was much smaller compared to the $P(\emptyset)$ of ethyl acetate. The results from mixtures containing large (40%) and small (3%) amounts of thermal monitor were equivalent in the sense that they demonstrated that negligible heating occurs at pressures below 0.05 torr. The magnitude of the thermal component was dependent on pressure of mixture, area of the beam and fluence as seen from Table 4.

Table 4. Irradiation of 3% Isopropyl Bromide and 97% Ethyl Acetate Mixture for Various Conditions.

P (torr)	$A_O \text{ cm}^2$	$V_O \text{ cm}^3$	d cm	$\emptyset \text{ J/cm}^2$	$P(\emptyset)_{IB}$	$P(\emptyset)_{IB}/P(\emptyset)_{EA}$
0.05	0.44	170.8	0.75	1.35	0.00008	0.0026
0.05	0.44	170.8	0.75	2.49	0.0011	0.0065
0.20	0.44	170.8	0.75	2.49	0.056	0.29
0.05	2.86	170.8	1.91	1.35	0.0021	0.072
0.05	0.72	170.8	0.96	3.31	0.0.01	0.038
0.05	0.70	13.4	0.15	4.95	0.03	0.044
0.05	0.70	13.4	0.15	3.46	0.008	0.014

Cell with $V_O = 170.8 \text{ cm}^3$ was 35.7 cm long and the one with $V_O = 13.4 \text{ cm}^3$ was 0.95 cm long. $P(\emptyset)_{IB}$ and $P(\emptyset)_{EA}$ refer to the reaction probability of isopropyl bromide and of ethyl acetate, respectively. The different A_O (and d) were obtained by using various iris sizes in front of the laser beam.

The most complicated effect is that of geometry. In our experiments only circular beams were used, so the irradiated volume has cylindrical shape. As seen in Table 6, the yield of ethyl acetate was not affected significantly unless very small diameter beams are used. The yield of the thermal monitor, however, changed orders of magnitude when the area of the beam was changed by less than a factor of 10. Further work is necessary in order to understand all factors affecting the yield of sample and thermal monitor when the beam diameter is varied.

2. Dependence of $P(\phi)$ on Parent Pressure.

From the previous section it was concluded that "thermal effects" were not significant below 0.05 torr for ethyl or sec-butyl acetate. In this section the effect of collisions on the yield for the $P(20)$ line at a given fluence measured at different pressures of ester are reported. The results are shown in Table 5 for constant geometry. For the 3 fluences investigated, no dependence of the yield on pressure was observed. Although the yield appears constant, the contribution of the thermal component was expected to be greater at $P \geq 0.1$ torr. The invariance of yield to pressure of parent molecule was an extremely important observation. One knows that collisions have occurred but there is no effect on yield.

3. Dependence of $P(\phi)$ and Thermal Effects on Geometry.

Because the reaction probability was measured at several different geometries, the effect of the size of the diameter of the laser beam on the yield for a given fluence and pressure, was investigated. It is seen in Table 6 that for ethyl acetate at 0.05 torr, the effect of varying the cross sectional area of the beam, A_0 , at $\phi = 1.35 \text{ J/cm}^2$ from 2.86 to 0.44 cm^2 produced the same yield, but reducing A_0 from 0.44 to 0.15 cm^2 resulted in a decrease of the yield. For a fluence of 2.5 J/cm^2 however, no variation of the yield was observed when A_0 changed from 2.85 to 0.15 cm^2 . This may be because at high fluence the cooling effect was not as severe as with lower fluence. To observe a decrease of the yield at high ϕ it may

Table 5. $P(\emptyset)_{EA}$ Dependence on Pressure for a 3% Isopropyl Bromide, 97% Ethyl Acetate Mixture.

P (torr)	\emptyset J/cm ²	$P(\emptyset)_{EA}$
0.1	2.49	0.19
0.01	2.49	0.17
0.00	2.49	0.18
0.1	1.35	0.07
0.01	1.35	0.08
0.004	1.35	0.07
0.1	1.00	0.02
0.01	1.00	0.04
0.004	1.00	0.03

Table 6. $P(\emptyset)$ Dependence on Geometry for a 3% Isopropyl Bromide, 97% Ethyl Acetate Mixture.

P (torr)	A_o cm ²	d cm	\emptyset J/cm ²	$P(\emptyset)_{EA}$
0.05	0.15	0.22	1.35	0.018
0.05	0.15	0.22	1.35	0.016
0.05	0.44	0.37	1.35	0.031
0.05	2.85	0.95	1.35	0.029
0.05	0.15	0.22	2.49	0.15
0.05	0.44	0.37	2.49	0.17
0.05	0.72	0.48	2.49	0.14
0.05	2.86	0.95	2.49	0.18

For Tables 5 and 6 cell was 35.7 cm long with $V_o = 170.8$ cm³. Focusing was obtained with a telescope arrangement. Different A_o were obtained by varying the size of the iris or by collimating the beam with the telescope.

be necessary to decrease the size of d even further than 0.15 cm^2 .

4. Effect of Quencher Bath Gas in the MPIUR of Ethyl Acetate.

Valuable information about the effects of collisions can be obtained from the extent of collisional deactivation of excited ester molecules with added bath gas molecules. As will be explained in the discussion, there have been reports of enhancement of the yield by addition of small amounts of rare gas to the absorbing species in some cases, as well as, quenching of the reaction at any amount of added bath gas. Therefore some studies were done with helium, nitrogen and isopropyl bromide added to ethyl acetate at various fluences.

a. Helium as Bath Gas

Helium was added to 0.02 torr of ethyl acetate (except at $\phi = 10 \text{ J/cm}^2$ where the ethyl acetate pressure was 0.04 torr) and the yield was plotted vs pressure using Stern-Volmer type plots, (see Fig. 8), from which the half quenching pressure was readily obtained. Three different fluences were used: high fluence where saturation occurs, moderate fluence at which the log probability vs log fluence plot was linear, and low fluence near the threshold for reaction, (see Fig. 11). Table 7 contains the data for the Stern-Volmer plots of ethyl acetate with added He and the half quenching pressure for the three fluences. The two different pressure scales for the high fluence results in Fig. 8 should be noted.

As the plots clearly indicate, the addition of He greatly affected the yield, with quenching strongly dependent upon fluence. This was consistent with the formation of lower energy molecules at the lower fluences. The nonlinearity of the quenching curves was expected because the pumping, as well as the collisional quenching, are multistep processes. The extreme quenching, even by He, contrasted with the independence of Y_0 (yield of neat sample) on acetate pressure.

Table 7. Stern-Volmer plots for Ethyl Acetate using He as bath gas.

$\phi = 0.8 \text{ J/cm}^2$				$\phi = 1.8 \text{ J/cm}^2$				$\phi = 10 \text{ J/cm}^2$			
$P_{\text{ester}} = 0.02 \text{ torr}$				$P_{\text{ester}} = 0.02 \text{ torr}$				$P_{\text{ester}} = 0.04 \text{ torr}$			
He (torr)	C_i/C_o	Y_o/Y		He (torr)	C_i/C_o	Y_o/Y		He (torr)	C_i/C_o	Y_o/Y	
0.00	0.937	1.0		0.00	0.719	1.0		0.00	0.291	1.0	
0.09	0.985	4.2		0.03	0.788	1.3		0.04	0.274	0.9	
0.13	0.987	4.8		0.07	0.828	1.6		0.05	0.305	1.0	
0.17	0.990	6.3		0.14	0.861	2.0		0.09	0.265	0.9	
0.23	0.993	9.0		0.20	0.909	3.1		0.23	0.287	1.0	
0.29	0.995	13.4		0.34	0.945	5.2		0.53	0.303	1.0	
				0.89	0.990	27.6		1.79	0.448	1.3	
								3.38	0.528	1.5	
								4.81	0.698	2.3	
								5.87	0.784	3.3	
								8.73	0.923	9.2	
$P_{1/2} = 0.04 \text{ torr}$				$P_{1/2} = 0.14 \text{ torr}$				$P_{1/2} = 4.2 \text{ torr}$			

All irradiations were with the P(20) line (long pulse); Y_o is the yield in absence of He. For $\phi = 0.8 \text{ J/cm}^2$ the cell was 20 cm long with $V_o = 152.5 \text{ cm}^3$ and 80 pulses were used. For $\phi = 1.8 \text{ J/cm}^2$, the same cell as above was used and 6 pulses were employed. For $\phi = 10 \text{ J/cm}^2$, a 3 cm long cell with $V_o = 16.0 \text{ cm}^3$ was placed 26 cm from a 50 cm focal length BaF_2 lens and pulsed 12 times. The half quenching pressures, $P_{1/2}$, were obtained from the plots in each case.

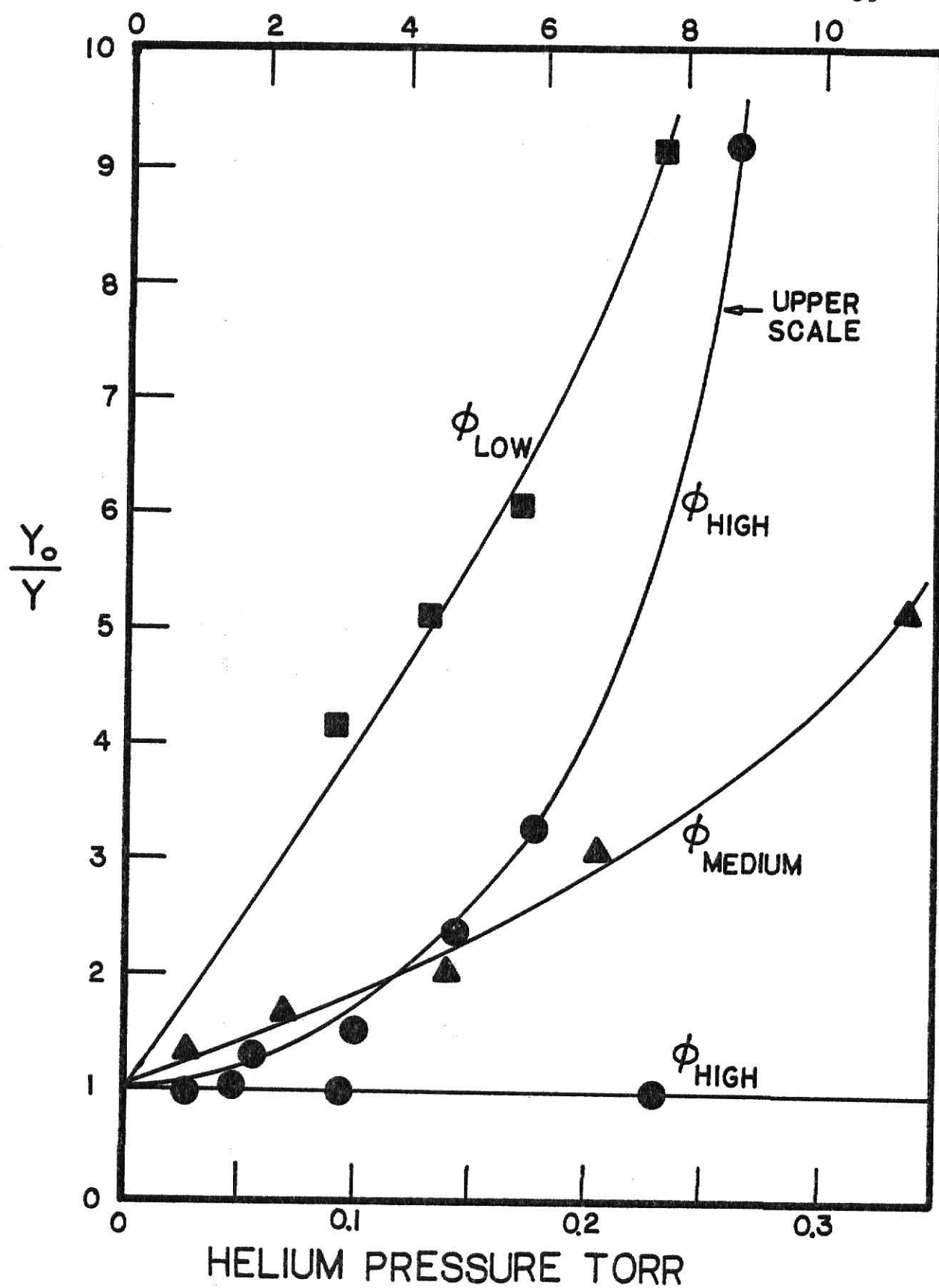


Fig. 8. Stern-Volmer Plots for He Added to Ethyl Acetate.

b. Nitrogen as Bath Gas.

Nitrogen was used as a bath gas with ethyl acetate in order to compare the degree of quenching with that of He. Being a diatomic, N_2 was able to acquire rotational and vibrational, as well as translational energy, from collisions with the excited ethyl acetate molecules. However, for similar fluence, N_2 was comparable to He in inhibiting reaction. Data for the Stern-Volmer plot of N_2 , the reaction probability and the half quenching pressure are shown in Table 8 and plotted in Fig. 9, together with the quenching plots of isopropyl bromide.

c. Isopropyl Bromide as Bath Gas.

This compound was used to investigate the quenching of ethyl acetate by a moderately large molecule. The added information regarding thermal enhancement resulting in the formation of propene from isopropyl bromide was also acquired. Because of its molecular complexity, isopropyl bromide was expected to quench the reaction of ethyl acetate significantly more than N_2 or He as was concluded from analysis of the data. Tables 9 and 10 contain the data for the Stern-Volmer plots at 2.0 and 3.6 J/cm², respectively together with the approximate half quenching pressures, the propene to ethene ratio and the reaction probability. The quenching curves are shown in Fig. 9. Note the two different pressure scales. At least for low fluence when only a small fraction of ethyl acetate molecules was above the threshold energy, the deactivation by collisions with another ethyl acetate and isopropyl bromide molecules were expected to be similar.

From the quenching experiments it was concluded that no thermal enhancement of the reaction of ethyl acetate was possible at any pressure of added bath gas under the range of fluence investigated. On the contrary, significant quenching resulted with even a small amount of bath gas present, especially at low fluence.

Table 8. Stern-Volmer plot for Ethyl Acetate using N_2 as Bath Gas.

N_2 torr	C_i/C_o	Y_o/Y	$P(\phi)$
0.00	0.568	1.0	0.15
0.01	0.607	1.1	0.13
0.03	0.660	1.3	0.11
0.06	0.674	1.4	0.10
0.10	0.730	1.6	0.08
0.14	0.803	2.2	0.06
0.19	0.874	3.4	0.04
$P_{1/2} = 0.12$ torr			

Pressure of ethyl acetate was 0.02 torr; fluence at $P(20)$ was 1.54 J/cm^2 , 10 pulses were used for all experiments. The reaction probability was calculated using equation (10) with $V_o/G_o = 2.66$.

Table 9. Stern-Volmer plot for Ethyl Acetate using Isopropyl Bromide as bath gas.

Br (torr)	C_i/C_o	Y_o/Y	$P(\emptyset)$	[Propene]/[Ethene]
0.00	0.480	1.0	0.19	0.00
0.03	0.694	1.7	0.10	0.0005
0.04	0.742	2.0	0.08	0.05
0.10	0.873	4.1	0.04	0.13
0.11	0.886	4.6	0.03	0.25
0.18	0.943	9.1	0.02	0.78
0.23	0.961	13.5	0.01	1.37
0.27	0.968	16.4	0.009	1.32
0.29	0.987	40.7	0.003	1.65
0.47	0.996	120.7	0.001	0.06

$$P_{1/2} = 0.04 \text{ torr}$$

Pressure of ethyl acetate was 0.02 torr; cell length 20 cm with $V_o/G_o = 2.66$; fluence of the P(20) line was 2.0 J/cm^2 , 10 pulses were used in all experiments.

Table 10. Stern-Volmer plot for Ethyl Acetate using Isopropyl Bromide as bath gas.

Br (torr)	C_i/C_o	Y_o/Y	$P(\emptyset)$	[Propene]/[Ethene]
0.00	0.817	1.0	0.78	0.00
0.06	0.821	1.0	0.76	0.03
0.18	0.871	1.4	0.53	0.05
0.61	0.910	2.0	0.36	0.18
1.20	0.957	4.3	0.17	1.10
2.10	0.979	8.7	0.08	6.29
3.14	0.989	16.7	0.04	37.35

$$P_{1/2} = 0.61 \text{ torr}$$

Same as above but $\emptyset = 3.6 \text{ J/cm}^2$ with $V_o/G_o = 77.4$.

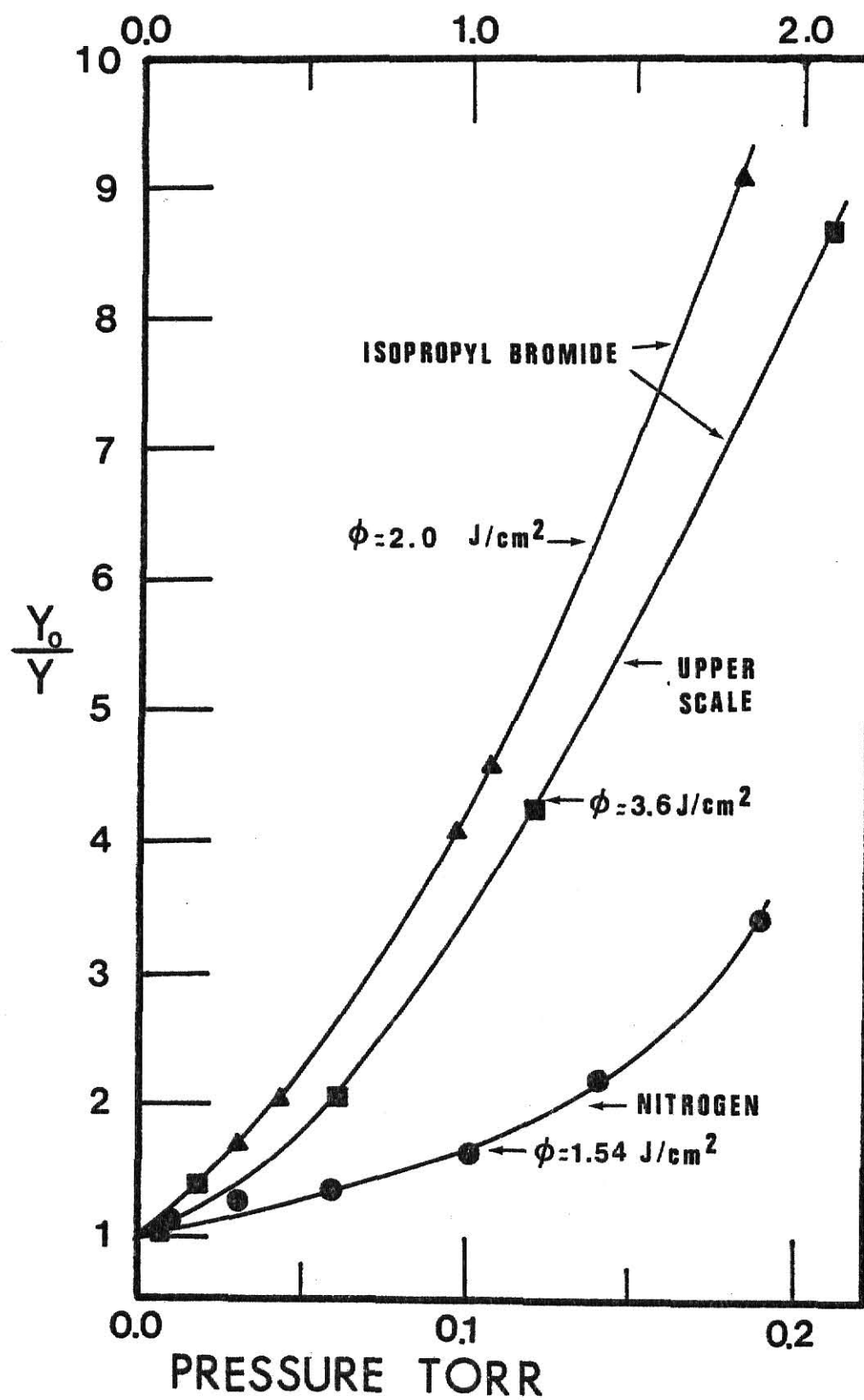


Fig. 9. Stern-Volmer Plots for N_2 and Isopropyl Bromide Added to Ethyl Acetate.

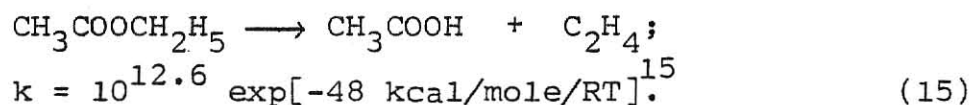
IV. EXPERIMENTAL DATA

A. Ethyl Acetate.

1. Reaction Probability Dependence on Fluence.

The results from the last section indicated that, in order to avoid effects of intermolecular energy transfer in the MPIUR of ethyl acetate, very low pressures (<0.05 torr) must be used. Because of experimental limitations to the measurement of small extent of reaction for analysis of low pressure samples, pressures from 0.02 to 0.1 torr were employed in this work.

Ethyl acetate is the simplest member of the acetate series that gives the characteristic unimolecular elimination reaction:



This reaction was investigated the most thoroughly. All experiments for ethyl acetate were done at 0.05 torr pressure (except where indicated otherwise) in a variety of constant fluence type irradiation cells. In the case of focused conditions, short cells and a 50 cm focal length BaF₂ lens were used to minimize the fluence gradient inside the cells.

The absorption spectrum of ethyl acetate and some of the laser lines used are shown in Fig. 10. The yields from irradiation at a given fluence and the derived reaction probability are shown in Tables 11 through 16 for five different laser lines. The $\log P(\phi)$ vs $\log \phi$ plots are shown in Fig. 11.

From the experimental results plotted in Fig. 11, the following conclusions were reached: (i) There is slight if any, variation in the $\log P(\phi)$ vs $\log \phi$ plots with laser frequency. This conclusion certainly must be true within the limitations of the ϕ measurement. (ii) At high enough fluence ($> 9 \text{ J/cm}^2$) ethyl acetate shows saturation meaning

that the reaction probability approaches a constant value.⁴⁵
In the case of ethyl acetate irradiated at 1053.9 cm^{-1} with the P(12) line, this value is close to 90%. (iii) At intermediate fluence corresponding to $P(\phi)$ values of 10^{-2} to 10^{-4} , a linear behavior of $\log P(\phi)$ vs $\log \phi$ that follows equation (12) for $\phi < \phi_r$, is observed. (iv) There is no power dependence of $P(\phi)$ for $P(\phi) \leq 10\%$, although at higher $P(\phi)$, higher power may produce more reaction as compared to low power of the same ϕ .

After the main experimental work was completed and the new fluence scale established, we made some checks to ascertain whether or not the adjusted ϕ values were correct. The new studies were done with P(20). These results are shown in bottom of Table 14. The new results are in very close agreement with the older data. Thus we believe that the new fluence scale is satisfactory except possibly for P(38).

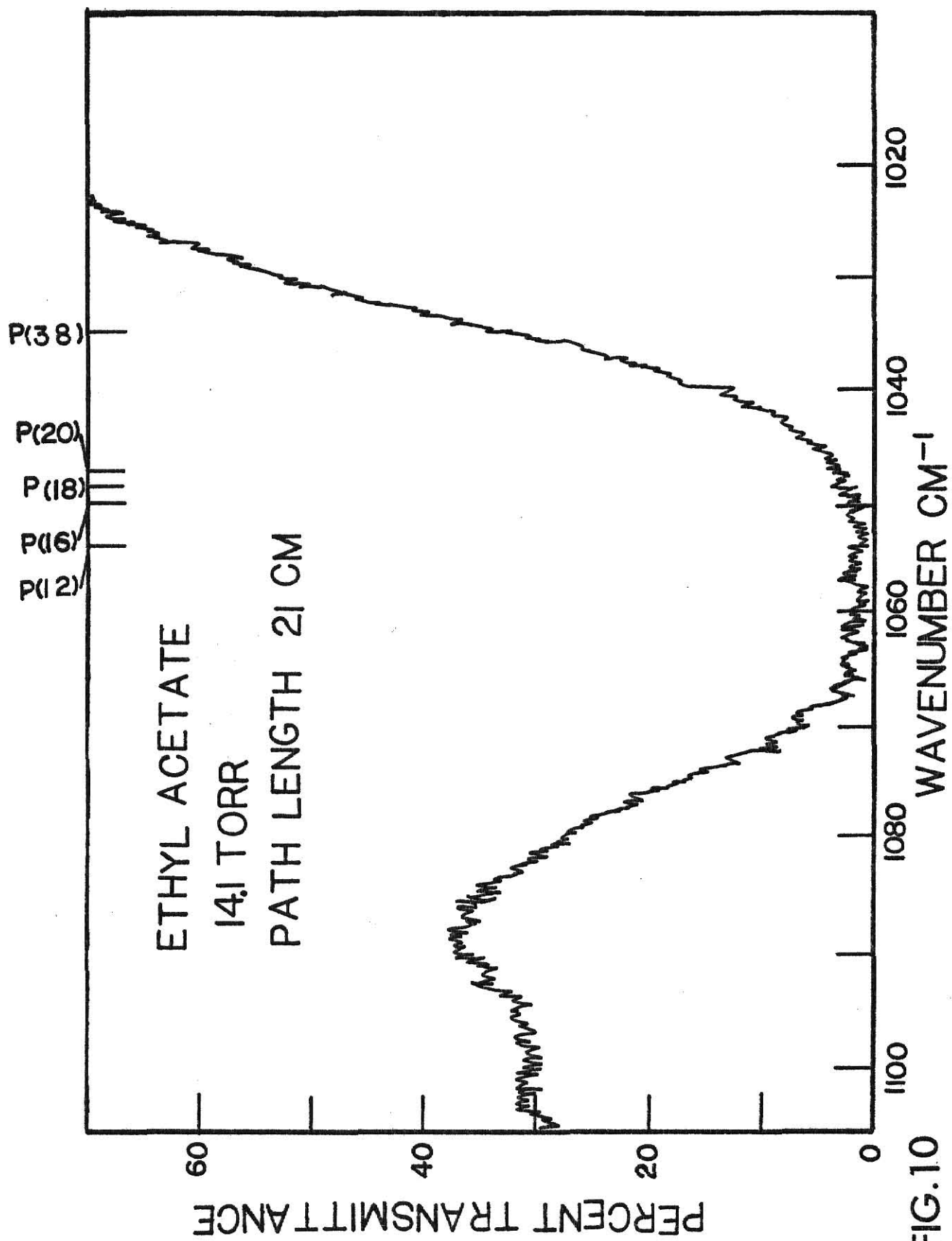


FIG.10

Table 11. Ethyl Acetate Irradiated with P(12), 1053.9 cm^{-1} .

i	C_i/C_o	$\phi \text{ J/cm}^2$	P(ϕ)
5	0.770	2.51	0.095
5	0.821	2.31	0.072
5	0.936	1.63	0.024
5	0.983	1.04	0.006
8	0.997	0.82	0.0007
30	0.995	0.76	0.0003
<hr/>			
5	0.983	1.81	0.028
5	0.957	2.60	0.071
5	0.874	3.05	0.21
5	0.851	3.35	0.26
5	0.675	4.27	0.61
5	0.640	6.72	0.69
5	0.562	7.51	0.88
5	0.563	9.32	0.88
5	0.588	9.71	0.82
5	0.592	9.92	0.81

Pressure of ethyl acetate = 0.05 torr; cell length = 3 cm;
 $V_o = 16.0 \text{ cm}^3$, G_o for focused and unfocused conditions were
 1.98 and 8.59 cm^3 , respectively. Fluence values for lower part
 of table were obtained using a BaF_2 lens, focal length 50 cm,
 the cell was placed at 26 cm from the lens and the area of
 the beam was measured with ir sensitive paper.

Table 12. Ethyl Acetate Irradiated with P(16), 1050.44 cm^{-1} .

i	C_i/C_o	$\phi \text{ J/cm}^2$	$P(\phi)$
30	0.512	1.50	0.055
70	0.604	1.11	0.018
80	0.877	0.84	0.0041
200	0.761	0.76	0.0034
220	0.795	0.72	0.0026
260	0.907	0.63	0.0009

Pressure of Ethyl Acetate = 0.05 torr; cell length = 26 cm;
 $V_o = 186 \text{ cm}^3$; $G_o = 74.5 \text{ cm}^3$ unfocused conditions.

Table 13. Ethyl Acetate Irradiated with P(18), 1048.66 cm^{-1} .

i	C_i/C_o	$\phi \text{ J/cm}^2$	$P(\phi)$
50	0.611	1.26	0.025
50	0.640	1.10	0.022
50	0.711	1.06	0.017
50	0.774	0.87	0.013
50	0.900	0.80	0.005
50	0.926	0.68	0.001

Same conditions as in Table 12.

Table 14. Ethyl Acetate Irradiated with P(20), 1046.85 cm^{-1} long pulse.

i	C_i/C_o	$\phi \text{ J/cm}^2$	$P(\phi)$
5	0.759	1.84	0.143
5	0.802	1.75	0.115
5	0.831	1.65	0.097
5	0.940	1.14	0.033
5	0.969	1.06	0.017
5	0.989	0.82	0.006
6	0.994	0.82	0.003
*100	0.996	0.32	0.0001

Pressure of ethyl acetate = 0.05 torr; cell length = 20 cm;
 $V_o = 152.5 \text{ cm}^3$; $G_o = 57.3 \text{ cm}^3$. Unfocused conditions were used.
 * cell was 35.7 cm long, $V_o = 268.3 \text{ cm}^3$, $G_o = 102.3 \text{ cm}^3$, unfocused.

i	C_i/C_o	$\phi \text{ J/cm}^2$	$P(\phi)$	$G_o \text{ cm}^3$
35	0.542	2.5	0.19	15.8
25	0.454	3.3	0.26	25.6
25	0.644	1.4	0.03	102.3
70	0.976	0.86	0.004	15.8

0.05 torr of ethyl acetate using a 35.7 cm long cell and a telescope arrangement to vary G_o .

Table 15. Ethyl Acetate Irradiated with P(20), 1046.85 cm^{-1} , Short Pulse.

i	C_i/C_o	$\phi \text{ J/cm}^2$	$P(\phi)$
6	0.892	1.52	0.33
6	0.948	1.26	0.15
15	0.954	1.01	0.055
15	0.989	0.83	0.013
30	0.994	0.66	0.0033
50	0.993	0.48	0.0023
<hr/>			
*70	0.996	0.47	0.0003
**100	0.989	0.31	0.0003

Pressure of ethyl acetate = 0.05 torr; cell length = 0.95 cm; $V_o = 13.4 \text{ cm}^3$; $G_o = 0.77 \text{ cm}^3$. For upper part of table cell was placed at 25 cm from BaF_2 lens and the area of the focused beam was measured with ir sensitive paper. * was done on the same cell as above with $G_o = 2.7 \text{ cm}^3$. ** was done with a 35.7 cm long cell with $V_o = 268.3 \text{ cm}^3$ and $G_o = 102.3 \text{ cm}^3$, unfocused conditions.

Table 16. Ethyl Acetate Irradiated with P(38), 1029.43 cm^{-1} .

i	C_i/C_o	$\phi \text{ J/cm}^2$	P(38)
10	0.829	3.67	0.39
10	0.847	3.44	0.35
10	0.850	2.94	0.34
16	0.833	2.24	0.24
16	0.919	1.47	0.11
20	0.993	0.96	0.008
<hr/>			
30	0.971	0.85	0.005
40	0.994	0.67	0.0008

Pressure of ethyl acetate = 0.05 torr; for upper part of table cell was 0.95 cm long; $V_o = 13.4 \text{ cm}^3$; $G_o = 0.63 \text{ cm}^3$. Cell was placed at 30 cm from BaF_2 lens and the area of the focused beam was measured with ir sensitive paper. Lower part of table was done unfocused with same cell and $G_o = 2.72 \text{ cm}^3$.

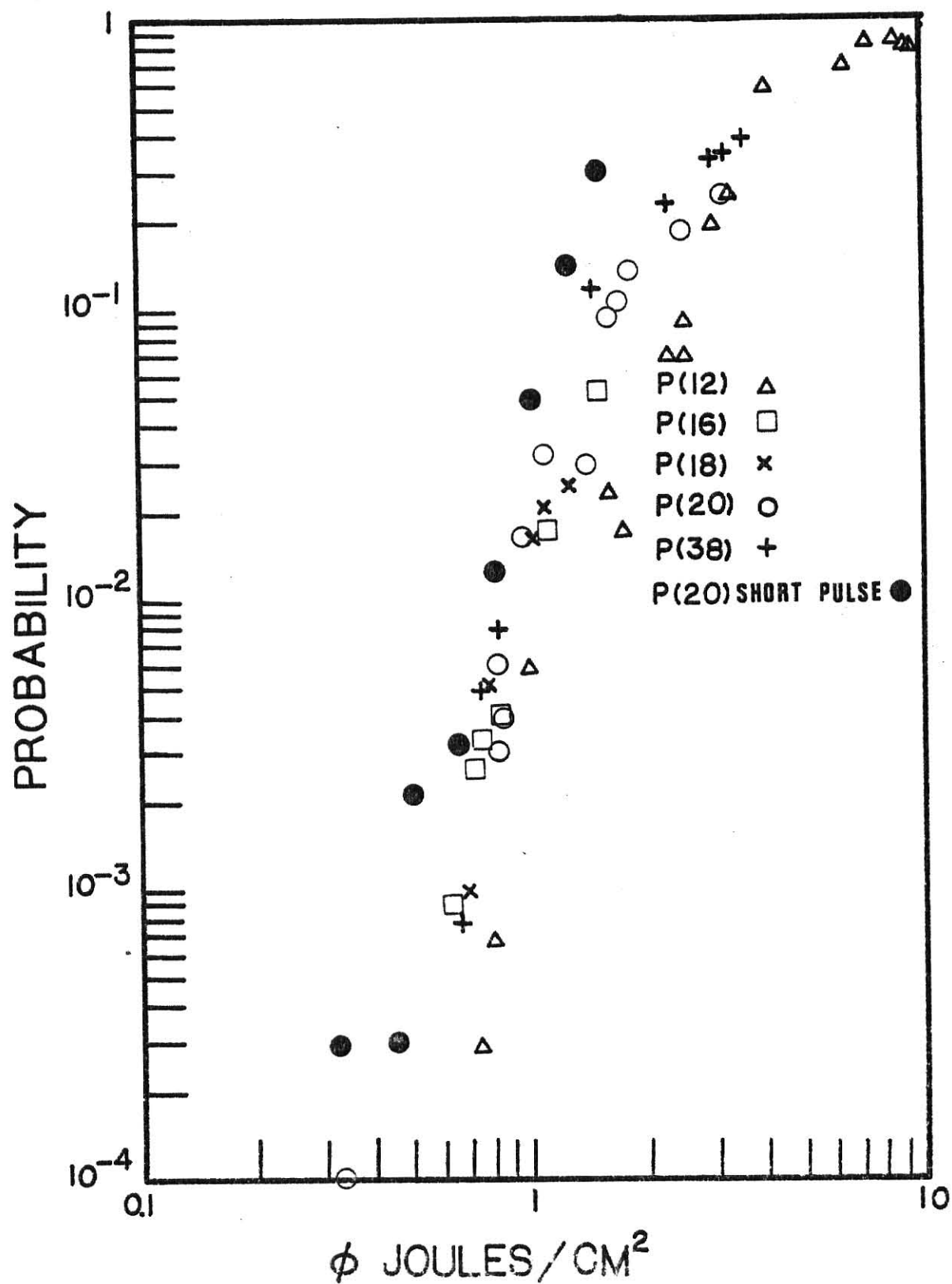


Fig. 11. Log $P(\phi)$ vs log ϕ for Ethyl Acetate.

2. Measurement of σ_L , \bar{n} and \bar{n}_r .

The absorption of the laser energy for different pressures of ethyl acetate and the other esters obeyed an equation with the same form as Beer's law in which intensities are replaced by fluences. Equation (4) was used to calculate σ_L and the results are tabulated in Tables 17 and 18 for P(20) and P(38), respectively. Fig. 12 shows the Beer's law type plots for the two lines and Fig. 13 depicts the calculated σ_L for the fluences and the frequencies used.

Measurements done by Quigley et al.¹⁷ and also by Knott and Pryor¹⁸ agreed with results obtained in this laboratory as can be verified from Table 45 where the reported σ_L values are compared with the ones obtained in this laboratory.

The slight increase in σ_L for P(38) with fluence may be explained by a red shift of the band. Looking at the ir spectrum in Fig. 10, a red shift of the vibrationally excited ethyl acetate at P(38) could raise the absorbance value resulting in a higher cross section. In the case of the decrease of σ_L with fluence at P(20) σ was already a maximum, it can only decrease by a red shift. It is worth noting that the values of σ_L presented in this work did not vary with pressure (the Beer's law-like relation for absorption of the laser radiation was obeyed up to pressures of 5 torr). With the present method for measuring σ_L it was not possible to employ focusing of the beam to enhance the fluence. Therefore, we were limited to fluences $< 3 \text{ J/cm}^2$ for absorption cross section measurements.

The σ_L vs ν plots indicate that for the esters a remarkable similarity exists between σ and σ_L for low fluence. This was unexpected because the laser output is much narrower than the band pass of the ir monochromator. The explanation of this agreement between σ and σ_L might be the very high density of rotational states for the esters. Even though the band width of the laser is less than 1 cm^{-1} , many rotational lines lie within the bandwidth of a laser line.

Data from previously described experiments can be used to obtain the \bar{n} and \bar{n}_r using (20) and (21), respectively. Note that in order to obtain the total mean vibrational energy in ethyl acetate or the other esters, the vibrational contribution to the thermal energy at 298 K must be added to the laser energy. This means an increase in \bar{n} of approximately one ir photon for ethyl acetate. The \bar{n} and \bar{n}_r for ethyl acetate at P(20) and P(38) are shown in Tables 19 and 20, respectively, together with the vibrational thermal energy.

For P(38) the \bar{n} values are very unreasonable. This is even more strongly illustrated by a plot of $P(\emptyset)$ vs $\bar{n} + 1$ ir photon (for ethyl acetate). This plot relates the yield to the absorbed energy and should be independent of laser frequency. It appears that the fluence measurement for P(38) was in error. This may be due to the fact that the \emptyset were measured using a NaCl flat instead of a Ge flat and the procedure for correcting \emptyset_{pyro} is only applicable to measurements done with a Ge flat.

Table 17 . Measurement of σ_L for Ethyl Acetate at P(20).

$\emptyset = 2.8 \text{ J/cm}^2$		$\emptyset = 1.9 \text{ J/cm}^2$		$\emptyset = 0.22 \text{ J/cm}^2$	
P (torr)	\emptyset/\emptyset_0	P (torr)	\emptyset/\emptyset_0	P (torr)	\emptyset/\emptyset_0
0.10	0.981	0.30	0.918	0.10	0.980
0.25	0.947	0.50	0.855	0.20	0.934
0.50	0.881	0.60	0.834	0.30	0.889
0.70	0.818	0.70	0.801	0.40	0.863
0.90	0.770	0.80	0.769	0.60	0.798
1.00	0.734			0.80	0.744
2.00	0.555				
$^* \sigma_L = 2.3 \pm 0.3$		$\sigma_L = 2.8 \pm 0.2$		$\sigma_L = 3.3 \pm 0.2$	

σ at 1046.85 cm^{-1} is $3.7 \times 10^{-19} \text{ cm}^2/\text{molecule}$. Cell was 35.7 cm long (except in * where cell was 40 cm long); all σ_L must be multiplied by $10^{19} \text{ cm}^2/\text{molecule}$.

Table 18 . Measurement of σ_L for Ethyl Acetate at P(38).

$\emptyset = 0.65 \text{ J/cm}^2$		$\emptyset = 0.37 \text{ J/cm}^2$		$\emptyset = 0.09 \text{ J/cm}^2$	
P (torr)	\emptyset/\emptyset_0	P (torr)	\emptyset/\emptyset_0	P (torr)	\emptyset/\emptyset_0
0.25	0.972	0.22	0.983	0.30	0.986
0.45	0.950	0.55	0.957	0.65	0.969
0.70	0.924	0.95	0.928	0.99	0.953
0.90	0.903				
$\sigma_L = 0.9 \pm 0.3$		$\sigma_L = 0.7 \pm 0.2$		$\sigma_L = 0.4 \pm 0.2$	

σ at 1029.43 cm^{-1} is $4.8 \times 10^{-20} \text{ cm}^2/\text{molecule}$. Cell was 35.7 cm long; all σ_L must be multiplied by $10^{-19} \text{ cm}^2/\text{molecule}$.

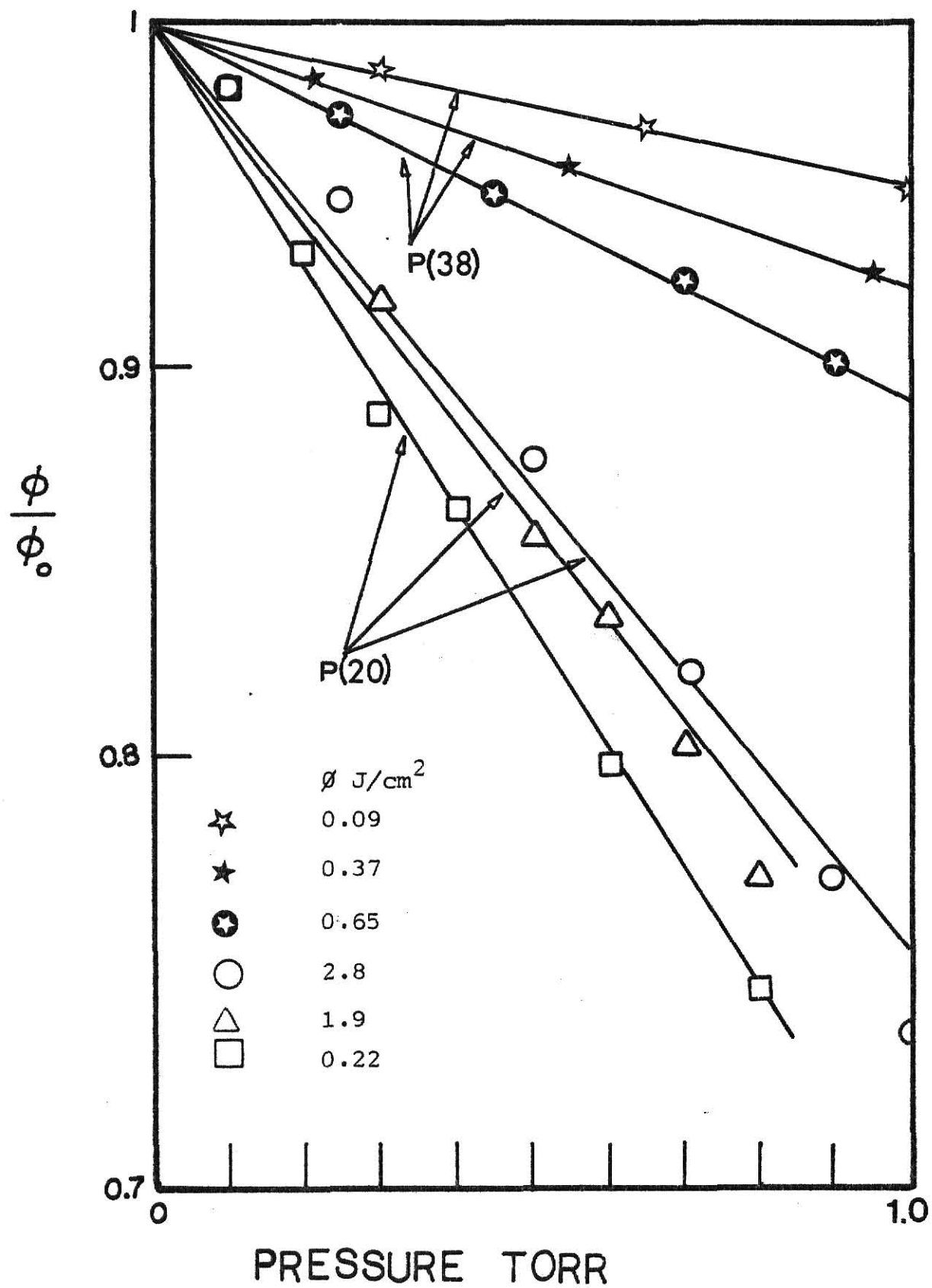


Fig. 12. Log Transmittance vs Ethyl Acetate Pressure.

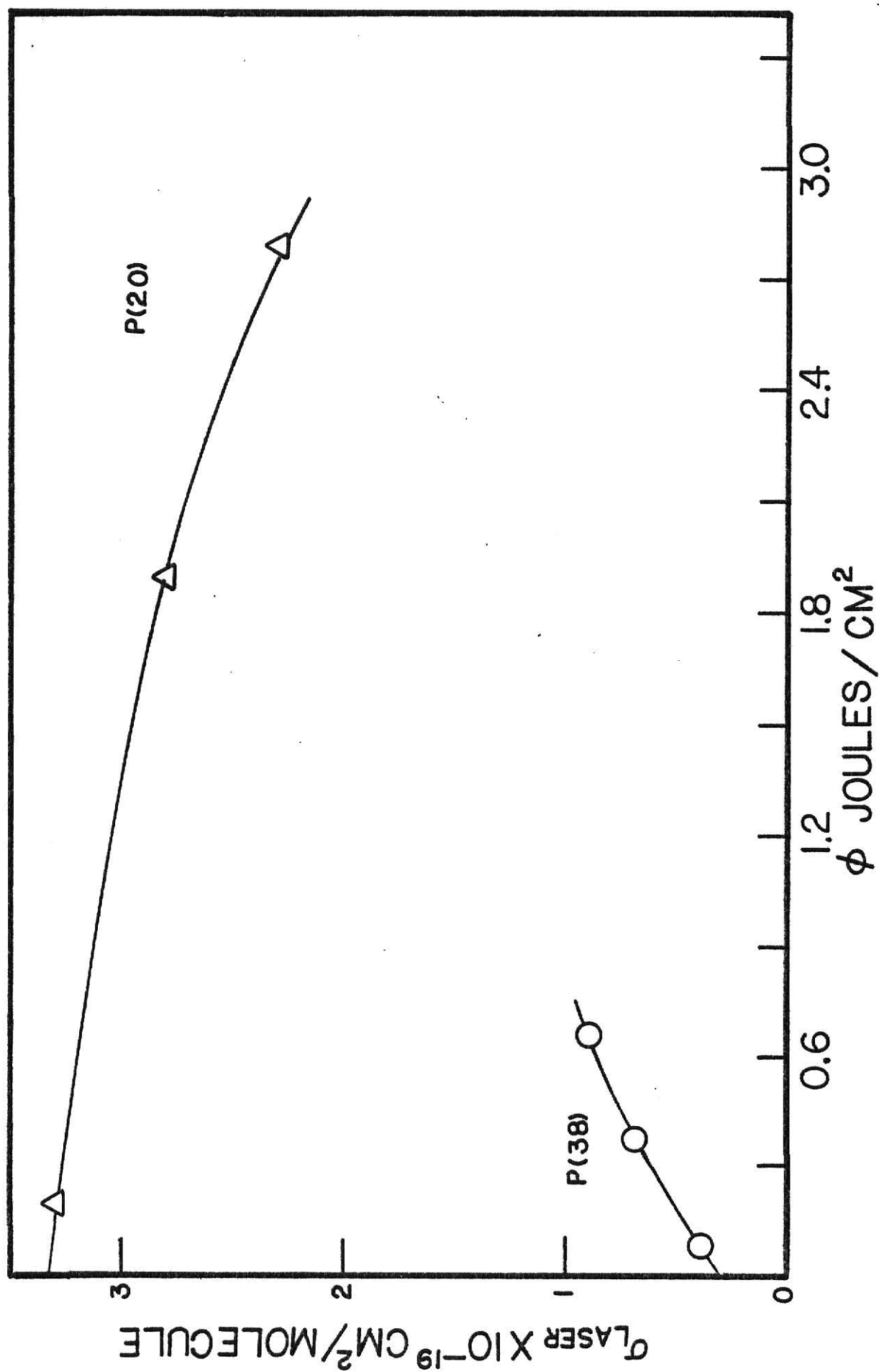


Fig. 13. σ_L vs ϕ for Ethyl Acetate.

Table 19. \bar{n} and \bar{n}_r for Ethyl Acetate Irradiated with P(20).

$\phi \text{ J/cm}^2$	σ_L	\bar{n}	$P(\phi)$	\bar{n}_r
2.80	2.2	31	0.22	141
1.84	2.8	25	0.16	156
1.75	2.8	24	0.14	171
1.65	2.9	23	0.12	190
1.14	3.0	17	0.03	560
1.06	3.1	16	0.02	790
0.82	3.1	13	0.007	1765
0.81	3.2	12	0.006	2050

Energy of a P(20) photon = 2.99 kcal/mole. σ_L must be multiplied by $10^{-19} \text{ cm}^2/\text{molecule}$. The vibrational thermal energy which must be added to \bar{n} to obtain the total energy is 3.0 kcal/mole at 298 K.

Table 20. \bar{n} and \bar{n}_r for Ethyl Acetate Irradiated at P(38).

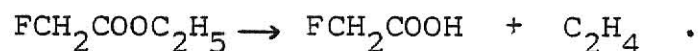
$\phi \text{ J/cm}^2$	σ_L	\bar{n}	$P(\phi)$	\bar{n}_r
1.00	1.1	5.5	0.008	688
0.74	0.9	3.3	0.003	1100
0.64	0.8	2.6	0.0007	3714

Energy of a P(38) photon = 2.93 kcal/mole. The vibrational thermal energy (3.0 kcal/mole) must be added to the \bar{n} to obtain the total energy. σ_L must be multiplied by $10^{-19} \text{ cm}^2/\text{molecule}$.

B. Ethyl Fluoroacetate.

1. Reaction Probability Dependence on Fluence.

Irradiation of this ester with the CO₂ laser induced the reaction,



$$k = 10^{12.6} \exp[-46.7 \text{ kcal mole}^{-1} / RT] .$$

This rate constant was deduced from consideration of rate constants of similar compound (see appendix). Fig. 14 shows the infrared spectrum of ethyl fluoroacetate and the lines used to induce MPIUR. The dependence of $P(\emptyset)$ on \emptyset is given in Tables 21 through 24. Irradiation of ethyl fluoroacetate at frequencies higher than 1080 cm⁻¹ was not possible for unfocused conditions due to the low energy output of the CO₂ laser beyond this frequency. The reaction probability for a given fluence varied with the frequency of the line used to induce MPIUR. This dependence was more evident in a plot of $\log P(\emptyset)$ vs \emptyset .

Saturation for ethyl fluoroacetate was observed at a fluence of approximately 8 J/cm² for R(20). This was the only line for which high fluence was obtained by focusing the laser beam. The $P(\emptyset)$ was somewhat higher for fluoroacetate than for ethyl acetate. The lower activation energy estimated for ethyl fluoroacetate might account for its higher reactivity compared to that of ethyl acetate.

The linearity of the $\log P(\emptyset)$ vs $\log \emptyset$ plots in Fig. 15 for $P(\emptyset) < 0.1$ was well described by equation (12) for low fluence with $n = 6$. This high dependence of the reaction probability on fluence was found to be characteristic of the esters investigated in this study. This n value did not show any dependence on frequency.

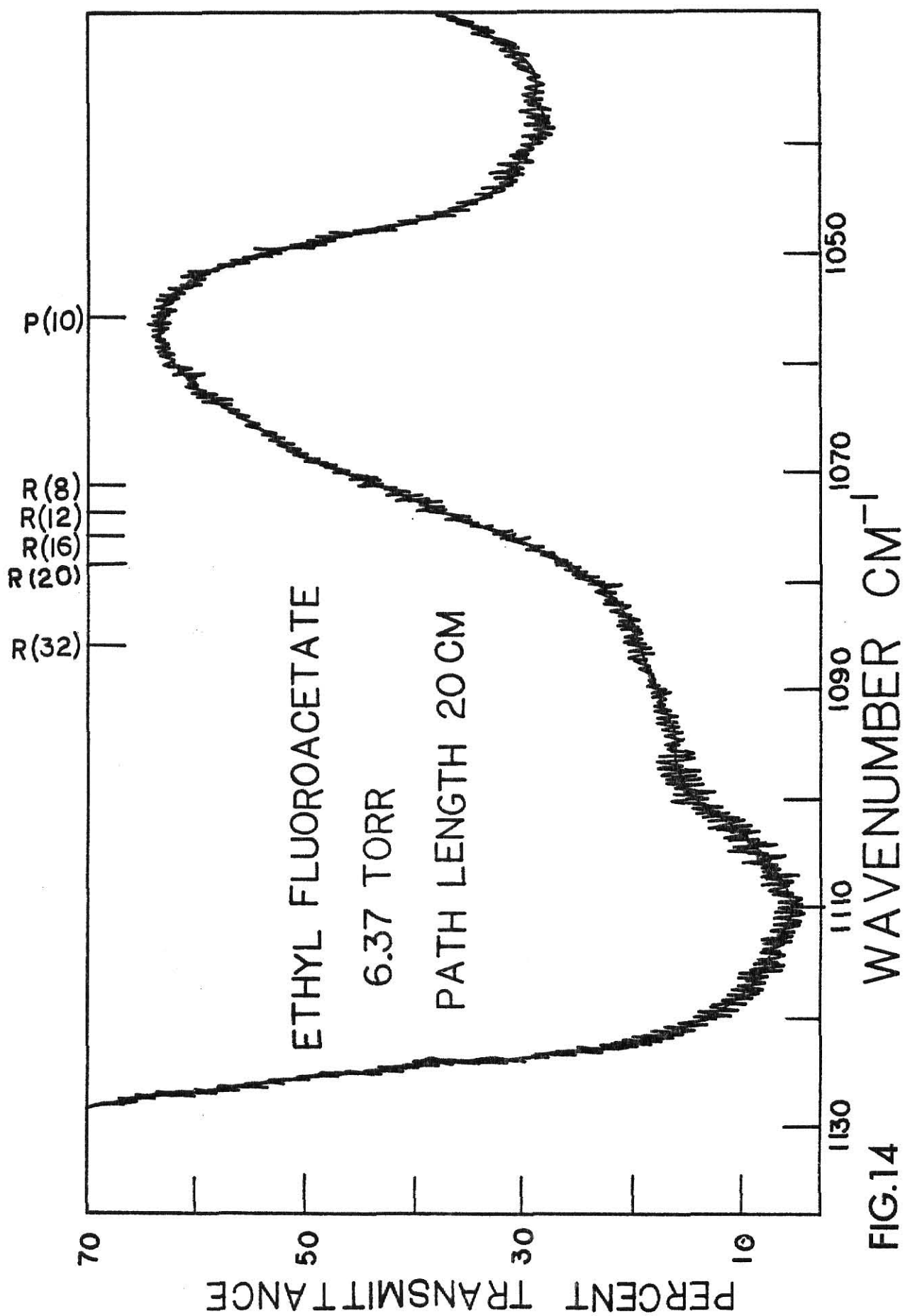


FIG.14

Table 21. Ethyl Fluoroacetate Irradiated with R(20),
 $\bar{\nu} = 1078.58 \text{ cm}^{-1}$.

i	C_i/C_o	$\phi \text{ J/cm}^2$	$P(\phi)$
4	0.892	8.5	0.70
4	0.894	8.0	0.69
4	0.890	7.0	0.71
4	0.896	6.0	0.67
4	0.906	4.0	0.61
4	0.924	2.5	0.49
6	0.901	2.3	0.43
8	0.917	1.4	0.27
12	0.975	1.0	0.05
20	0.991	0.7	0.01
<hr/>			
10	0.472	1.7	0.35
10	0.823	1.2	0.09
15	0.908	0.93	0.03
20	0.991	0.58	0.0022

Pressure of ethyl fluoroacetate = 0.05 torr; cell length = 0.95 cm; $V_o = 13.4 \text{ cm}^3$ for upper part of table where cell was placed at 29 cm from BaF_2 lens with $G_o = 0.54 \text{ cm}^3$. For lower part of table unfocused conditions were used with $G_o = 2.7 \text{ cm}^3$.

Table 22. Ethyl Fluoroacetate Irradiated with R(12),
 $\bar{\nu} = 1073.27 \text{ cm}^{-1}$.

i	C_i/C_o	$\phi \text{ J/cm}^2$	$P(\phi)$
5	0.536	1.59	0.31
5	0.599	1.50	0.26
5	0.704	1.27	0.18
5	0.877	1.10	0.07
5	0.930	0.97	0.04
5	0.969	0.82	0.017
5	0.993	0.68	0.004

Pressure of ethyl fluoroacetate = 0.07 torr; cell length = 20 cm; $V_o = 156.5 \text{ cm}^3$; $G_o = 57.3 \text{ cm}^3$, unfocused conditions.

Table 23. Ethyl Fluoroacetate Irradiated with P(10),
 $\bar{\nu} = 1055.62 \text{ cm}^{-1}$.

i	C_i/C_o	$\phi \text{ J/cm}^2$	$P(\phi)$
5	0.686	1.57	0.19
5	0.785	1.48	0.13
5	0.844	1.38	0.09
5	0.926	1.19	0.04
5	0.979	0.86	0.01
5	0.992	0.75	0.004

Same conditions as in Table 22.

Table 24 . Ethyl Fluoroacetate irradiated with R(8),
 $\bar{\nu} = 1070.46 \text{ cm}^{-1}$.

i	C_i/C_o	$\phi \text{ J/cm}^2$	$P(\phi)$
5	0.642	1.27	0.23
5	0.734	1.21	0.16
5	0.751	1.15	0.15
5	0.844	1.00	0.09
5	0.883	0.85	0.07
5	0.962	0.80	0.02
5	0.981	0.63	0.01
5	0.991	0.57	0.005
5	0.998	0.50	0.001

Pressure of ethyl fluoroacetate = 0.07 torr; cell length = 20 cm,
 $V_o = 156.5 \text{ cm}^3$, $G_o = 57.3 \text{ cm}^3$. Unfocused conditions.

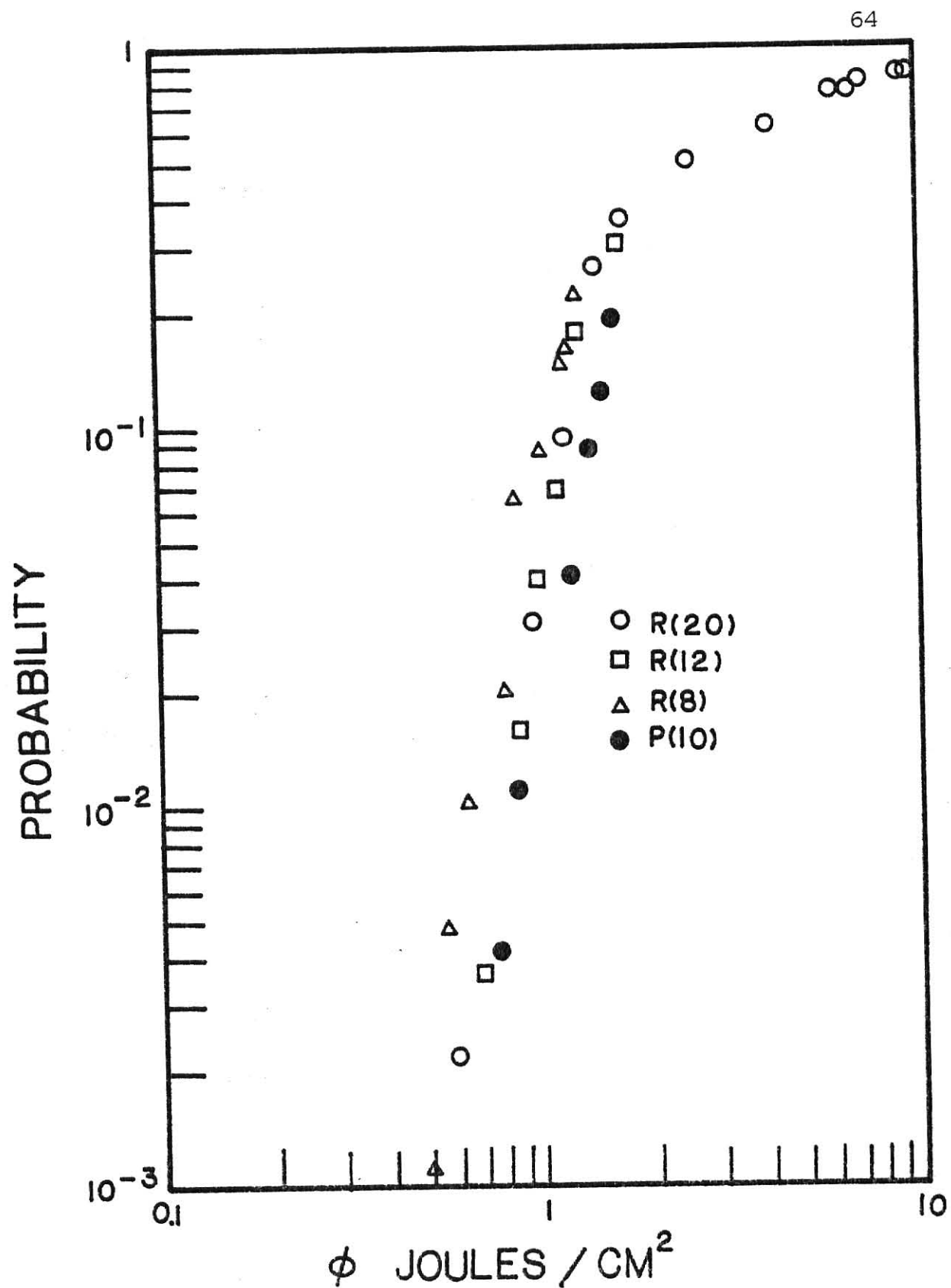


Fig. 15. Log $P(\phi)$ vs log ϕ for Ethyl Fluoroacetate.

2. Measurement of σ_L , \bar{n} and \bar{n}_r .

Equation (4) was also valid for ethyl fluoroacetate and was used to obtain σ_L for this ester. Transmittance vs pressure data at various fluences for the frequencies corresponding to R(12) and P(10) are shown in Tables 25 and 26, and are plotted in Figures 16 and 17, respectively. The white light absorption cross sections at each frequency are included at the bottom of the Tables. The σ_L obtained from Figures 16 and 17 are plotted in Figure 18. In contrast to ethyl acetate the σ_L for ethyl fluoroacetate increased with fluence. The increase in σ_L for both lines can be readily explained by a red shift of the absorbing band. According to Fig. 14, the effect should be more pronounced for P(10) than for R(12) as indeed was observed. The absorption data only go to $\sim 2.5 \text{ J/cm}^2$ because the method of measurement was not suitable for focused geometry.

Data for the calculation of \bar{n} and \bar{n}_r at R(12) and P(10) were obtained from Tables 20 and 22, and values of σ_L for a given ϕ were taken from Fig. 18. Tables 27 and 28, contain the \bar{n} and \bar{n}_r with the fluence, reaction probability and σ_L necessary to calculate them. Also given was the vibrational contribution to the thermal energy of ethyl fluoroacetate at 298 K. This thermal energy must be added to \bar{n} to obtain the mean vibrational energy of the excited ethyl fluoroacetate.

Comparison of the yield resulting from a given \bar{n} in Tables 27 and 28 indicates a difference of approximately 2. This is attributed to a combination of experimental error

in the measurement of ϕ (which is further amplified by the shift to the new scale) and uncertainty in the values of σ_L .

Table 25. Laser Absorption Cross Section of Ethyl Fluoroacetate at R(12), $\bar{\nu}=1073.27 \text{ cm}^{-1}$.

$\phi = 2.25 \text{ J/cm}^2$		$\phi = 1.20 \text{ J/cm}^2$		$\phi = 0.17 \text{ J/cm}^2$		$\phi = 0.01 \text{ J/cm}^2$	
P (torr)	ϕ/ϕ_0	P (torr)	ϕ/ϕ_0	P (torr)	ϕ/ϕ_0	P (torr)	ϕ/ϕ_0
0.10	0.974	0.15	0.946	0.06	0.977	0.10	0.957
0.20	0.934	0.25	0.929	0.35	0.900	0.20	0.940
0.30	0.925	0.45	0.870	0.45	0.865	0.30	0.909
0.39	0.895	0.55	0.830	0.60	0.847	0.40	0.887
0.50	0.846	0.75	0.779	0.65	0.815	0.60	0.850
0.70	0.797			0.85	0.783	0.70	0.832
0.80	0.767			1.00	0.745	0.80	0.800
1.00	0.721					1.00	0.763
$\sigma_L = 2.9 \pm 0.3$		$\sigma_L = 2.9 \pm 0.2$		$\sigma_L = 2.5 \pm 0.2$		$\sigma_L = 2.3 \pm 0.2$	

Path length 35.7 cm; σ_L must be multiplied by $10^{-19} \text{ cm}^2/\text{molecule}$.
 White light absorption cross section at 1073.27 cm^{-1} is $2.27 \times 10^{-19} \text{ cm}^2/\text{molecule}$.

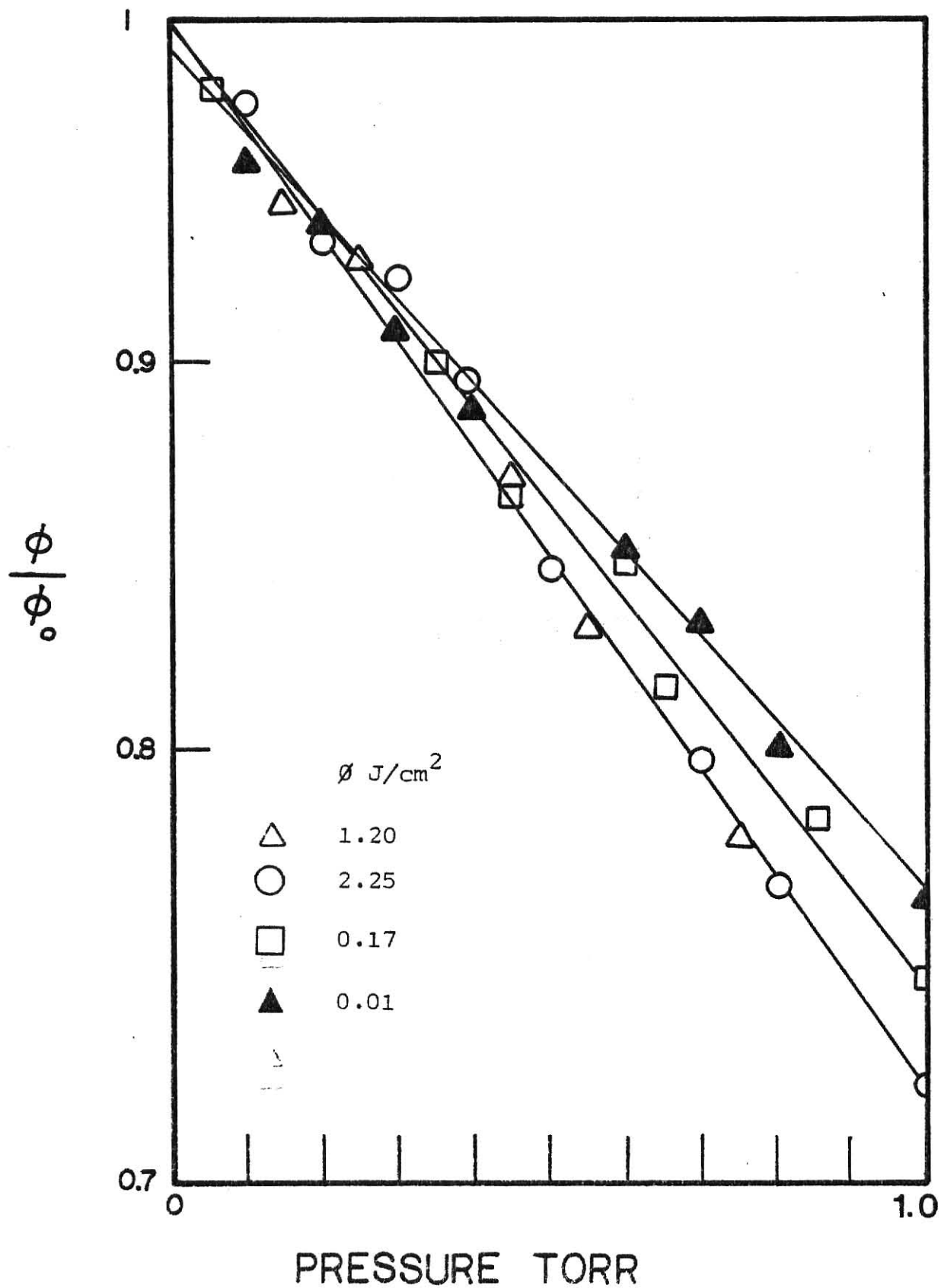


Fig. 16. Log Transmittance vs Ethyl Fluoroacetate Pressure at R(12).

Table 26. Laser Absorption Cross Section of Ethyl Fluoroacetate at P(10), $\bar{\nu}=1055.62 \text{ cm}^{-1}$.

$\sigma = 1.96 \text{ J/cm}^2$		$\sigma = 0.98 \text{ J/cm}^2$		$\sigma = 0.16 \text{ J/cm}^2$		$\sigma = 0.07 \text{ J/cm}^2$	
P (torr)	σ/σ_0	P (torr)	σ/σ_0	P (torr)	σ/σ_0	P (torr)	σ/σ_0
0.10	0.977	0.15	0.958	0.20	0.973	0.15	0.989
0.20	0.957	0.35	0.929	0.40	0.945	0.25	0.973
0.30	0.919	0.55	0.883	0.60	0.920	0.35	0.965
0.50	0.868	0.75	0.843	0.80	0.900	0.45	0.951
0.70	0.828	0.95	0.810	1.00	0.877	0.55	0.932
1.00	0.757					0.60	0.934
						0.75	0.915
						0.85	0.908
						1.00	0.897
						4.66	0.584
$\sigma_L = 2.4 \pm 0.3$		$\sigma_L = 1.9 \pm 0.2$		$\sigma_L = 1.1 \pm 0.2$		$\sigma_L = 1.0 \pm 0.2$	

Path length 35.7 cm; σ_L must be multiplied by $10^{-19} \text{ cm}^2/\text{molecule}$.
 White light absorption cross section at 1055.62 cm^{-1} is $0.95 \times 10^{-19} \text{ cm}^2/\text{molecule}$.

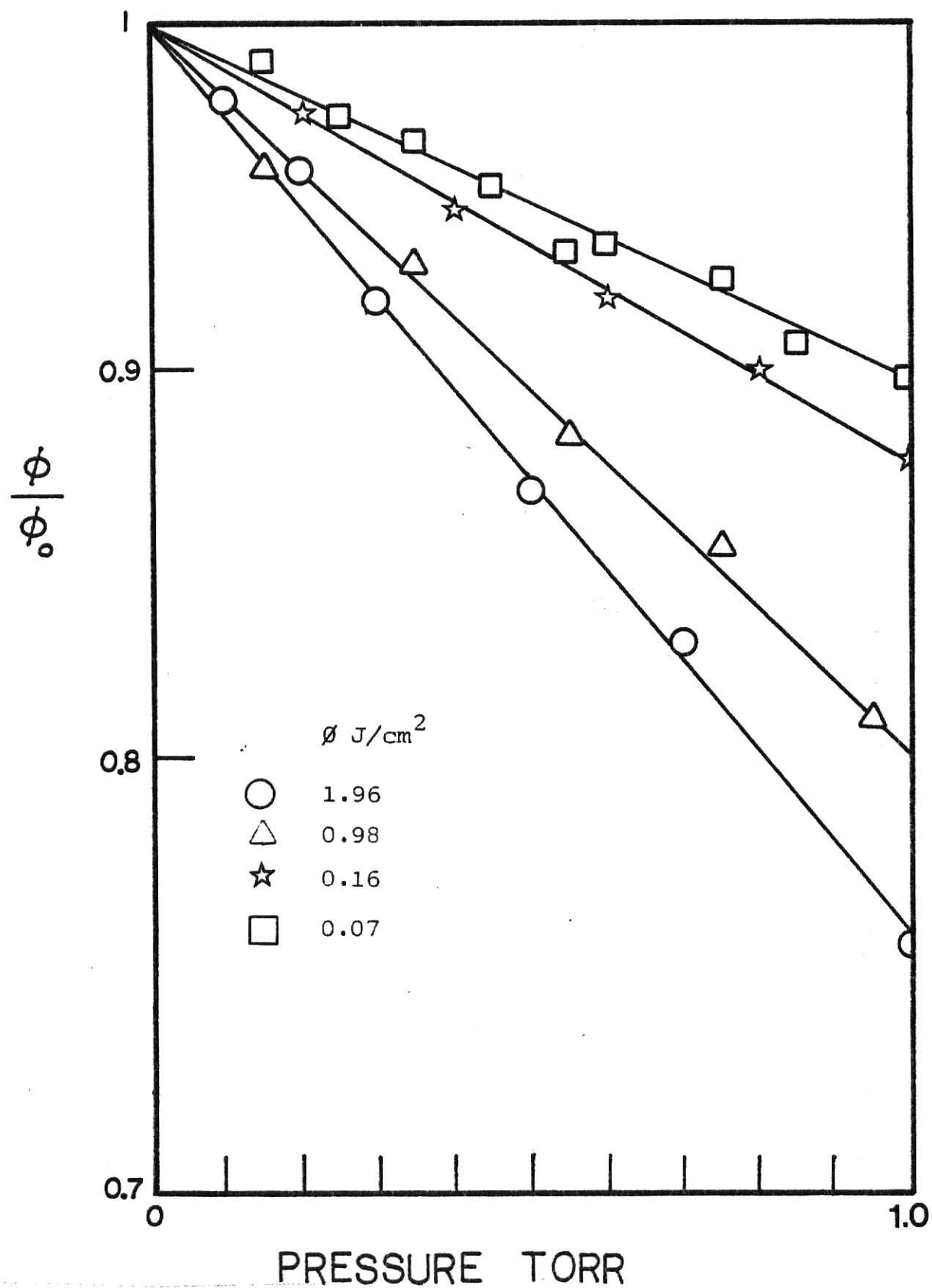


Fig. 17. Log Transmittance vs Ethyl Fluoroacetate Pressure at P(10).

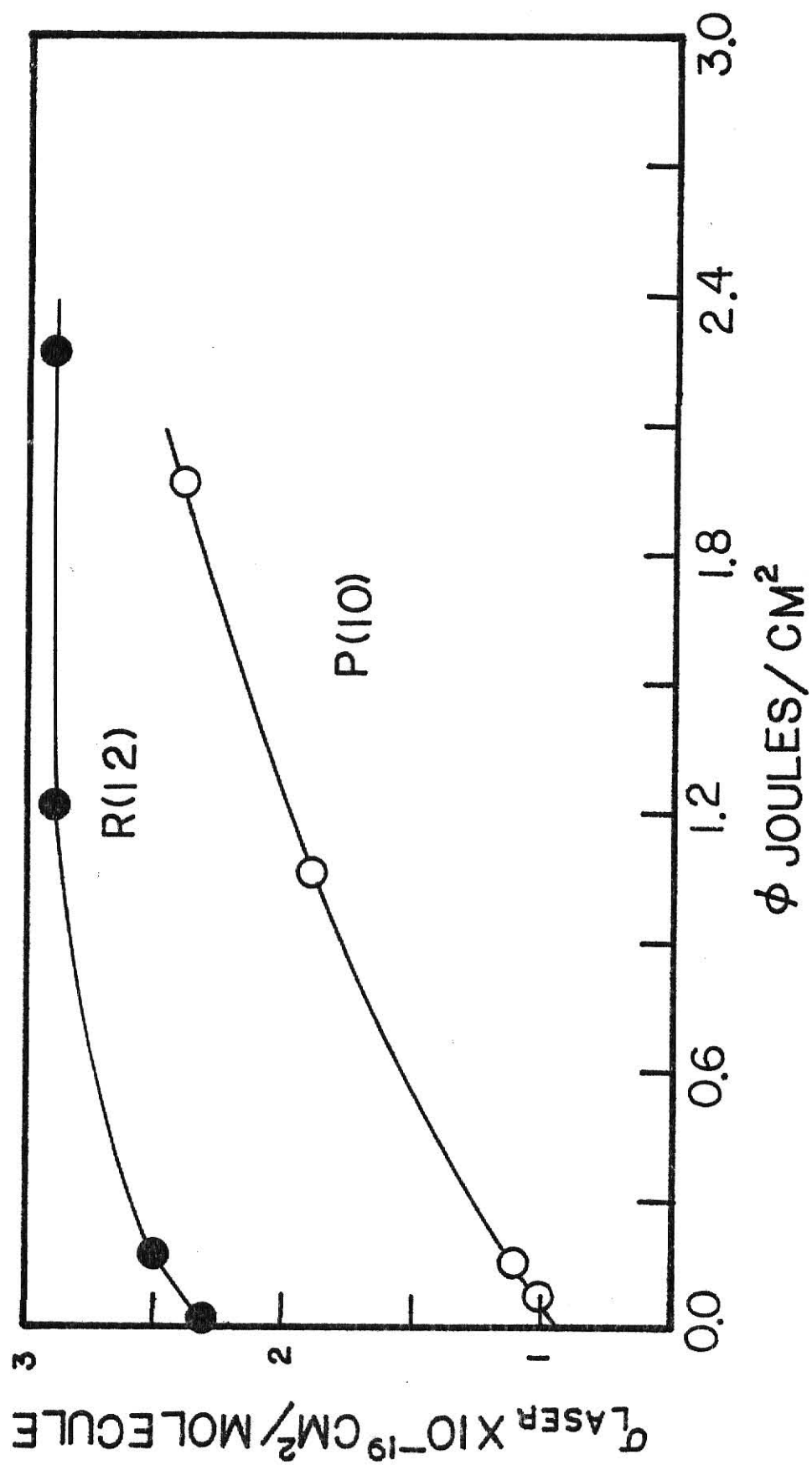


Fig. 18. σ_L vs ϕ for Ethyl Fluoroacetate.

Table 27. \bar{n} and \bar{n}_r Values for Ethyl Fluoroacetate at R(12).

ϕ J/cm ²	σ_L	\bar{n}	P(ϕ)	\bar{n}_r
2.2	2.9	30.6	0.45	68
2.0	2.9	27.2	0.40	68
1.8	2.9	24.5	0.36	68
1.4	2.9	19.0	0.20	95
1.2	2.9	16.3	0.07	233
0.9	2.8	11.8	0.025	473
0.6	2.7	7.6	0.0013	5850

$hc\bar{\nu} = 2.13 \times 10^{-20}$ J for R(12) photons. σ_L must be multiplied by 10^{-19} cm²/molecule. The thermal vibrational energy at 298 K that must be added to \bar{n} to obtain the mean energy is 3.1 kcal mole⁻¹.

Table 28. \bar{n} and \bar{n}_r Values for Ethyl Fluoroacetate at P(10).

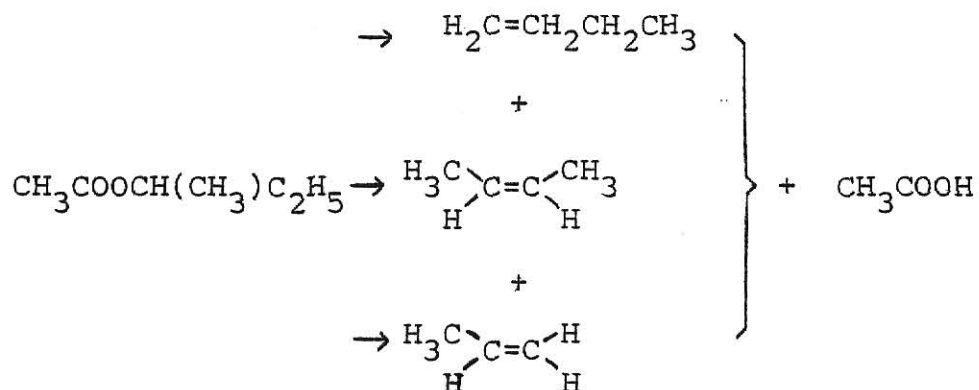
ϕ J/cm ²	σ_L	\bar{n}	P(ϕ)	\bar{n}_r
1.5	2.2	15.7	0.15	104
1.2	2.0	11.4	0.042	272
1.0	1.9	9.0	0.017	532
0.7	1.6	5.3	0.003	1777

$hc\bar{\nu} = 2.10 \times 10^{-20}$ J for P(10) photons. σ_L must be multiplied by 10^{-19} cm²/molecule. The thermal vibrational energy at 298 K must be added to \bar{n} to obtain the mean energy.

C. sec-Butyl Acetate.

1. Laser and Thermal Initiated Butene Product Distribution

The infrared spectrum of sec-butyl acetate (Fig. 19) shows an absorption band from 1050 cm^{-1} to 1000 cm^{-1} . The P(38) line at 1029.43 cm^{-1} was used to induce the reaction:



$$k = 10^{13.3} \exp[-46.6 \text{ kcal mole}^{-1}/RT]^{15},$$

$$A_{1\text{-Butene}} = 12.6, \quad A_{2\text{-Butene}} = 12.4.$$

Because of analytical difficulties, separate experiments were done to find the butene ratios. The butene isomers were resolved on a propylene carbonate column connected to a 10 % carbowax 20M on chromasorb W column operated at 0°C and the sec-butyl was not measured. The ester decomposition was followed in another set of experiments.

The butene product distribution was independent of ester pressure in the range of 1.0 to 0.05 torr, as shown in Table 29. This product distribution was the same as that obtained by conventional thermal reaction of sec-butyl acetate as demonstrated by a sensitizing experiment in which a mixture of 90 % SiF_4 and 10 % sec-butyl acetate at a total pressure of 0.8 torr was irradiated with 40 pulses of the P(42) line where SiF_4 absorbs strongly but the ester does not. The same product distribution was obtained. The product distribution was also invariant to the number of pulses and to \emptyset . The former means the butene formed is not itself dissociated by the laser, while the later demonstrated that, although sec-butyl acetate has two reaction channels, no enhancement of one channel over the other was caused by MPIUR.

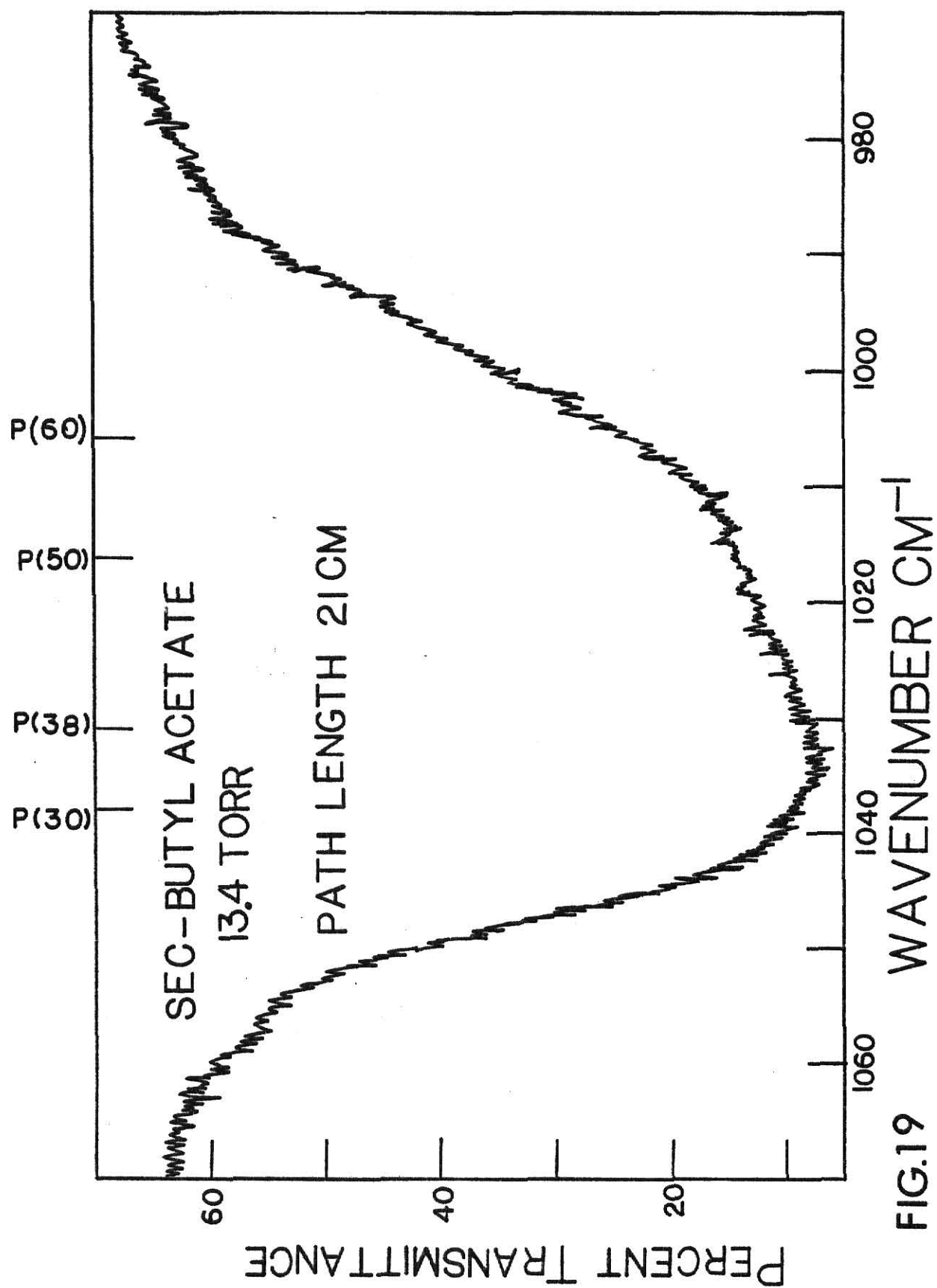


FIG.19

Table 29 . Butene Product Distribution of sec-Butyl Acetate.

P (torr)	% [1-Butene]	% [<u>trans</u> -2-Butene]	% [<u>cis</u> -2-Butene]
0.82	52	29	19
0.60	54	28	18
0.40	57	25	18
0.30	50	30	20
0.20	53	28	19
<hr/>			
* 0.05	49	31	19
** 0.80	52	29	19

For upper part of Table, a 1 cm long cell was used with $V_0 = 8.5 \text{ cm}^3$. Fluence was 5 J/cm^2 . Focused conditions (25 cm from a Germanium lens of focal length = 40 cm).

* Same cell but cell was placed at 30 cm from Germanium lens, resulting in a fluence, $\phi = 8 \text{ J/cm}^2$. ** Same cell, unfocused P(42) with $\phi = 0.5 \text{ J/cm}^2$, (for the 90% SiF_4 : 10% sec-butyl acetate mixture).

2. Reaction Probability Dependence on Fluence.

The reaction probability for sec-butyl acetate was investigated over a fluence range of 0.5 to 6 J/cm² for the P(38) line (Fig. 19). In order to reach fluences greater than 0.5 J/cm², it was necessary to focus the beam. Attention was focused on the middle and high P(\emptyset) ranges, rather than on the threshold fluence. For fluences above 4 J/cm², virtually 100% reaction per pulse was observed. The dependence of P(\emptyset) on \emptyset is high at P(\emptyset) below 10% reaction as is evident by the value of the slope (5.8). At higher reaction probabilities there was less change of P(\emptyset) with \emptyset until saturation was reached. There seems to be a rather sharp break in the log P(\emptyset) vs log \emptyset curve between the two regimes. This may reflect error caused by the dependence of the yield on the fluence at high focused conditions.

Table 30. sec-Butyl Acetate Irradiated with P(38), 1029.43 cm^{-1}

i	C_i/C_o	$\phi \text{ J/cm}^2$	$P(\phi)$
5	0.886	5.8	1.04
8	0.833	4.6	0.98
8	0.859	4.2	0.82
12	0.826	3.3	0.69
14	0.825	2.6	0.59
14	0.861	2.1	0.46
<hr/>			
7	0.852	1.5	0.31
7	0.880	1.2	0.24
7	0.922	0.9	0.16
15	0.938	0.7	0.06
18	0.986	0.54	0.011
<hr/>			
30	0.913	0.55	0.015

Pressure of sec-butyl acetate = 0.07 torr; cell length = 0.95 cm; $V_o = 13.4 \text{ cm}^3$, for upper part of table cell was placed 35 cm from BaF_2 lens with $G_o = 0.31 \text{ cm}^3$. For middle part of table cell was placed 22 cm from lens with $G_o = 1.09 \text{ cm}^3$. The area of the focused beam was measured with ir sensitive paper in both cases. The point at the bottom of the table was done unfocused with $G_o = 2.72 \text{ cm}^3$.

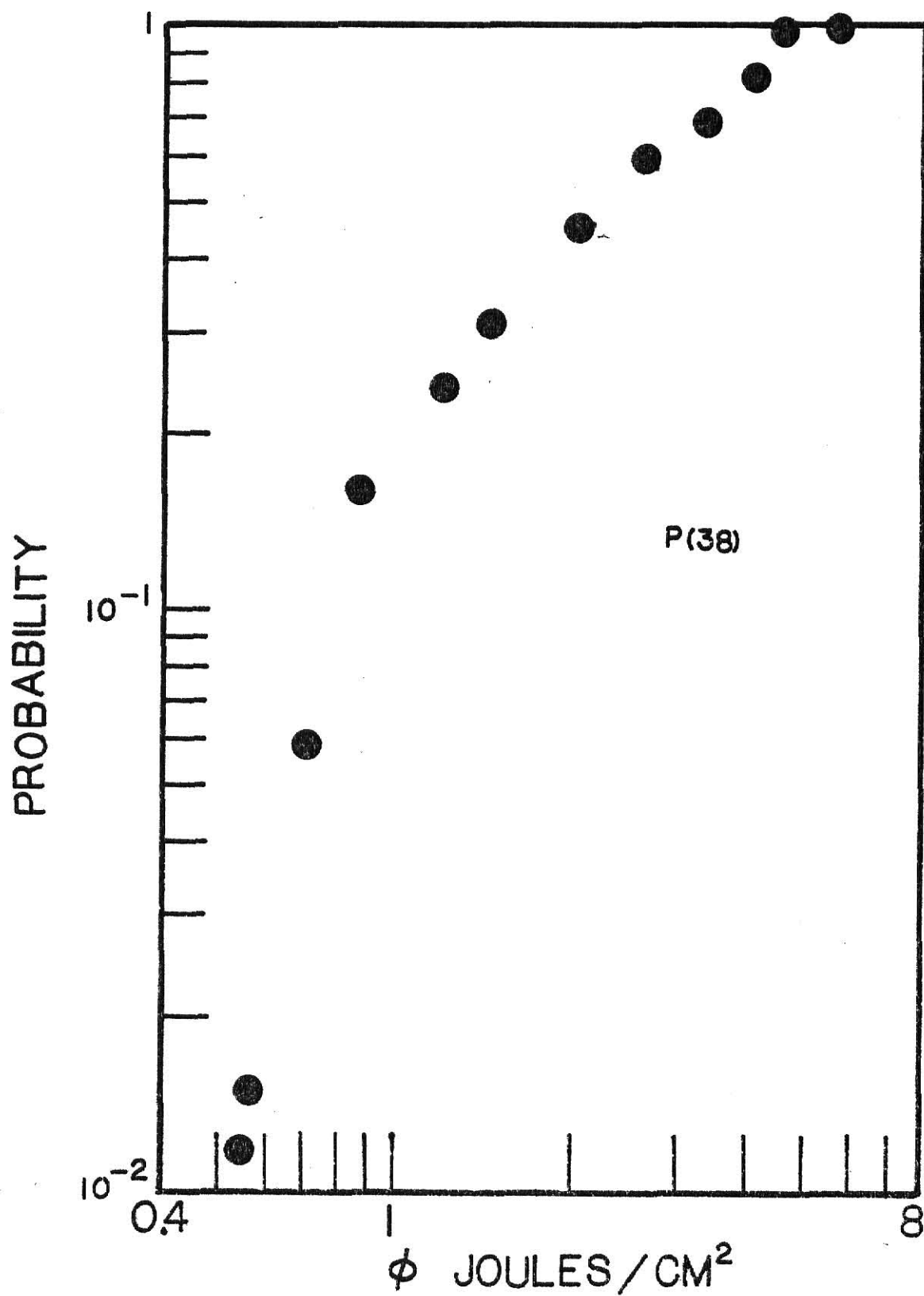


Fig. 20. Log $P(\phi)$ vs log ϕ for sec-Butyl Acetate.

3. Measurement of σ_L , \bar{n} and \bar{n}_r .

As in previous cases, the absorption of sec-butyl acetate follows Beer's law (see Fig. 21) and σ_L was calculated from equation (4) using data in Table 31. Fig. 22 shows a plot of σ_L vs ϕ . The decrease in σ_L with ϕ can be explained by a red shift of the absorbing band at high fluence (see Fig. 19). Due to the manner in which σ_L is measured, a lens can not be used to increase the fluence, so the maximum fluence available is obtained with arrangement A (see Fig. 4). In the case of P(38), which is a low energy line (see Fig. 1), the limiting fluence is about 0.67 J/cm^2 . By comparison with other esters studied, a further decrease in σ_L is predicted at higher ϕ . As in previous cases, σ_L extrapolated to σ at low ϕ .

Values for \bar{n} and \bar{n}_r for sec-butyl acetate are presented in Table 32. The σ_L at 0.9 J/cm^2 was obtained by smooth extrapolation of the curve in Fig. 22. The thermal vibrational energy of this ester at 298 K is 3.3 kcal/mole, which must be added to the \bar{n} values to obtain the mean energy of the molecule. The \bar{n} are pressure independent and are affected only by the magnitude of σ_L for a given ϕ .

Table 31. Measurement of σ_L for sec-Butyl Acetate at P(38).

$\phi = 0.67 \text{ J/cm}^2$		$\phi = 0.07 \text{ J/cm}^2$	
P (torr)	ϕ/ϕ_0	P (torr)	ϕ/ϕ_0
0.10	0.972	0.15	0.958
0.20	0.944	0.30	0.917
0.30	0.915	0.45	0.870
0.50	0.866	0.70	0.807
0.70	0.824	0.85	0.767
0.90	0.771	1.00	0.728
1.00	0.746		
$\sigma_L = 2.5 \pm 0.3$		$\sigma_L = 2.7 \pm 0.2$	

Path length = 35.7 cm. σ_L must be multiplied by $10^{-19} \text{ cm}^2/\text{molecule}$
 $\sigma = 2.8 \times 10^{-19} \text{ cm}^2/\text{molecule}$ at 1029.43 cm^{-1} .

Table 32. \bar{n} and \bar{n}_r for sec-Butyl Acetate irradiated with P(38).

$\phi \text{ J/cm}^2$	σ_L	\bar{n}	P(ϕ)	\bar{n}_r
0.9	2.2	10	0.14	71
0.7	2.4	8	0.06	140
0.6	2.5	7	0.03	250

The thermal vibrational energy for sec-butyl acetate at 298 K is 4.0 kcal/mole. This energy must be added to \bar{n} to obtain the mean energy of the ester. The σ_L must be multiplied by $10^{-19} \text{ cm}^2/\text{molecule}$.

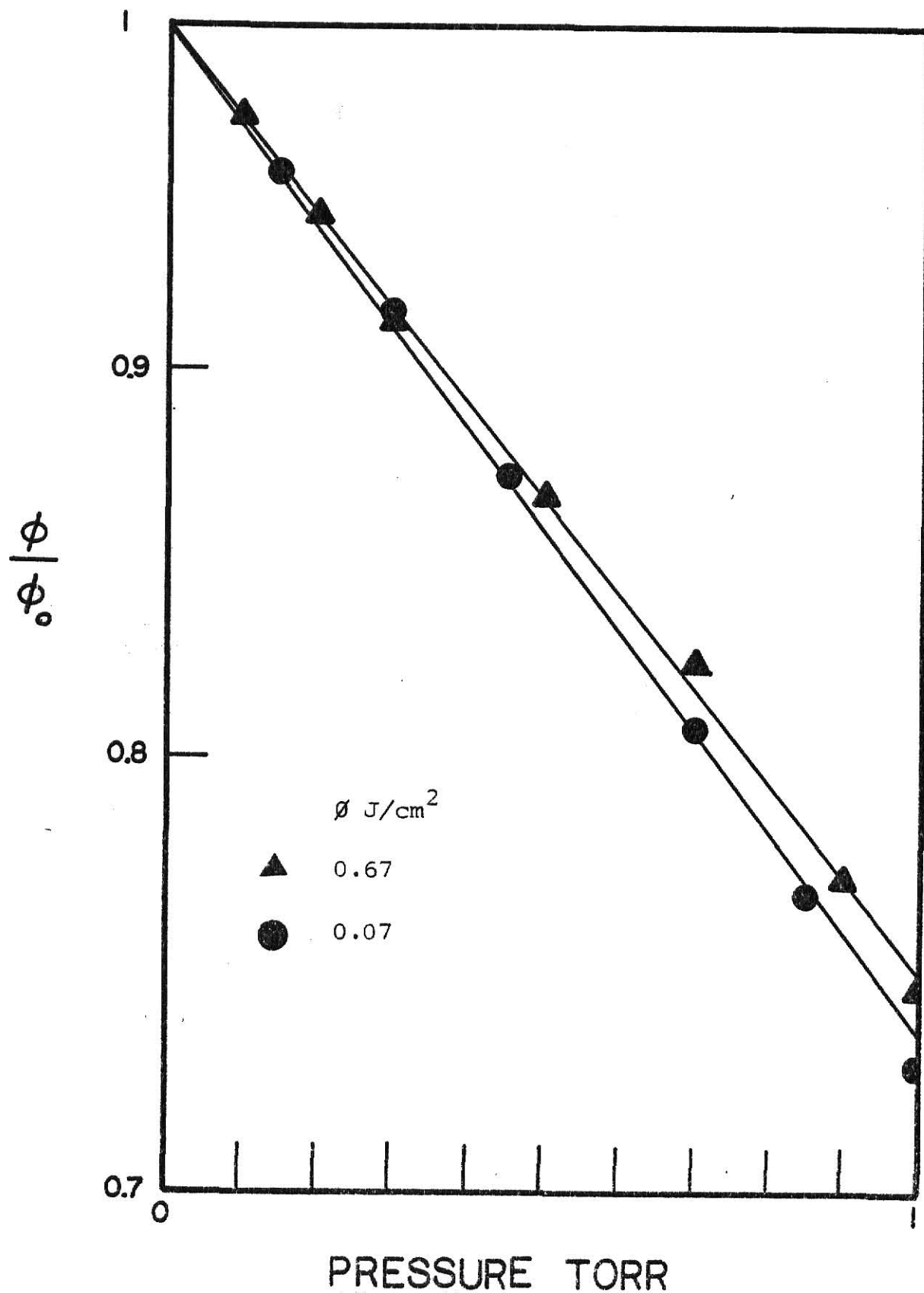


Fig. 21. Log Transmittance vs sec-Butyl Acetate Pressure

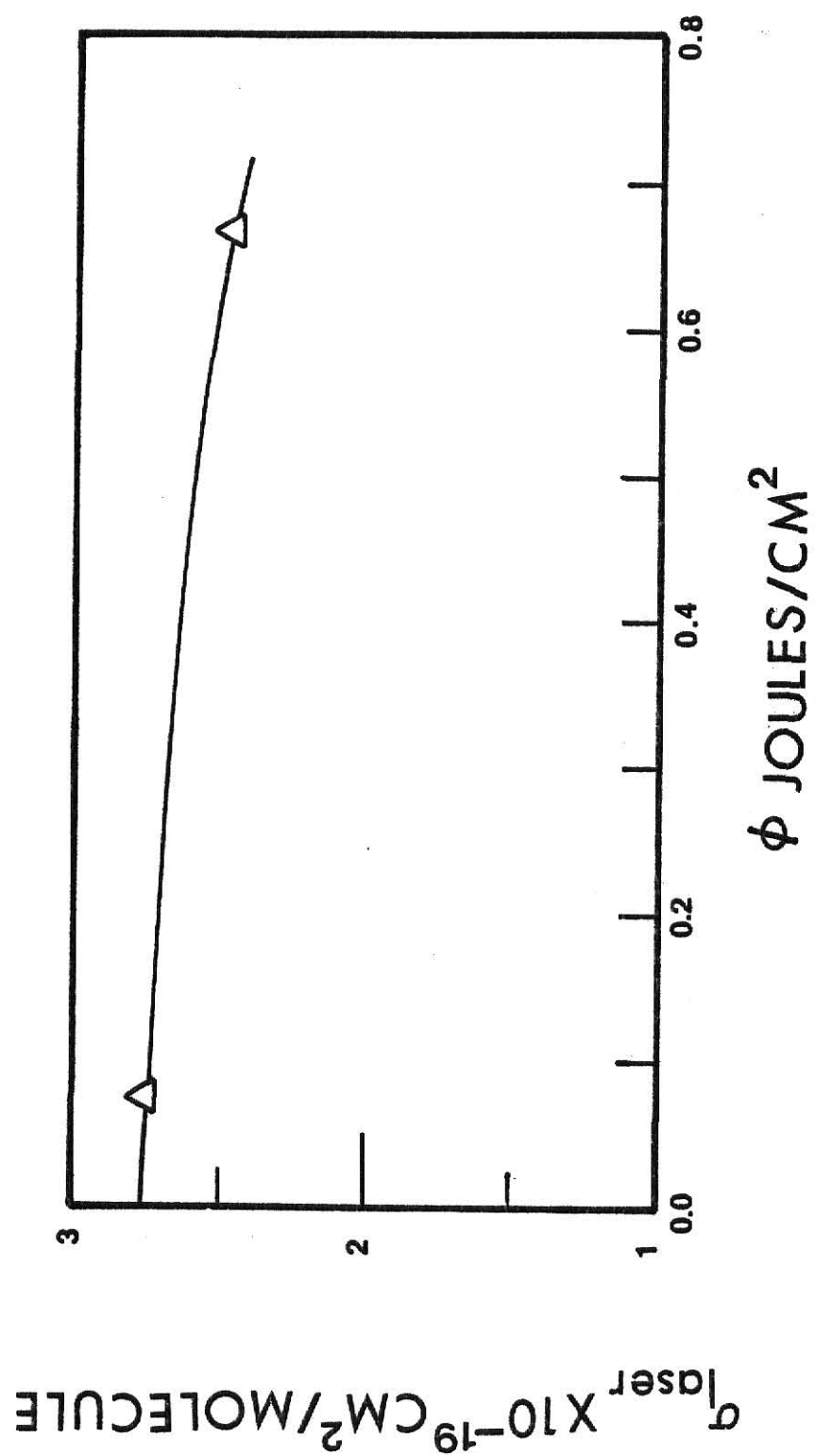
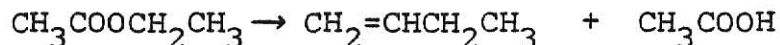


Fig. 22. σ_L vs ϕ for sec-Butyl Acetate.

D. n-Butyl Acetate.

1. Reaction Probability Dependence on Fluence.

The infrared spectrum of n-butyl acetate (Fig. 23) shows two peaks overlapping each other with maxima corresponding to the frequencies of the R(8) and P(26) lines of the $00^0_1-02^0_0$ vibrational band. The MPIUR of n-butyl acetate was the same as found in thermal excitation:



$$k = 10^{12.4} \exp[-46.0 \text{ kcal mole}^{-1}/RT]^{15}.$$

The reaction probability data for P(26) were extended to low fluence to examine threshold behavior. However, a linear plot of $\log P(\emptyset)$ vs $\log \emptyset$ was still obtained. Experiments were then done with R(8). Except for the points at $P(\emptyset) = 0.12$ for R(8) there was no significant difference between the two frequencies.

All data were taken under mildly focused conditions. the saturation region was not investigated for this ester. For the same fluence, $P(\emptyset)$ was a factor of 3 lower for n-butyl acetate than for sec-butyl acetate. This occurs in spite of the fact that the absorption cross sections are nearly equal. This is qualitatively consistent with the smaller reaction rate constants for n-butyl acetate.

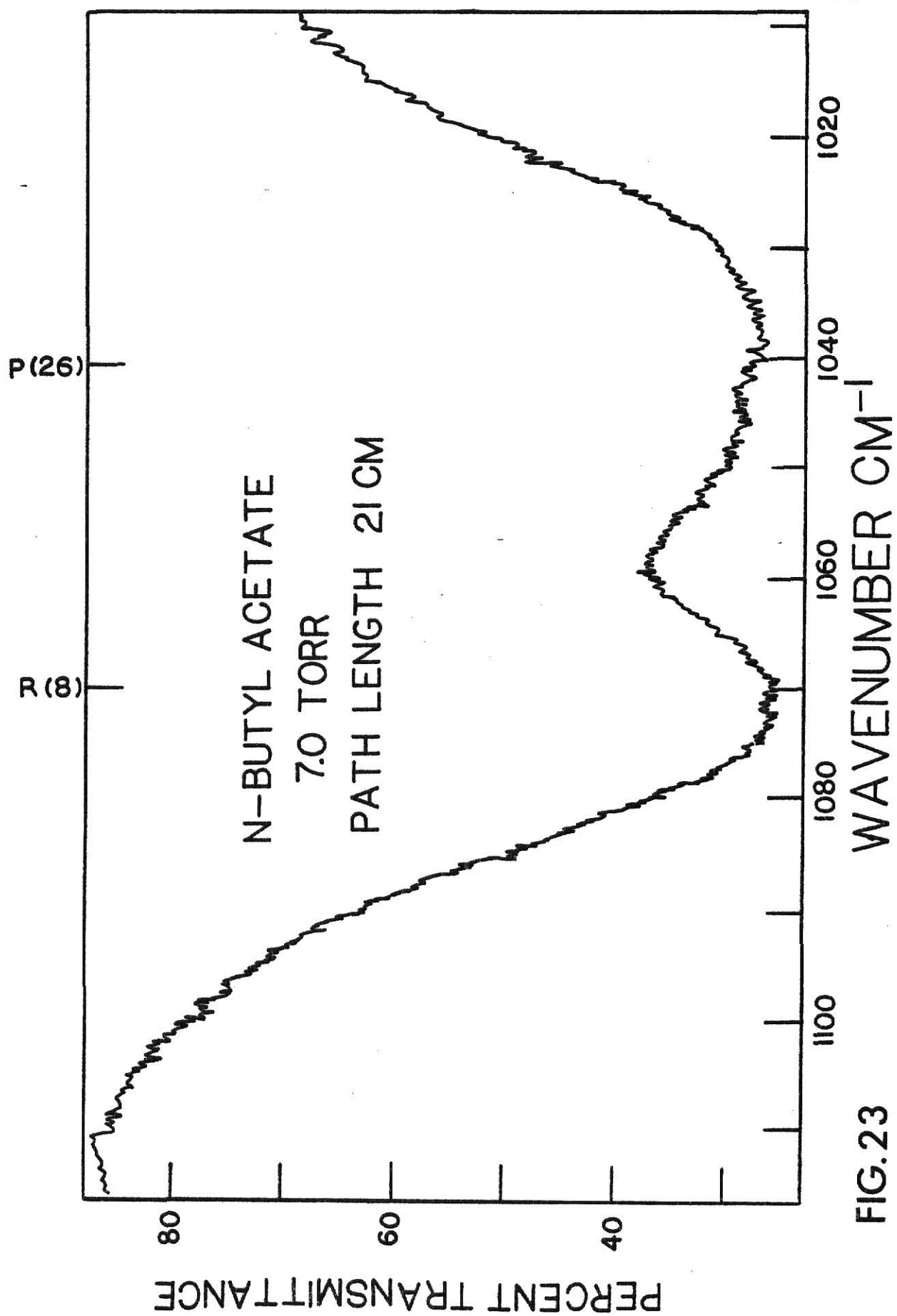


FIG. 23

Table 33. Reaction Probability vs Fluence for n-Butyl Acetate.

i R(8)	C_i/C_o	ϕ J/cm ²	P(ϕ)	i P(26)	C_i/C_o	ϕ J/cm ²	P(ϕ)
5	0.736	3.20	0.482	3	0.865	2.64	0.383
5	0.759	3.04	0.433	3	0.826	2.64	0.500
5	0.775	2.95	0.403	5	0.894	1.95	0.179
5	0.821	2.60	0.313	7	0.919	1.87	0.097
5	0.868	2.05	0.226	10	0.910	1.69	0.076
5	0.926	1.71	0.124	6	0.989	1.45	0.015
5	0.929	1.52	0.119	9	0.984	1.45	0.014
5	0.977	1.38	0.038	12	0.991	1.09	0.0063
5	0.977	1.38	0.038	15	0.997	0.90	0.0015

Pressure of n-butyl acetate 0.10 torr; cell length 3 cm; $V_o = 16.04$ cm³, $G_o = 1.98$ cm³, for focused conditions with cell placed 26 cm from a 50 cm focal length BaF₂ lens. Conditions were the same for R(8) and P(26).

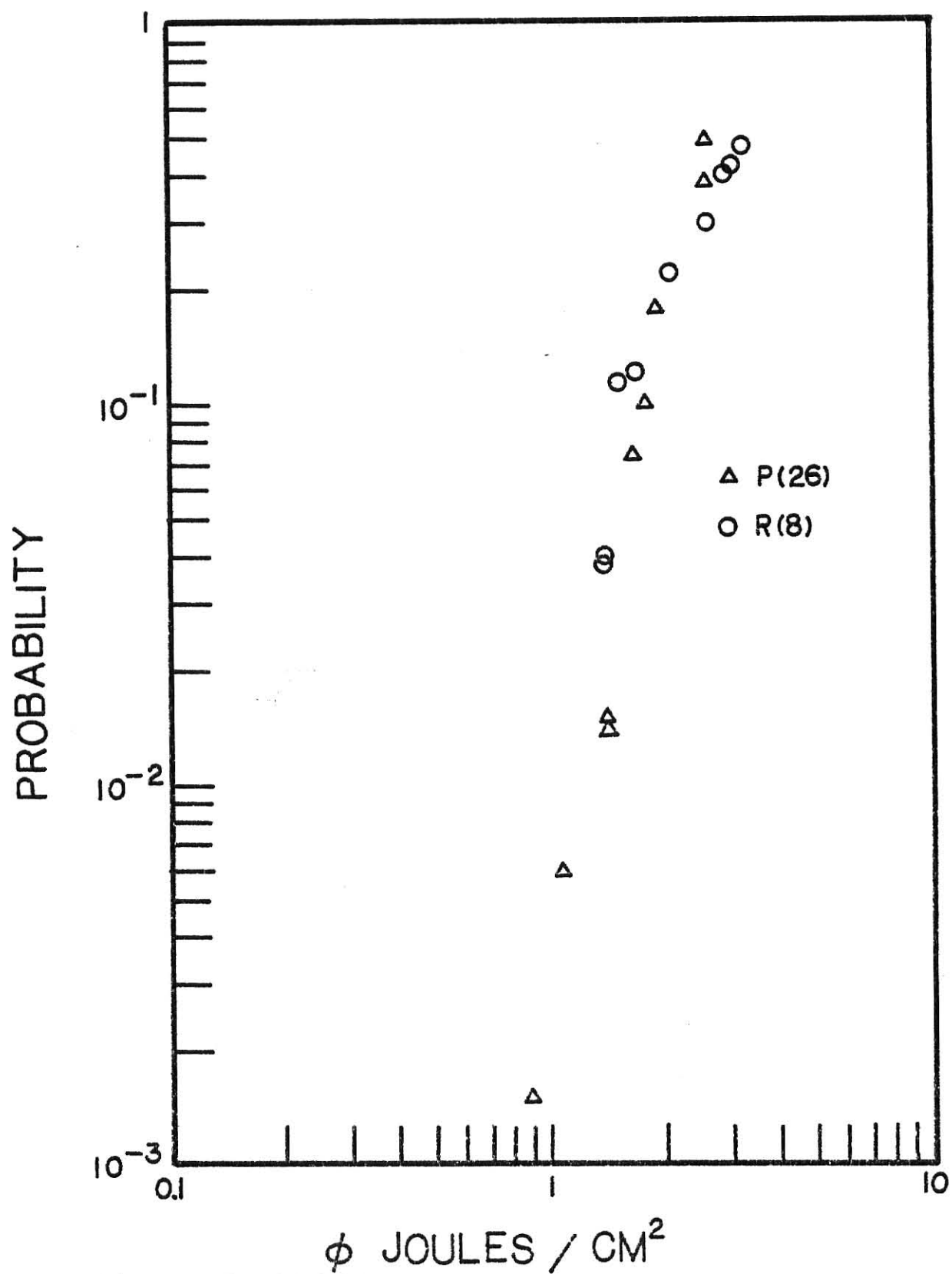


Fig. 24. Log $P(\phi)$ vs log ϕ for n-Butyl Acetate.

2. Measurement of σ_L , \bar{n} and \bar{n}_r .

Transmittance vs n-butyl pressure data from Table 34 were plotted in Fig. 25. The linearity of the curve warranted the use of equation (4) to calculate σ_L , which was determined for high for high and low fluence at R(8) and P(26). The decrease in σ_L at high fluence observed in Fig. 26 is again attributed to a red shift of the absorption band, see Fig. 23. The σ_L in both cases extrapolated to σ , when measured at low fluence. The point at $\phi = 0.15 \text{ J/cm}^2$ was taken from reference 17.

The σ_L for R(8) at $\phi = 0.67 \text{ J/cm}^2$ is in good agreement with the σ_L reported for n-butyl acetate at this frequency in reference 17 (see Table 45). The σ_L at $\phi = 1.35 \text{ J/cm}^2$ is suspected to be too high because a red shift of the band (Fig. 23) would cause a very sharp decrease of cross section at R(8) with increasing fluence.

The \bar{n} values for P(26) at $\phi \leq 2 \text{ J/cm}^2$ were obtained from Table 33 and Fig. 26, no \bar{n} values were tabulated for R(8) because of lack of σ_L data at the higher fluences employed to irradiate n-butyl acetate at this frequency.

Table 35. \bar{n} and \bar{n}_r Values for n-Butyl Acetate at P(26).

$\phi \text{ J/cm}^2$	σ_L	\bar{n}	$P(\phi)$	\bar{n}_r
1.7	2.1	18	0.10	180
1.2	2.5	15	0.08	187
1.0	2.6	13	0.04	325

σ_L must be multiplied by $10^{-19} \text{ cm}^2/\text{molecule}$. The vibrational thermal energy of n-butyl acetate at 298 K is 4.0 kcal/mole. This energy must be added to the \bar{n} to obtain the mean energy of the molecules.

Table 34. Laser Absorption Cross Section of n-Butyl Acetate at R(8) and P(26) with $\bar{\nu} = 1070.46 \text{ cm}^{-1}$ and $\bar{\nu} = 1041.27 \text{ cm}^{-1}$, respectively.

P(26)		P(26)		R(8)		R(8)	
$\sigma = 1.73 \text{ J/cm}^2$		$\sigma = 0.13 \text{ J/cm}^2$		$\sigma = 1.35 \text{ J/cm}^2$		$\sigma = 0.67 \text{ cm}^2$	
P (torr)	σ/σ_0	P (torr)	σ/σ_0	P (torr)	σ/σ_0	P (torr)	σ/σ_0
0.25	0.946	0.20	0.938	0.10	0.973	0.15	0.964
0.50	0.899	0.31	0.905	0.20	0.945	0.30	0.930
0.65	0.859	0.56	0.836	0.41	0.911	0.49	0.889
0.75	0.839	0.70	0.791	0.80	0.825	0.70	0.850
0.95	0.795	0.86	0.751	1.00	0.800	0.90	0.811
		0.99	0.712				
$\sigma_L = 2.1 \pm 0.3$		$\sigma_L = 3.0 \pm 0.2$		$\sigma_L = 2.0 \pm 0.3$		$\sigma_L = 2.0 \pm 0.2$	

Cell length is 35.7 cm; σ_L must be multiplied by $10^{-19} \text{ cm}^2/\text{molecule}$. the σ at R(8) and P(26) are $2.97 \times 10^{-19} \text{ cm}^2/\text{molecule}$ and $2.88 \times 10^{-19} \text{ cm}^2/\text{molecule}$, respectively

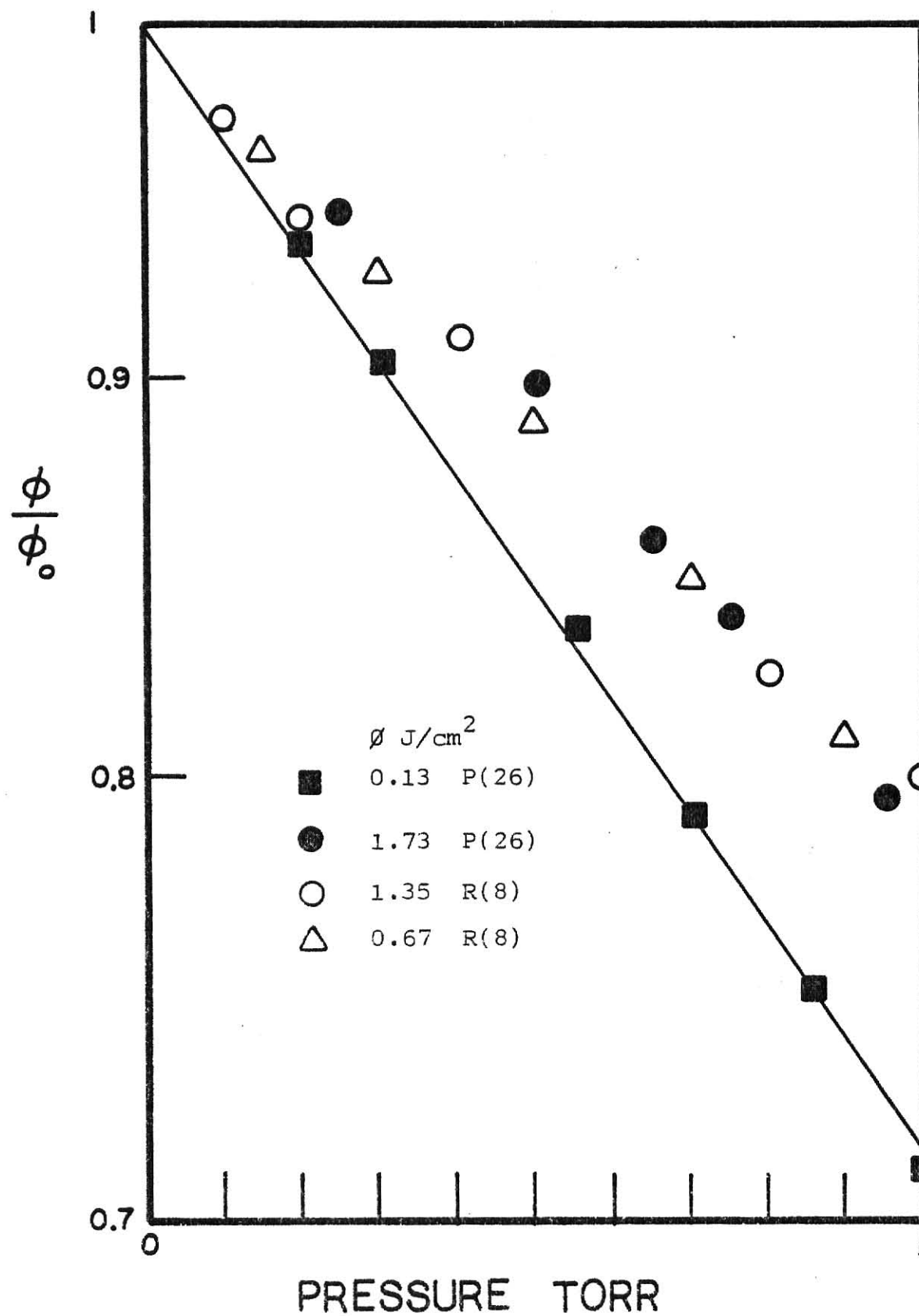


Fig. 25. Log Transmittance vs n-Butyl Acetate Pressure.

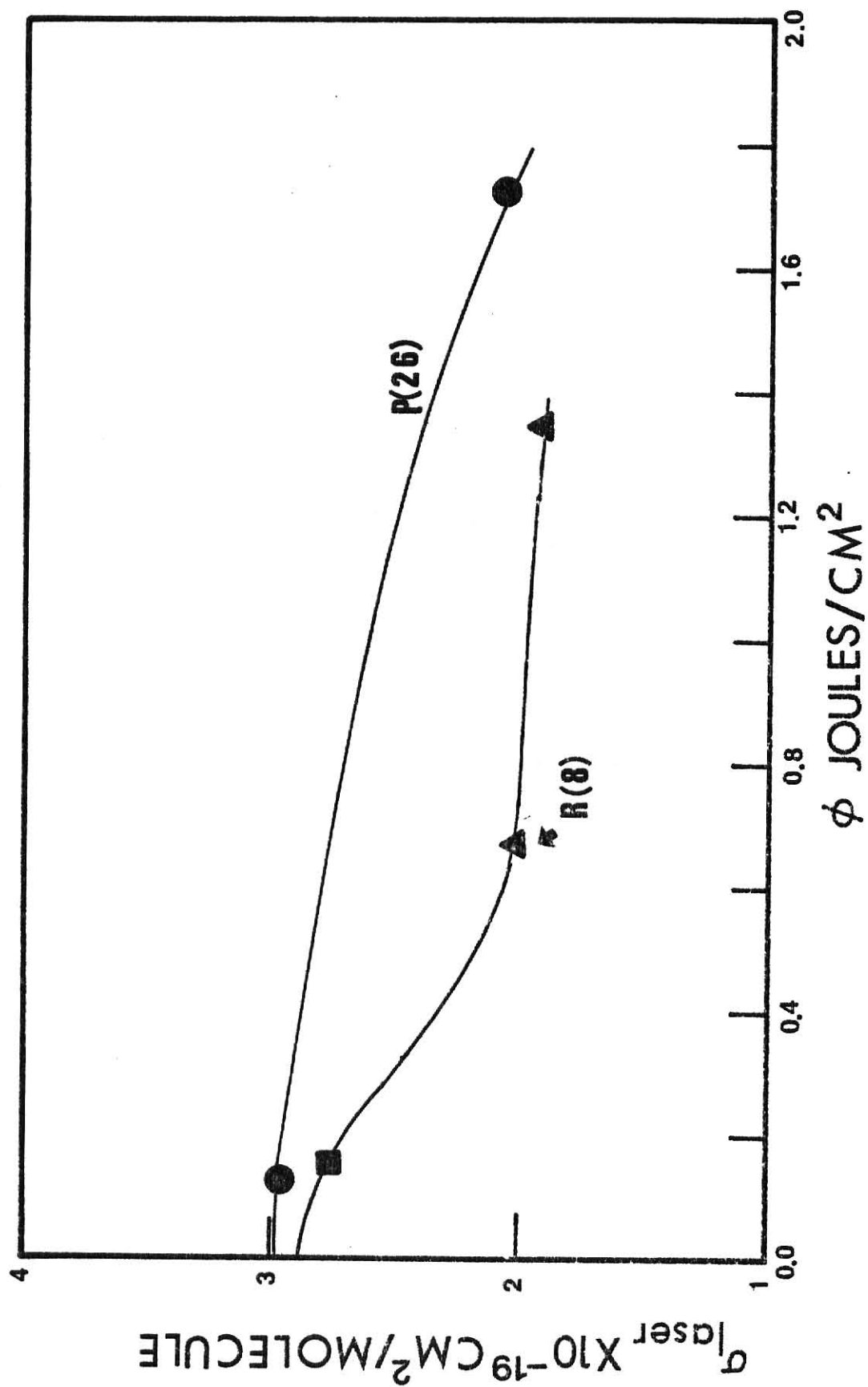


Fig. 26. σ_L vs ϕ for n-Butyl Acetate.

E. Ethyl 2-Bromopropionate.

1. Reaction Probability Dependence on Fluence.

The infrared spectrum of this ester (see Fig.27) displays a rather narrow band centered at about 1070 cm^{-1} with a FWHM of 20 cm^{-1} . The other esters had bands with FWHM from 50 to 70 cm^{-1} . The MPIUR of ethyl 2-bromopropionate can occur via two reaction channels; one is the elimination of ethylene and the other is elimination of HBr:

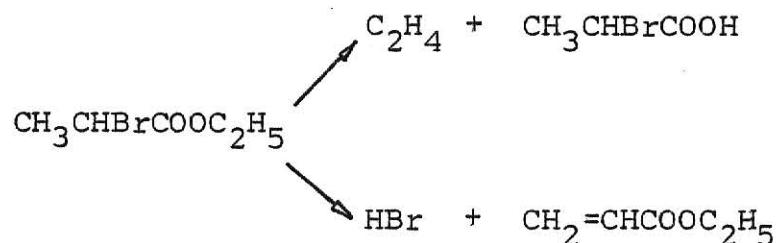


Table 36 shows the dependence of the ratio of the C_2H_4 elimination to the HBr elimination upon fluence for MPIUR and sensitized excitation. The thermal rate constants for these two channels are not known. The channel leading to elimination of C_2H_4 was favored by both MPIUR and sensitized excitation. There was no indication of a C-Br rupture channel. For low fluence, the ratio of ethylene to ethyl acrylate was about 3 and did not vary with number of pulses or frequency of line used. However, for higher fluence the ethylene channel becomes more dominant. This also is found for the sensitized excitation experiments.

A puzzling aspect is that the same change in ratio occurs for the sensitized excitation experiments. One explanation for the increase in ethylene in MPIUR is that at high fluence ethyl acrylate is formed during the pulse and subsequently begins absorbing energy during the pulse and contributes to the amount of ethylene observed. At 1.8 J/cm^2 $P(\emptyset)$ is 0.2 and at 4 J/cm^2 the saturation region has been reached. The variation in the product ratio begins at $\sim 2\text{ J/cm}^2$ and this coincides with the region where appreciable reaction occurs during the pulse.-

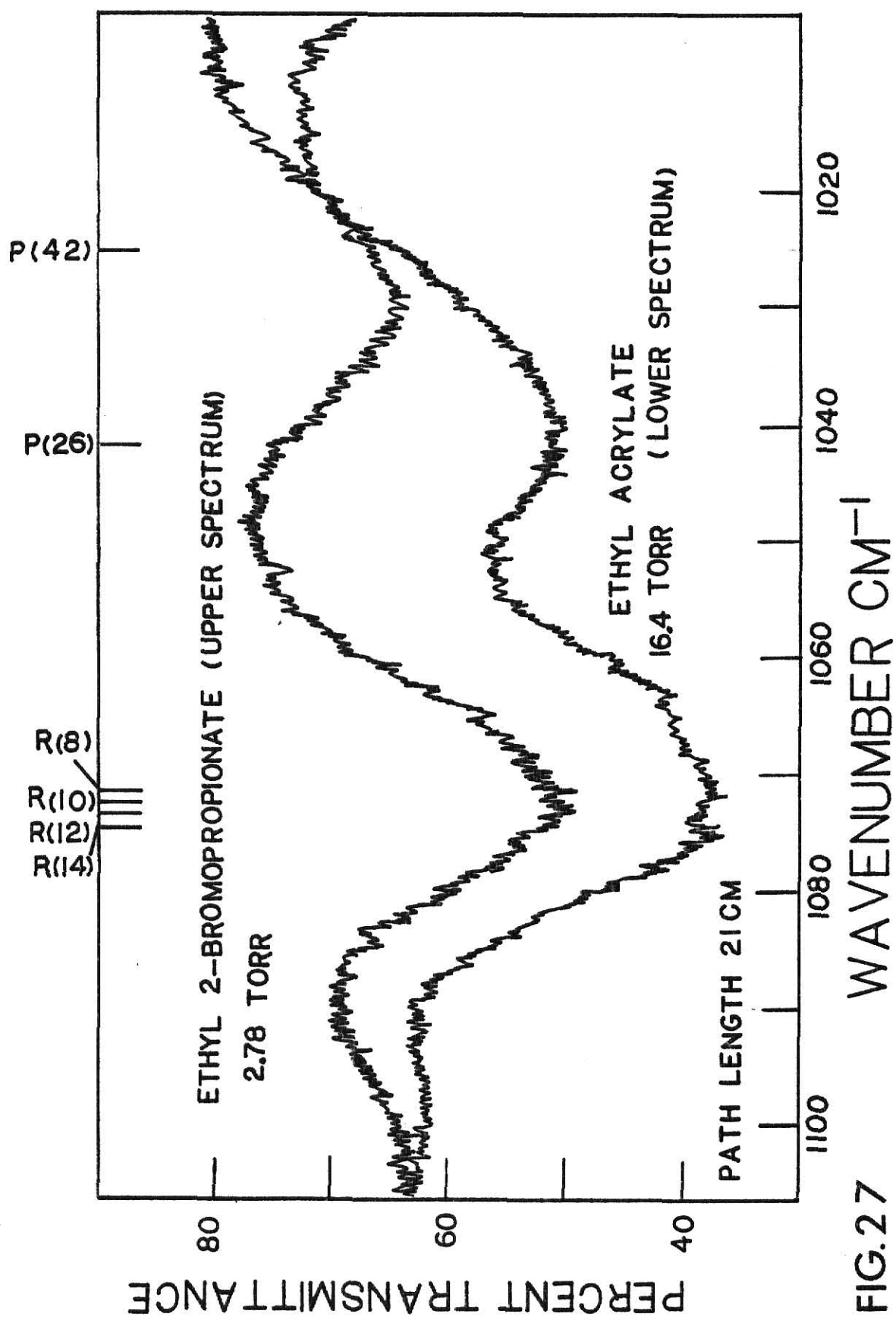


FIG. 27

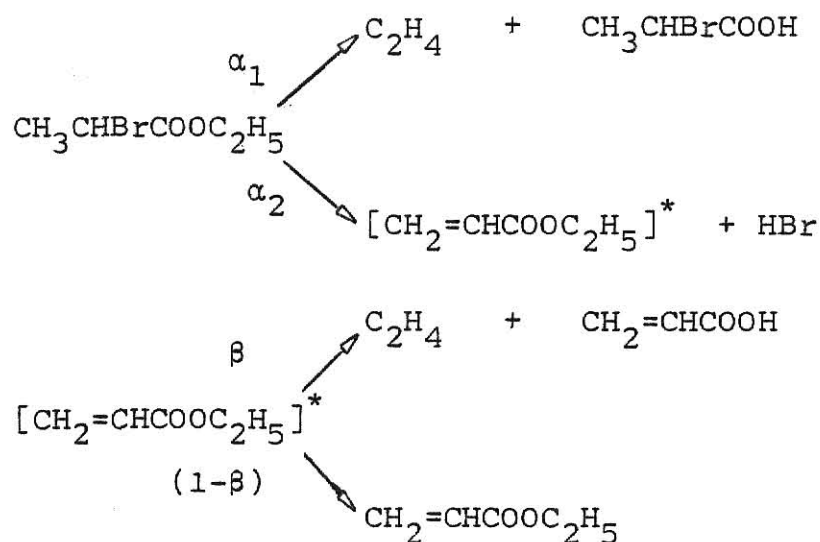
Table 36. Ratio of Products vs Fluence for MPIUR and Thermal Excitation of Ethyl 2-Bromopropionate.

ϕ J/cm ²	[Ethylene]/[Ethyl Acrylate]		Frequency
5.1	31.2		R(14)
4.0	12.6		
2.8	5.0		
1.7	3.1		
1.3	3.0		
1.0	3.4	MPIUR	
1.2	3.1		
0.7	3.2		R(12)
1.6	4.2		R(10)
1.2	3.1		P(42)
3.3	3.1		P(42)
<hr/>			
0.8	5.1	Sensitized	P(42)
3.3	12.7	Excitation	P(42)

For upper part of table the pressure of ethyl 2-bromopropionate was 0.1 torr (except for P(42) where pressure was 0.05 torr, and the reaction probability was 0.08). The ratios from lower part of table resulted from a sensitized experiment where a mixture of 81 % SiF₄ and 19 % ethyl 2-bromopropionate at a pressure of 0.1 torr was pulsed ten times with low and high fluence.

The results from Table 36 indicate a similar behavior with fluence for MPIUR and sensitized excitation of ethyl 2-bromopropionate.

A possible mechanism that could account for the observed behavior of the MPIUR of ethyl 2-bromopropionate is:



$$\frac{\text{C}_2\text{H}_4}{\text{HBr}} = \frac{\alpha_1 + \alpha_2(\beta)}{\alpha_2 + (1-\beta)} .$$

At $\beta = 0.5$, half the excited ethyl acrylate formed during the pulse reacts giving a ratio equal to 7.0. At higher β the ratio increases. For this mechanism to take place, the excited ethyl acrylate must absorb the laser energy. For the thermal reaction the vibrationally excited ethyl acrylate could absorb energy from the laser pulse.

Certainly no conclusive proof that the ethylene elimination channel is favored over the HBr elimination channel at high fluence can be obtained because of the possibility of secondary reaction by ethyl acrylate. Ethyl 2-bromopropionate was irradiated with the R(14) line and the reaction probability vs fluence data is tabulated in Table 37 and the results are plotted in Fig. 28. The slope of the linear portion of the plot was 4.3. This was the smallest n for the esters investigated and indicated that, for this ester, a less severe dependence of $P(\emptyset)$ on \emptyset is followed.

Table 37. Ethyl 2-Bromopropionate Irradiated with R(14),
 $\bar{\nu} = 1074.64 \text{ cm}^{-1}$.

i	C_i/C_o	$\phi \text{ J/cm}^2$	$P(\phi)$
8	0.649	3.8	0.62
8	0.680	3.0	0.55
10	0.732	2.1	0.36
<hr/>			
5	0.819	1.8	0.19
8	0.908	1.4	0.06
12	0.964	1.0	0.015

Pressure of ester = 0.1 torr; cell length 0.95 cm; $V_o = 13.4 \text{ cm}^3$; for upper part of table cell was placed 21 cm from BaF_2 lens with $G_o = 1.13 \text{ cm}^3$. For lower part of table experiments were done unfocused with $G_o = 2.72 \text{ cm}^3$.

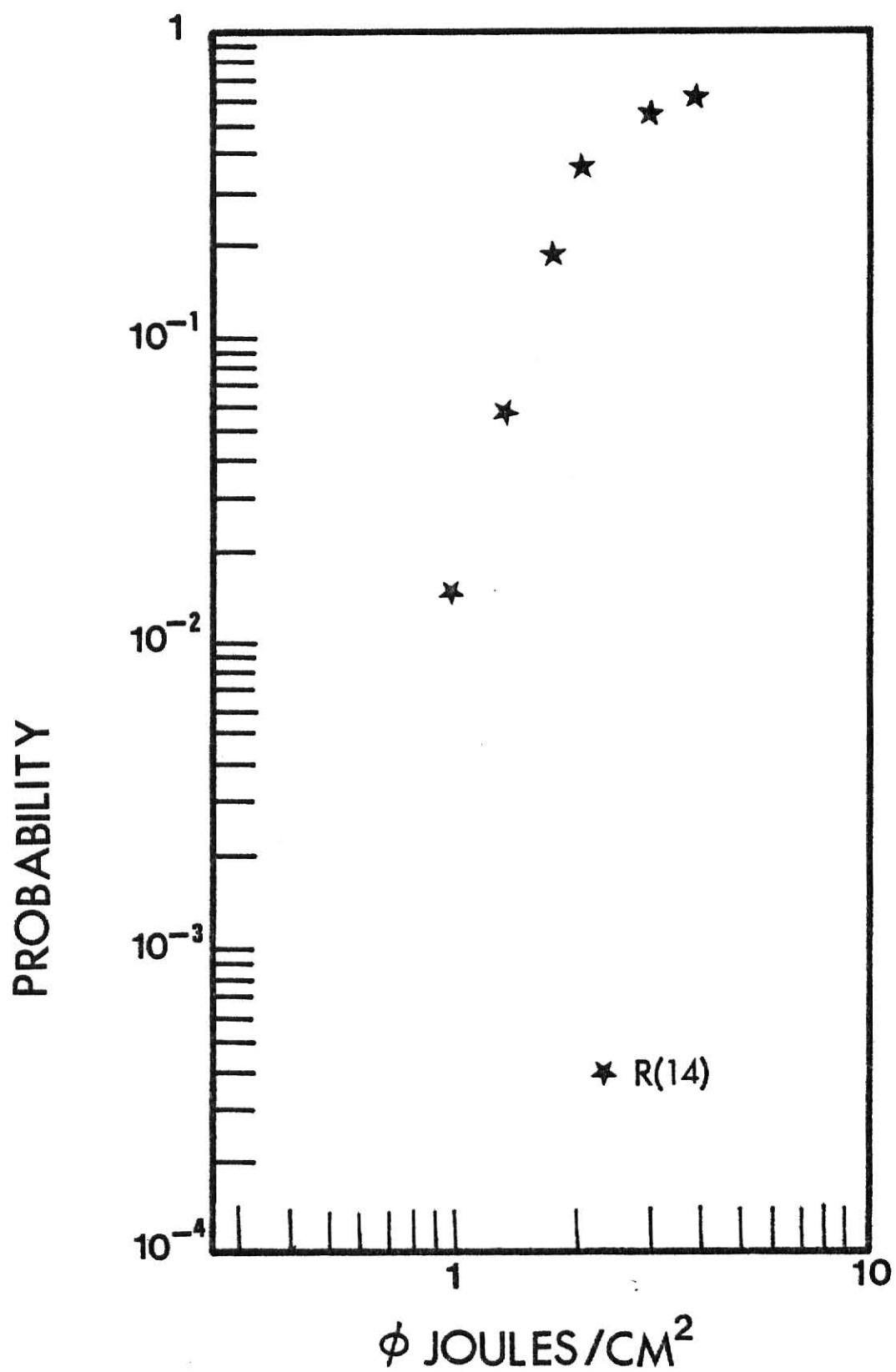


Fig. 28. $\log P(\phi)$ vs $\log \phi$ for Ethyl 2-Bromopropionate.

2. Measurement of σ_L , \bar{n} and \bar{n}_r .

Values of σ_L were obtained from the slopes of the linear plots of transmittance vs ester pressure in Fig. 29 using equation (4). The data for the plots are given in Table 39 together with the white light absorption cross section at 1073.27 cm^{-1} . Table 39 contains the transmittance vs pressure data for a 96% He, 4% ethyl 2-bromopropionate mixture and the measured σ_L . From Fig. 30, it is observed that σ_L decreases substantially with fluence due to a red shift of the absorption band. The σ_L extrapolated to σ at low ϕ , as was the case with other esters.

Trial experiments were done with added He to investigate the effect upon σ_L . These experiments were done at high pressure, before the extent of quenching by added inert gas was fully appreciated. At the pressures used, collisions occurred during the laser pulse and this may have resulted in collisional modification of the distributions during the pulse and these measurements, although interesting, are not useful for interpreting σ_L in the neat ester. The curve produced by the helium-propionate mixture showed that σ_L did not decline with fluence. One explanation is that the red shift of the absorbing band was inhibited because the pressure was so high that helium collisions interfered with the MPA process, as well as deactivating the ester molecules above E_0 . This quenching did not allow the molecules to absorb a sufficient number of photons to cause the large anharmonicity necessary for a red shift of the band. Further experiments for a lower range of helium composition would be valuable.

Data for \bar{n} and \bar{n}_r were taken from Fig. 28 and from Fig. 30 and tabulated in Table 40. The σ_L at $\phi = 1.55 \text{ J/cm}^2$ is believed to be too low, making the \bar{n} values at high ϕ unreasonably low.

Table 38. Laser Absorption Cross Sections of Ethyl
2-Bromopropionate at 1073.27 cm^{-1} , R(12).

$\phi = 1.55 \text{ J/cm}^2$		$\phi = 0.79 \text{ J/cm}^2$		$\phi = 0.13 \text{ J/cm}^2$	
P	ϕ/ϕ_0	P	ϕ/ϕ_0	P	ϕ/ϕ_0
0.20	0.96	0.10	0.96	0.15	0.93
0.30	0.95	0.20	0.93	0.25	0.90
0.40	0.93	0.30	0.91	0.35	0.87
0.50	0.90	0.40	0.88	0.45	0.83
0.70	0.88	0.50	0.85	0.65	0.77
1.00	0.83	0.60	0.83	0.70	0.75
		0.90	0.76		
$\sigma_L = 1.6 \pm 0.3$		$\sigma_L = 2.6 \pm 0.2$		$\sigma_L = 3.5 \pm 0.2$	

P refers to pressure of pure ester in torr; cell length was 35.7 cm; σ_L must be multiplied by $10^{-19} \text{ cm}^2/\text{molecule}$.

Table 39. Laser Absorption Cross Sections of Ethyl 2-Bromo-
propionate in a 4% ester, 96% Helium Mixture.

$\phi = 2.00 \text{ J/cm}^2$		$\phi = 1.12 \text{ J/cm}^2$		$\phi = 0.48 \text{ J/cm}^2$		$\phi = 0.22 \text{ J/cm}^2$	
P	ϕ/ϕ_0	P	ϕ/ϕ_0	P	ϕ/ϕ_0	P	ϕ/ϕ_0
8.78	0.87	7.68	0.88	7.38	0.89	6.35	0.90
5.50	0.91	4.80	0.92	5.01	0.92		
$\sigma_L = 3.4 \pm 0.4$		$\sigma_L = 3.5 \pm 0.3$		$\sigma_L = 3.4 \pm 0.3$		$\sigma_L = 3.5 \pm 0.3$	

P refers to the total pressure of the mixture in torr; cell length was 35.7 cm; σ_L must be multiplied by $10^{-19} \text{ cm}^2/\text{molecule}$. R(12) was also used for the data in Table 39.

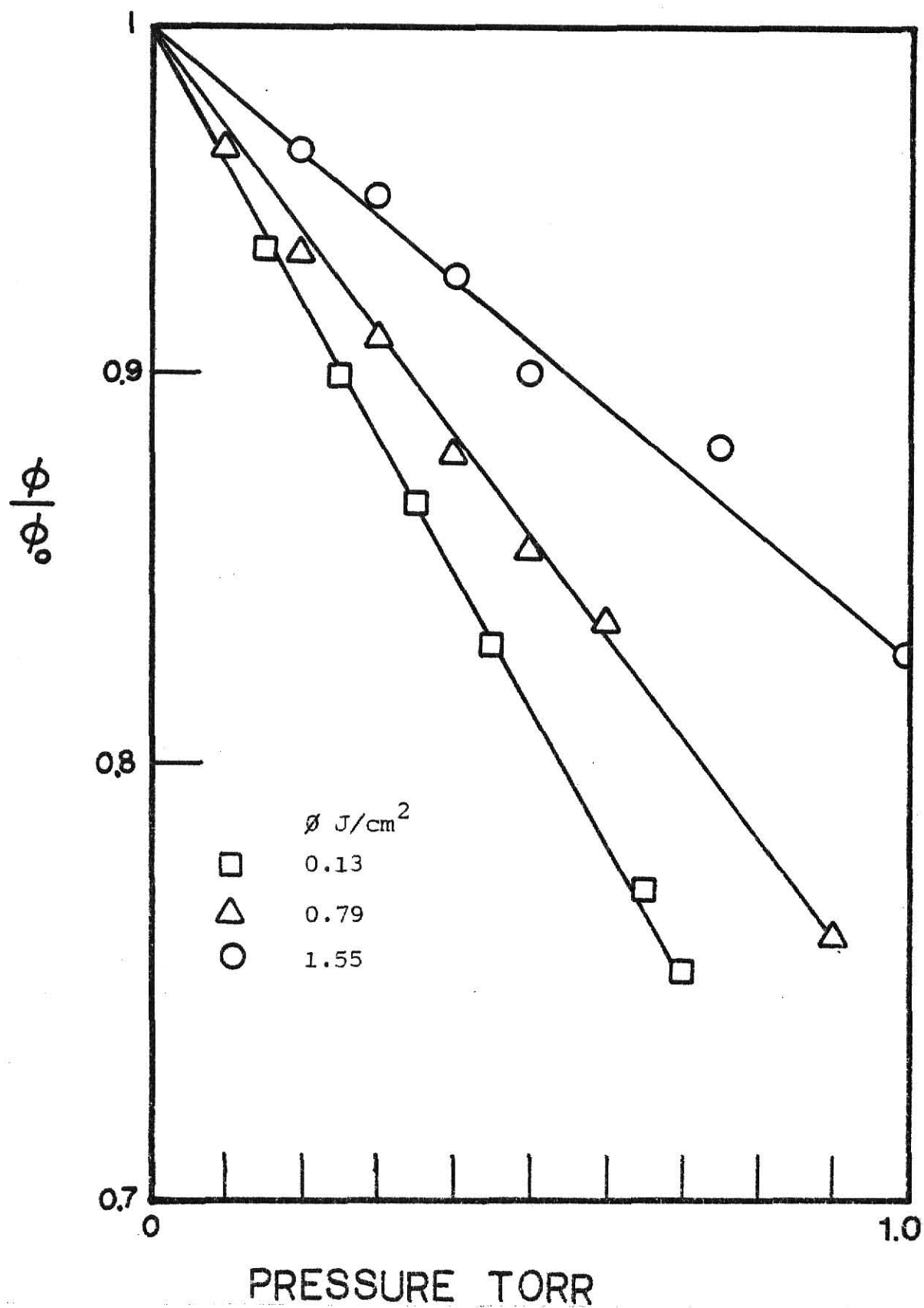


Fig. 29. Log Transmittance vs Ethyl 2-Bromopropionate Pressure.

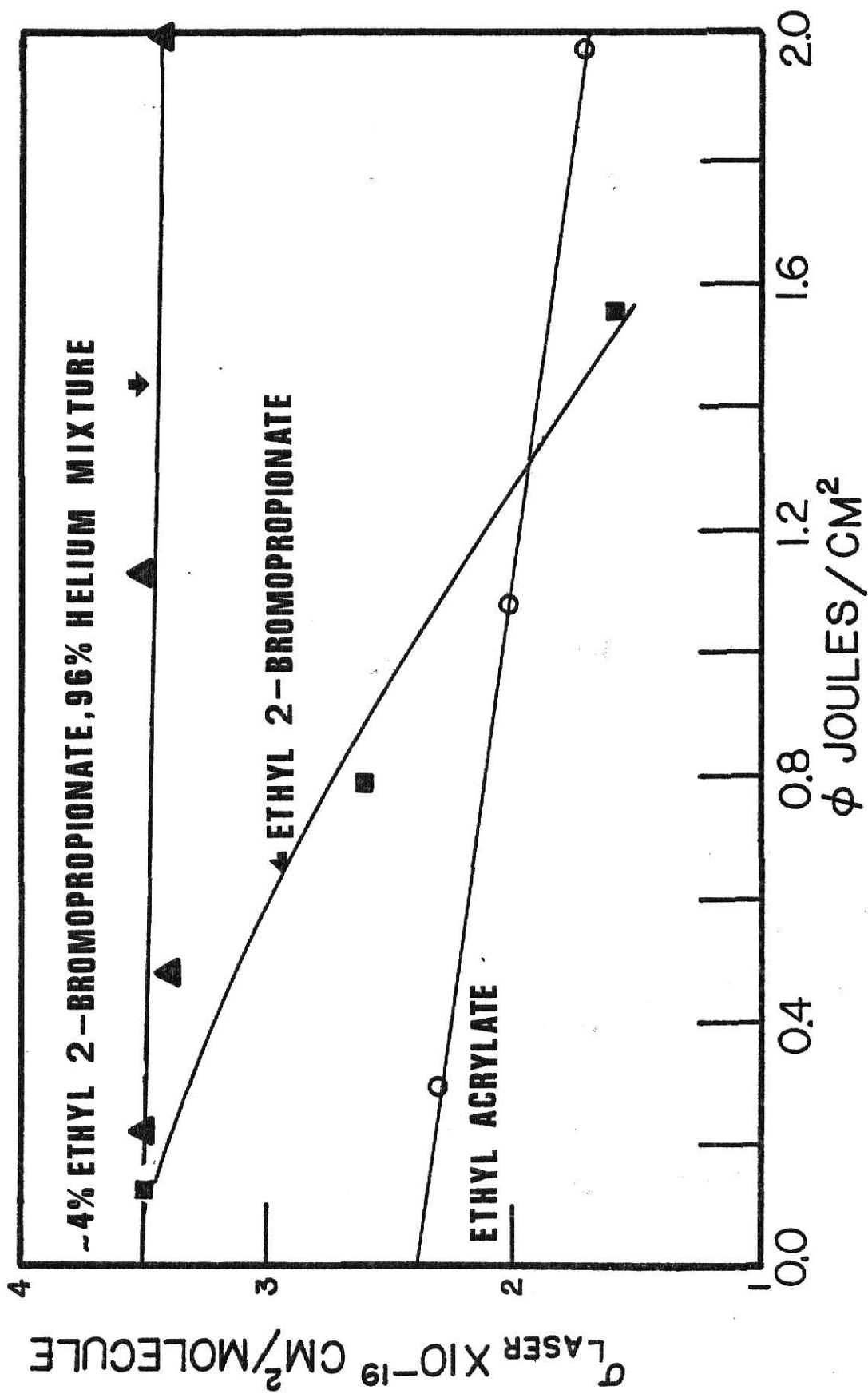


FIG. 30 σ_L vs ϕ for Ethyl 2-Bromopropionate and Ethyl Acrylate.

Table 40. \bar{n} and \bar{n}_r values for Ethyl 2-Bromopropionate.

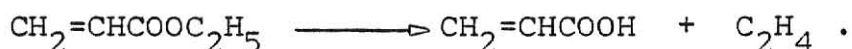
ϕ J/cm ²	σ_L	\bar{n}	P(ϕ)	\bar{n}_r
1.8	*1.2	10.8	0.20	54
1.6	1.5	12.0	0.12	100
1.2	2.1	12.6	0.04	315
0.8	2.7	10.8	0.006	1800
0.6	3.0	9.0	0.0012	7500

σ_L have been multiplied by 10^{-19} cm²/molecule. The vibrational thermal energy of ethyl 2-bromopropionate at 298 K is 4.4 kcal/mole, which corresponds to 1.47 ir photons. This energy must be added to the \bar{n} values to obtain the average energy of the molecules. * σ_L was obtained by smooth extrapolation of the absorption curve.

F. Ethyl Acrylate.

1. Reaction Probability Dependence on Fluence.

Ethyl acrylate was investigated because it was a product of the MPIUR of ethyl 2-bromopropionate, and because it has an absorption band very much like that of the propionate (see Fig. 27). The MPIUR of ethyl acrylate was the same as that obtained from thermal excitation:



Contrary to ethyl 2-bromopropionate, ethyl acrylate required high fluence to show measurable reaction. A very wide range of $P(\emptyset)$ was studied for this ester. Based upon the calculated irradiated volume at 31 and 29 cm from the BaF_2 lens, a $P(\emptyset) = 1.0$ was obtained for the high fluence range. Due to uncertainty in the G_0 measurement, the $P(\emptyset)$ could be as low as 0.8 for the highest points.

The dependence of the reaction probability on fluence for ethyl acrylate irradiated at R(10) is shown in Table 41 and plotted in Fig. 31. The linear region of the plot in Fig. 31 for $P(\emptyset)$ from 10^{-1} to 10^{-4} has a slope of 6.6, thus this ester exhibits the highest $P(\emptyset)$ dependence upon fluence. The difference in reactivity between ethyl acrylate and ethyl 2-bromopropionate might be caused by a high rate constant of the later. This is supported by the fact that ethylene is higher than HBr elimination for the propionate.

Table 41. Ethyl Acrylate irradiated with R(10), 1071.88 cm^{-1} .

i	C_i/C_o	$\phi \text{ J/cm}^2$	P(ϕ)
*4	0.812	13.0	1.00
4	0.812	9.9	1.00
4	0.815	9.5	0.98
4	0.818	8.6	0.97
4	0.827	7.8	0.92
5	0.820	6.5	0.77
7	0.767	5.3	0.73
10	0.779	3.8	0.48
12	0.839	2.9	0.29
15	0.874	2.5	0.18
20	0.918	2.2	0.08
20	0.967	2.1	0.04
40	0.984	1.4	0.008
50	0.995	1.2	0.002
70	0.999	1.1	0.0003
<hr/>			
2	0.776	7.9	1.05
2	0.813	6.9	0.87
2	0.865	4.8	0.62
10	0.698	3.0	0.31
20	0.652	2.5	0.19

For upper part of Table pressure of ethyl acrylate = 0.05 torr; cell length = 0.95 cm, $V_o = 13.4 \text{ cm}^3$, $G_o = 0.677 \text{ cm}^3$ at 29 cm from lens (* $G_o = 0.673 \text{ cm}^3$ at 31 cm from lens). For lower part of Table pressure was 0.1 torr; cell length = 3 cm, $V_o = 16.0 \text{ cm}^3$, $G_o = 1.37 \text{ cm}^3$ at 30 cm from lens. Areas of the focused beam were measured with ir sensitive paper.

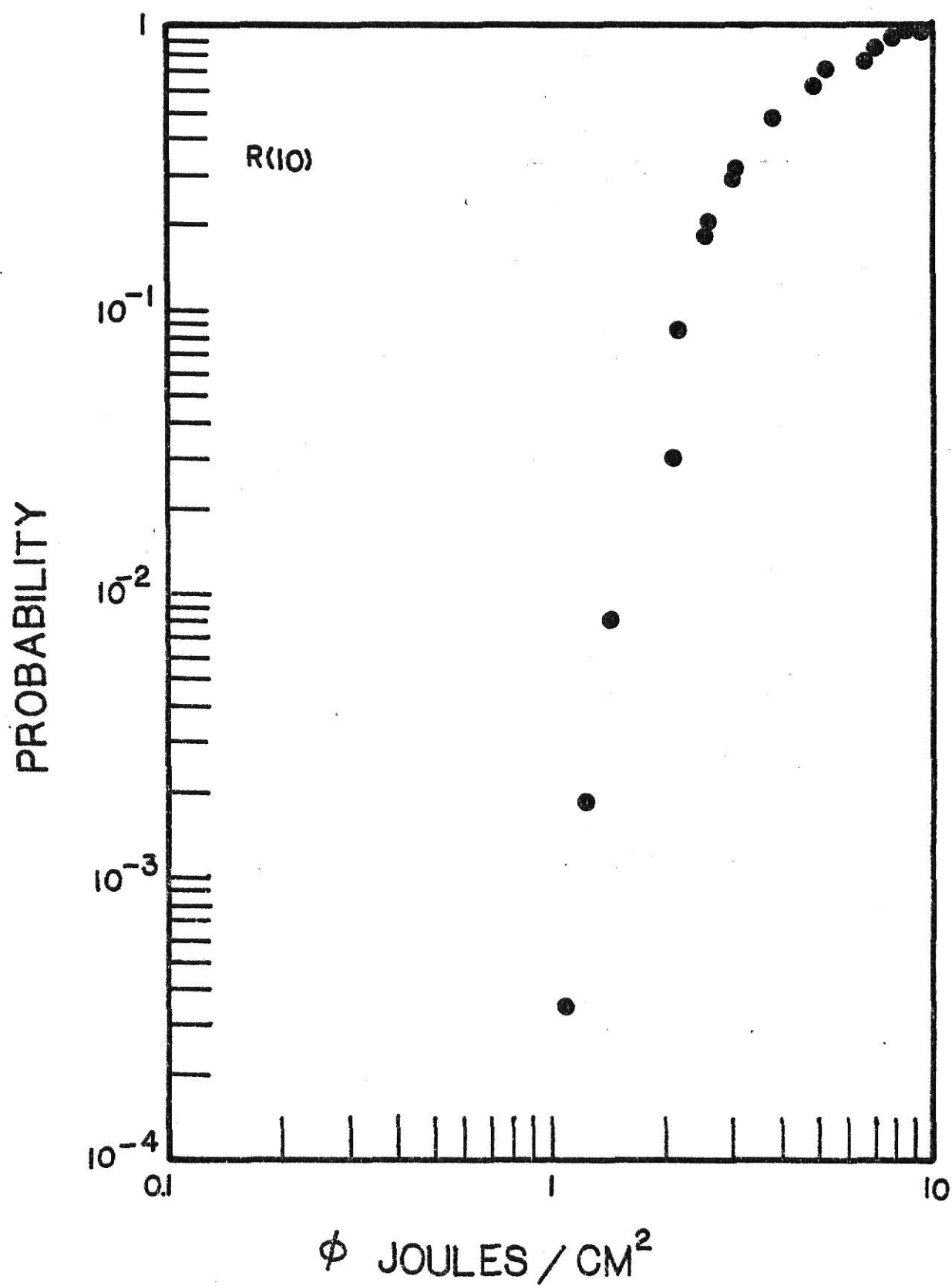


Fig. 31. Log $P(\phi)$ vs log ϕ for Ethyl Acrylate.

2. Measurement of σ_L , \bar{n} and \bar{n}_r .

Plots of log transmittance vs ethyl acrylate pressure at three different fluences yielded a straight line and equation (4) was used to obtain σ_L . The values of transmittance resulting from acrylate pressures below 1.0 torr are tabulated in Table 42, which also contains the σ_L for a given ϕ and the σ for the frequency used. The decrease of σ_L with ϕ was attributed to a red shift of the band at high ϕ . The decline of σ_L , even at moderate fluence, where reaction is low, can not be attributed to depletion of the absorbing molecules and is further evidence for the red shift as the explanation of the observed behavior of σ_L with fluence.

Data from Figs. 30 and 31 were used to obtain \bar{n} and \bar{n}_r employing equations (20) and (21), respectively. No \bar{n}_r can be calculated at high $P(\phi)$ due to the requirement of high fluence at which no σ_L were available.

Table 42. Measurement of σ_L for Ethyl Acrylate at R(10).

$\emptyset = 1.98 \text{ J/cm}^2$		$\emptyset = 1.08 \text{ J/cm}^2$		$\emptyset = 0.30 \text{ J/cm}^2$	
P (torr)	\emptyset/\emptyset_0	P (torr)	\emptyset/\emptyset_0	P (torr)	\emptyset/\emptyset_0
0.91	0.83	1.00	0.79	0.95	0.78
0.70	0.86	0.85	0.82	0.75	0.82
0.50	0.89	0.53	0.87	0.65	0.84
0.40	0.92	0.35	0.91	0.45	0.89
0.30	0.93	0.17	0.93	0.25	0.95
0.20	0.96				
$\sigma_L = 1.7 \pm 0.3$		$\sigma_L = 2.0 \pm 0.2$		$\sigma_L = 2.3 \pm 0.2$	

Path length 35.7 cm; σ_L must be multiplied by 10^{-19}
 $\text{cm}^2/\text{molecule}$. σ at R(10) is $2.4 \times 10^{-19} \text{ cm}^2/\text{molecule}$.

Table 43. \bar{n} and \bar{n}_r values for Ethyl Acrylate.

$\emptyset \text{ J/cm}^2$	σ_L	\bar{n}	P(\emptyset)	\bar{n}_r
2.5	*1.5	18.8	0.16	117
2.0	1.7	17.0	0.05	340
1.4	1.9	13.3	0.005	2660
1.2	2.0	12.0	0.001	12000

Vibrational thermal energy of ethyl acrylate at 298 K is
 3.6 kcal/mole. σ_L^* was obtained by smooth extrapolation
 of the absorption curve. The vibrational thermal con-
 tribution must be added to the \bar{n} values to obtain the total
 energy of the molecules.

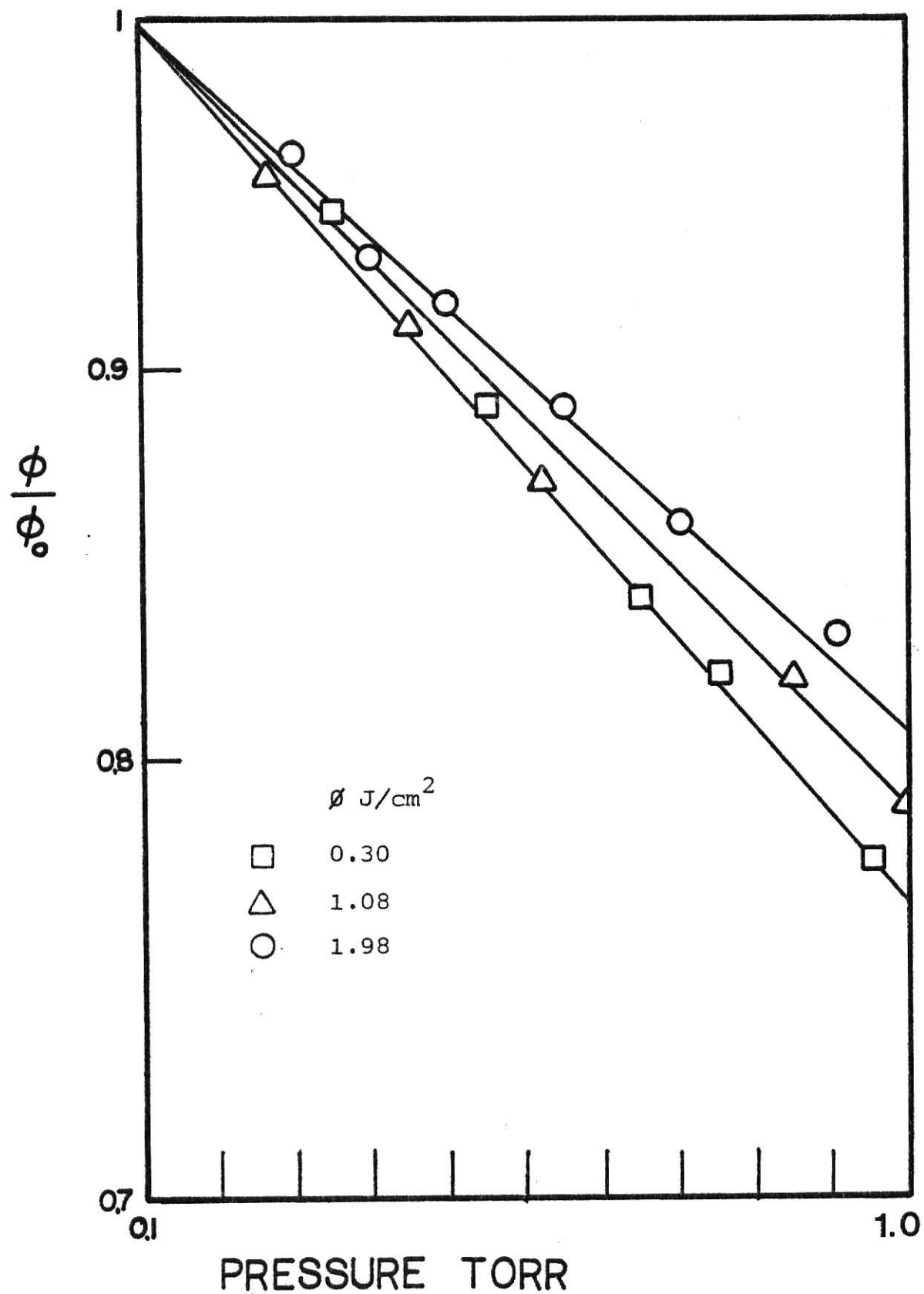


Fig. 32. Log Transmittance vs Ethyl Acrylate Pressure.

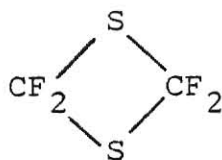
V. DISCUSSION

The ester molecules investigated in this thesis contained more atoms than the molecules investigated by most other workers studying the MPA and MPIUR processes. As a consequence, one cannot expect a complete similarity in the behavior between the case studied here and the usual case of the small molecules. Nevertheless, a brief literature survey will be useful before discussing the results of our work.

A. Literature Review.

1. Effect of Pressure in the MPIUR and MPA Processes.

Quigley¹⁹ reported that for fluences where no MPIUR occurs, but MPA is still taking place, the σ_L of SF_6 , in a mixture of SF_6 and added gas, increased with decreasing fluence (in the range from 1 J/cm² to 80 mJ/cm²), size of collision partner and added gas pressure (for 0 to 100 torr). The dependence of σ_L on added gas pressure can be explained by collisionally enhanced absorption that promotes rotational hole filling. This results in the \bar{n} being larger for a mixture of SF_6 and an added gas than for pure SF_6 . On the other hand, Lyman *et al.*¹³ found that the yield from mixtures of SF_6 and H_2 decreased with increasing pressure when either the total pressure of the mixture was increased or only the partial pressure of H_2 was increased from 0.025 to 2 torr and the SF_6 was held constant at 0.1 torr. In both cases the variation of the yield with total pressure was the same for fluences from 1 to 4 J/cm². These investigators also found that there was a significant decrease in the yield for pressures above 0.1 torr and that the yield asymptotically approached a maximum value for pressures below 0.1 torr, which imply that the pressure must be low in order to keep the time between collisions larger than the time it takes the excited molecules to dissociate. Lin *et al.*²⁰ observed small enhancements (< 20%) in the reaction yield when small quantities (mtorr) of rare gas are added to SF_6 . In contrast to SF_6 , Plum and Houston²¹ reported on the MPIUR of the ring compound



and found that the fraction reacted ($\sim 10\%$) at a fluence of 0.28 J/cm^2 did not vary systematically with tetrafluoro 1-, 3-dithietane pressure in the 0.002 to 2.0 torr range. But that addition of 2 torr of argon reduced the yield by roughly a factor of two. No pressure dependence on the reaction probability was reported by Stephenson and King²² for the dissociation of CF_2HCl in the 0.001 to 1.0 torr range. Upon addition of Ar²³, the dissociation of this compound increased until at ~ 50 torr of Ar the rate became independent of Ar pressure up to atmospheric pressure. Enhancement of the yield with increasing pressure was reported by Proch and Schroder²⁴ for the MPIUR of O_3 at a constant fluence, and they observed that O_3 kept dissociating after the termination of the laser pulse. Quick *et al.*²⁴ report enhancement of the reaction yield of fluorinated ethane and ethylene with the addition of inert gas. They used long pulse focused conditions, and reported that the threshold fluence for dissociation did not change with the addition of inert gas. The enhancement was very dependent upon the pressure of the bath gas, a sharp increase in yield occurred with a small increase in inert gas pressure, followed by quenching of the reaction at high pressures of inert gas. Setser and Jang²⁶ showed that both the collisional enhancement and collisional quenching depended upon pulse duration (laser intensity).

Another interesting effect of pressure is reported in Ref. 3 for the dissociation of ethyl vinyl ether, (EVE). This compound can react via a low energy dissociation channel ($E_a = 44 \text{ kcal/mole}$) and a high energy dissociation channel ($E_a = 65 \text{ kcal/mole}$) with k_1 and k_2 , respectively. The ratio of k_2/k_1 decreases with increasing EVE pressure for a constant

fluence. For pressures below 0.002 torr, no change in k_2/k_1 was observed, implying that collisional quenching was not important for the lower pressures.

2. Yield vs Fluence Behavior.

The dependence of the yield or, equivalently, the reaction probability on the laser fluence for MPIUR is a strong one. Investigators working with molecules that dissociate by MPIUR, have frequently plotted their results as $\log P(\phi)$ vs $\log \phi$. Although some other workers have suggested plotting $\log P(\phi)$ vs ϕ instead.²⁷ In the first type of plot, approximate linearity usually is observed for $P(\phi)$ 10^{-2} to 10^{-5} and the slope of this linear region is a measure of the reaction probability dependence on fluence.

For SF_6 ¹³ the $\log P(\phi)$ vs $\log \phi$ had slopes of 1.87 and 2.77 at 0.5 and 0.25 torr, respectively. Since the slope increased as the pressure decreased, collisions may affect the magnitude of the slope by collisional quenching, which is more effective at lower ϕ .

Invariably, at sufficiently high fluence, the yield approaches a constant value. The transformation from the linear, rapidly rising portion of the $\log P(\phi)$ vs $\log \phi$ to the constant yield region, occurs rather gradually with the exact shape depending on the molecule. If slopes are assigned to the curves in the transformation region rather low values will be obtained. This may be the reason small values frequently are reported for focused experimental conditions. For large molecules the maximum yield seems to approach 100%, but the maximum may be much smaller for smaller molecules. For smaller molecules the maximum may ultimately be related to bottleneck phenomenon in the absorption mechanism.

Using a molecular beam in order to work under true collisionless conditions, Brunner and Proch²⁸ investigated the dependence of yield on fluence for SF_6 and found it to be pronouncedly dependent on the laser frequency, thus, making the threshold energy and saturation yield also dependent on the

frequency. For a given fluence, the most effective line (that producing the lowest threshold energy) was found to be a few wavenumbers (5 cm^{-1}) to the red of the maximum of the absorbing band, and those lines to the blue of the band were discovered to have the highest threshold energies.

3. Fluence vs Power as the Critical Parameter for Yield.

In reference 13, work done on SF_6 suggested that little change in the reaction probability occurred by changing the pulse length. Kolodner et al.²⁹ compared the MPA of SF_6 using 0.5, 10 and 100 ns. pulses at a fluence of 1.5 J/cm^2 . They found a variation in the yield of only 20% even though the peak power changed by over a factor of 200. Gower and Billman³⁰, varied the pulse duration by a factor of five and showed that the MPIUR of polyatomic molecules had energy thresholds but no power thresholds.

Setser and Jang²⁶ reported that for the fluorinated ethanes with different inert gases, there was collision assisted enhancement of MPIUR. This effect is greater for a short pulse (high power) than for a long pulse (low power) of the same fluence. Kwok³¹ has measured the average number of photons absorbed per SF_6 molecule as a function of laser fluence for several pulse widths. He showed that there is significant difference in the \bar{n} values for the pulses with the same fluence but different pulse width, resulting in the σ_L being power dependent. Work done on ethyl vinyl ether³ showed an interesting effect of pulse length in the ratio of the dissociation channels of this compound using 0.2 and 2 μs . pulses. The channel with the higher activation energy was favored when using the 0.2 μs . pulse; but, the low activation energy channel was the only one occurring when the 2 μs . pulse was used. For the dissociation of CF_2HCl ²², major power effects were observed: 1) for constant fluence (1 J/cm^2), the dissociation yield increased by a factor of 6, from 6.5 to 40 MW/cm^2 ; 2) for pulses of constant fluence, modelocked pulses

produced 5-10 times more product than do nonmodelocked pulses; 3) for pulses of low intensity there were induction times of up to 200 ns. between the start of the pulse and any laser excited fluorescence from the CF_2 produced in the dissociation; 4) when high pressure of an inert gas was added, the effects of laser intensity were substantially reduced, and the reaction became mainly fluence dependent.

At the present time it appears that power is important for small molecules, but that fluence is important for large molecules, providing that experiments are done in the collision free pressure regime.

B. Discussion of Experimental Results of the Acetates

1. Effect of Pressure on the MPIUR of Ethyl Acetate

From experiments described in section III E, it was found that a pressure of ≤ 0.1 torr was needed to avoid collisional effects leading to intermolecular redistribution of laser energy (i.e. heating). This conclusion was based on the thermal monitor experiments. In doing such experiments care should be exercised to avoid altering the heat capacity of the irradiated volume. The experiments done with a 3% isopropyl bromide, 97% ethyl acetate mixture met this criterion. They showed that insignificant heating occurred at 0.05 torr from the small amount of dissociation of isopropyl bromide compared to that undergone by ethyl acetate at high fluence ($\geq 2.5 \text{ J/cm}^2$); the effect was even smaller at lower fluences. At a pressure of 0.2 torr the probability of isopropyl bromide reacting was greater and became even more severe with increasing pressure.

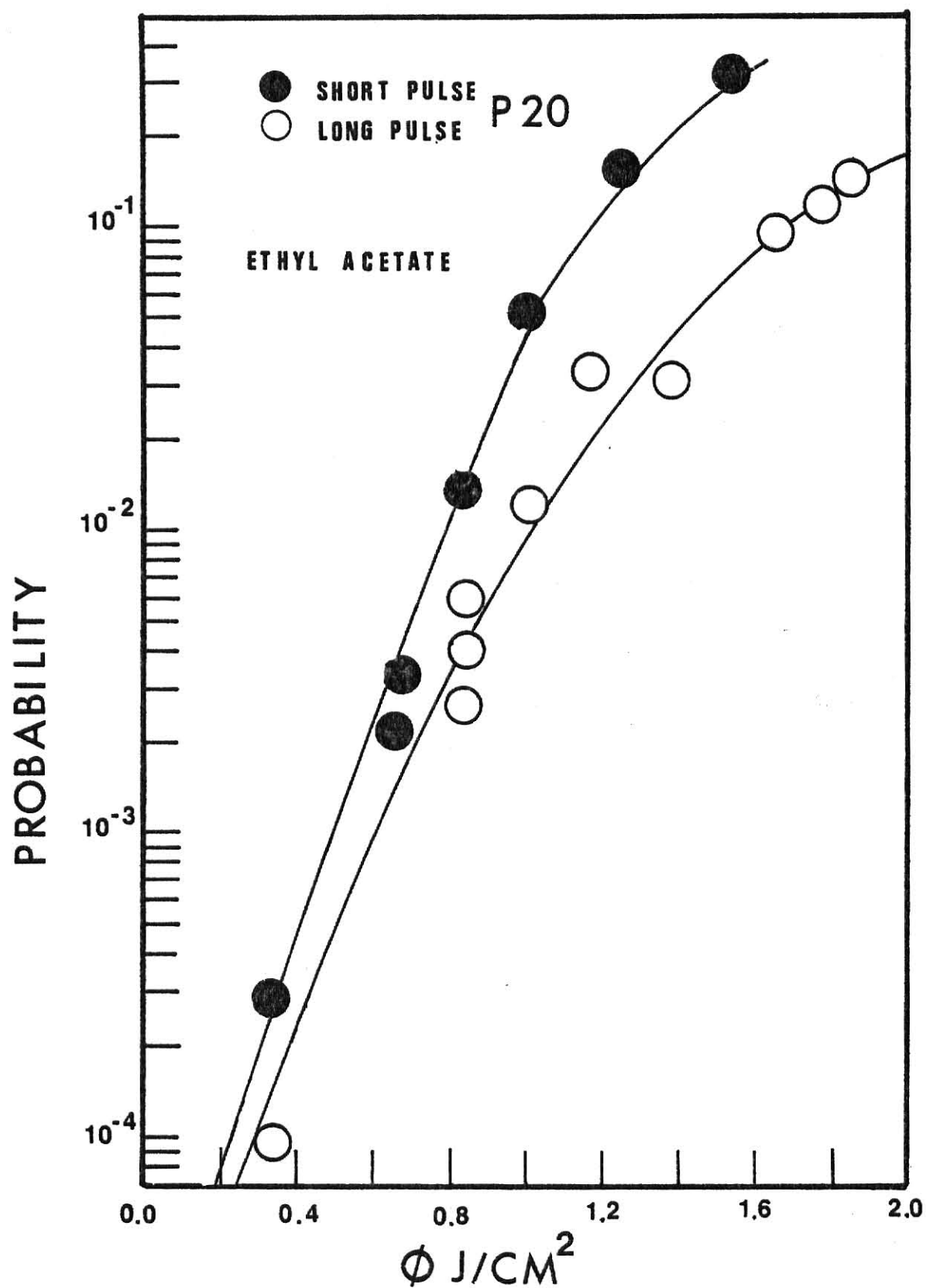
The effect of collisions between ethyl acetate and He, N_2 , isopropyl bromide, and other ethyl acetate molecules was investigated. The decrease in yield of ethyl acetate with the addition of a bath gas was shown as Stern-Volmer plots in Figs. 8 and 9. In all cases a sharp decrease in the yield of ethyl acetate was observed with addition of small amounts of bath gas at low fluence ($< 1 \text{ J/cm}^2$). For higher fluence ($> 5 \text{ J/cm}^2$), this decrease in yield was less severe. The bath gases differed in their ability to quench with isopropyl

bromide being the most effective and He and N₂ having comparable effect. The half quenching pressure (defined as the pressure of bath gas required to reduce the yield by 50%) for ethyl acetate was much smaller than those for small molecules activated by MPIUR.

The most puzzling aspect of the pressure dependence was that for pure neat samples. Experiments were done from 0.001 to 0.5 torr pressure with ethyl acetate at several different fluence and geometry conditions. For constant fluence and geometry the $P(\emptyset)$ values were independent of pressure. For high fluence (focused conditions) there may be a dependence upon geometry but for the conditions used in this work the effect was insignificant. Thus, $P(\emptyset)$ decreased with added gas pressure but was independent (up to 0.5 torr) of parent gas pressure. However, collisions were observed to result in sufficient intermolecular energy transfer to cause isopropyl bromide to react at pressures above 0.1 torr. The basic reason that pressure does not affect the $P(\emptyset)$ is that all of the molecules are excited and collisions only redistribute energy rather than remove energy. This will be examined more fully in the model section. This has the important implication that in the pure sample collisions are not the rate limiting factor for reaction. Rather, the cooling of the irradiated volume is the limiting factor.

2. Yield Dependence on Power.

The duration of the laser pulse can be varied by changing the amount of N₂ in the lasing mixture, producing pulses with different power for a given fluence. We investigated the effect of laser power on the MPIUR of ethyl acetate at $P(20)$ by using the short and long pulses (Fig. 3). No appreciable change in the $\log P(\emptyset)$ vs \emptyset plot (Fig. 33) for $P(\emptyset) < 10^{-3}$ was detected even though the power changed by a factor of ten. However, at higher reaction probability there may be a dependence of $P(\emptyset)$ on power with more reaction occurring for higher power at the same fluence. From the above one concluded that for laser pulses in the range of

FIG.33 $P(\phi)$ DEPENDENCE ON POWER

100 to 1000 ns., no dependence of the yield on power below 10% reaction was observed for ethyl acetate at 0.05 torr and the range of fluences shown in Fig. 33. Therefore we compared our yields on the basis of the laser fluences rather than power.

3. Yield vs Fluence for Esters.

In almost all of our work, the 1.3 s. long pulse was used. For the long pulse, the reaction probability of the esters investigated depended strongly on fluence at low $P(\phi)$ where there was a linear relationship between $\log P(\phi)$ and $\log \phi$. The values of the slopes for the linear portions of this plots ranged from 4.8 to 6.6 for the points with $P(\phi)$ below 10^{-2} .

At high $P(\phi)$, ($> 10^{-2}$), the $\log P(\phi)$ vs $\log \phi$ plot began to curve decreasing the magnitude of the slope until a constant value of $P(\phi)$ at high fluence (saturation) was observed. Focusing of the laser beam from 3 to 10 J/cm² was required for all esters in order to observe saturation. Considerable difficulty in measuring the irradiated volume made the measurement of $P(\phi)$ at high fluence somewhat uncertain. Nevertheless, saturation was observed in the sense that further increase in fluence produced little or no more reaction. The $P(\phi)$ values indicated that for some esters it was possible to obtain nearly 100% reaction at the saturation limit. For other cases still higher fluences may be required. This type of fluences were not readily obtained due to cracking of the NaCl windows, as mentioned in the experimental section. For the cases with $P(\phi) < 1.0$ at saturation, there also may be restrictions on the molecules at 300 K that can initially absorb energy. That is, not all quantum states are in resonance with the laser frequency.

An expression that has been used to represent the variation of $P(\phi)$ with ϕ is equation (12):

$$P(\phi) = C[1.0 - \exp(-(\phi/\phi_r)^n)] , \quad (12)$$

with C , n and ϕ_r being constants for a given molecule. C is

the saturation yield at \emptyset . For present purposes let $C = 1.0$. For $\emptyset/\emptyset_r \leq 1.0$ the exponential can be expanded to obtain

$$\log P(\emptyset) = \log[1.0 - [1.0 - (\emptyset/\emptyset_r)^n + (\emptyset/\emptyset_r)^{2n} - \dots]], \text{ and}$$

$$\log P(\emptyset) \approx \log (\emptyset/\emptyset_r)^n.$$

Thus, plots of $P(\emptyset)$ vs \emptyset give n , if the plots are linear in the low to moderate \emptyset region of a $\log P(\emptyset)$ vs $\log \emptyset$ plot. In order to check the behavior of the reaction probability with respect to fluence, the experimental data were plotted in section IV as $\log P(\emptyset)$ vs $\log \emptyset$ from which n values were obtained from the slopes of the linear portions. The n values are: 4.2, 6.0, 5.5, 5.0, 4.3 and 6.6 for ethyl acetate, ethyl fluoroacetate, sec-butyl acetate, n-butyl acetate, ethyl 2-bromopropionate and ethyl acrylate, respectively. These can be used together with \emptyset_r in equation (12). Figs. 34, 35, 36 and 37 show the experimental data plotted as $\log P(\emptyset)$ vs \emptyset for ethyl acetate, ethyl fluoroacetate, sec-butyl acetate and ethyl acrylate, respectively. Also plotted in the figures are the curves calculated using Eq. (12). It is evident that with the proper choice of n and \emptyset_r parameters, the curves calculated with Eq. (12) give a fairly good approximation to the experimental data. The agreement is especially good for ethyl acetate and ethyl acrylate.

In the case of ethyl fluoroacetate and sec-butyl acetate the calculated curves differed from the experimental results. For ethyl fluoroacetate, a change of \emptyset_r from 3 to 1.5 J/cm² resulted in a better agreement with low \emptyset experimental data and it was possible to get a reasonable analytical fit with Eq. (12). The disagreement at high \emptyset is a consequence of the saturation value being less than 1.0. By choosing $C < 1.0$ the fit can be improved. This disagreement was greatest for sec-butyl acetate, the reason being the much more gradual approach to the limiting $P(\emptyset)$. The fit could be improved at low $P(\emptyset)$ with lower \emptyset_r .

No precise values for the threshold energies of these reactions, which are the fluences at which the reactions

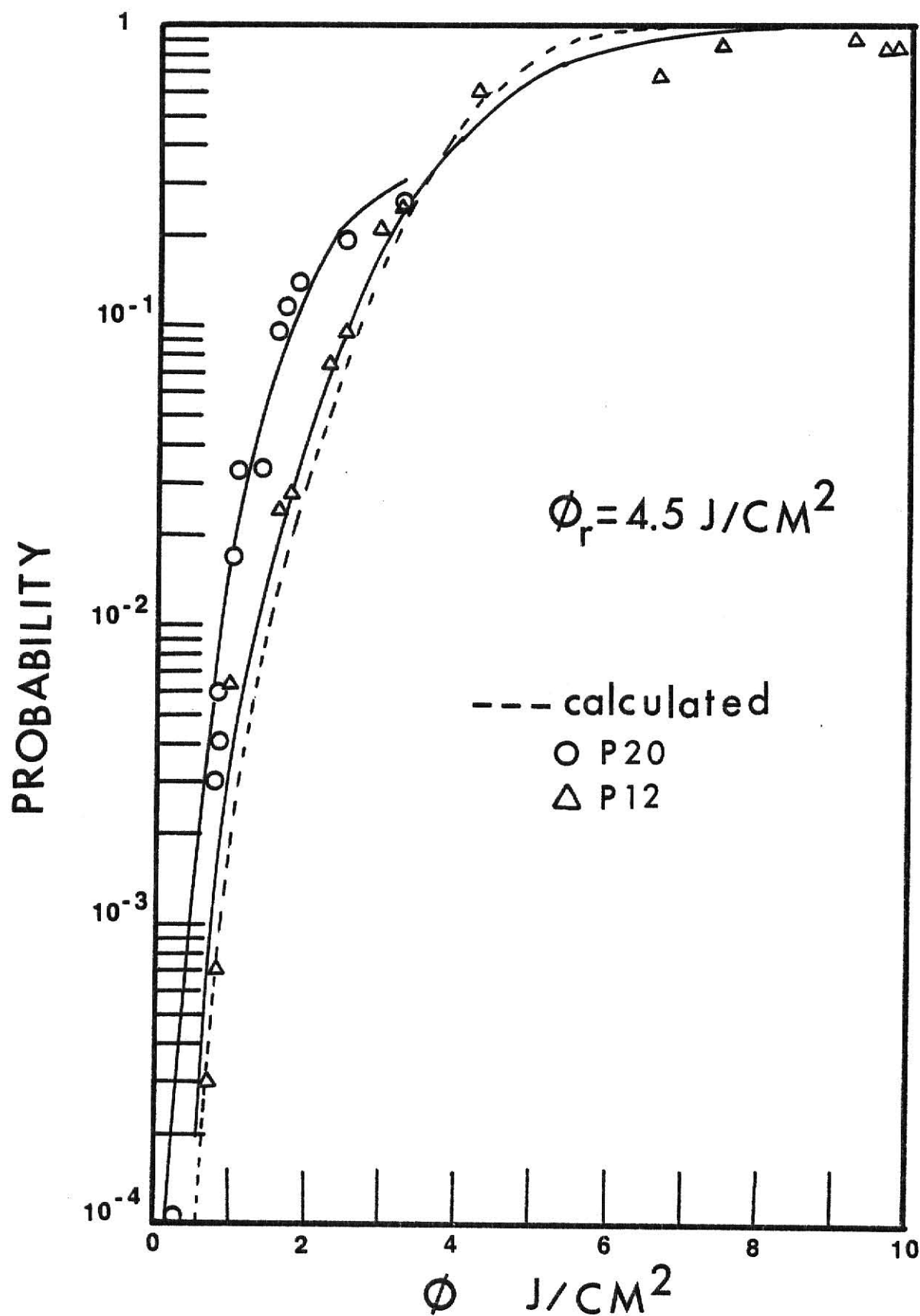


Fig. 34. Log $P(\Phi)$ vs Φ for Ethyl Acetate.

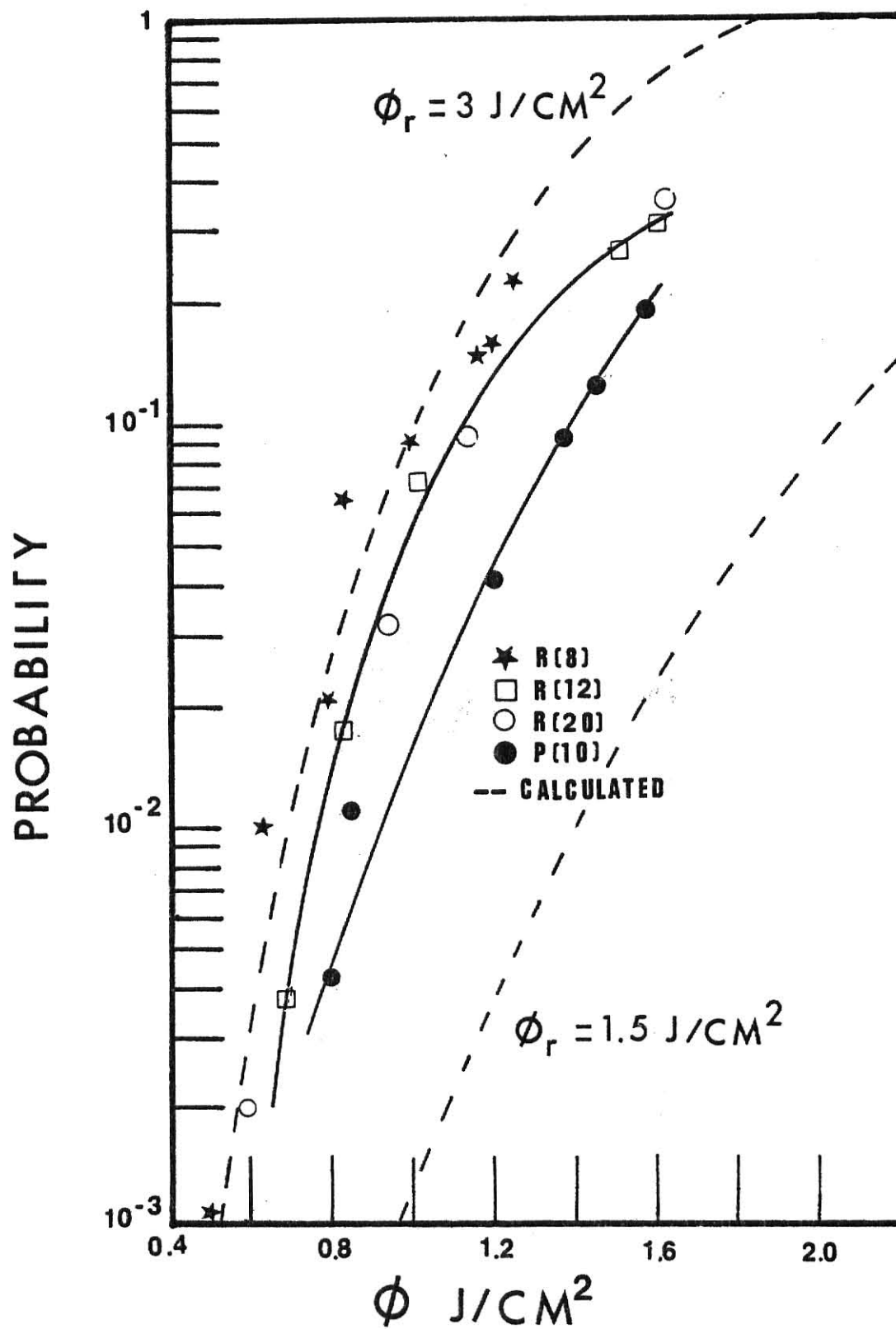


Fig. 35. Log $P(\phi)$ vs ϕ for Ethyl Fluoroacetate.

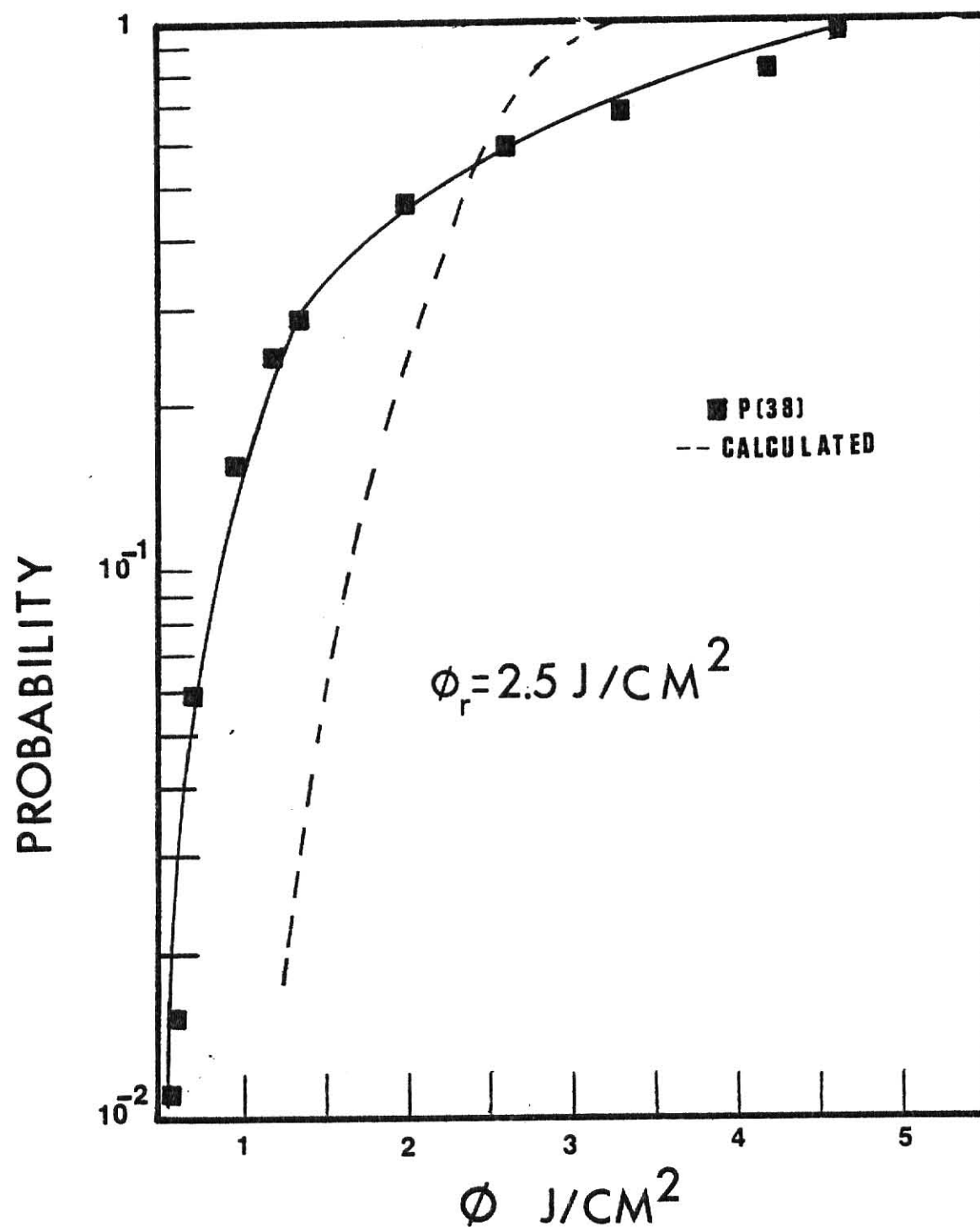


Fig. 36. Log $P(\Phi)$ vs Φ for sec-Butyl Acetate.

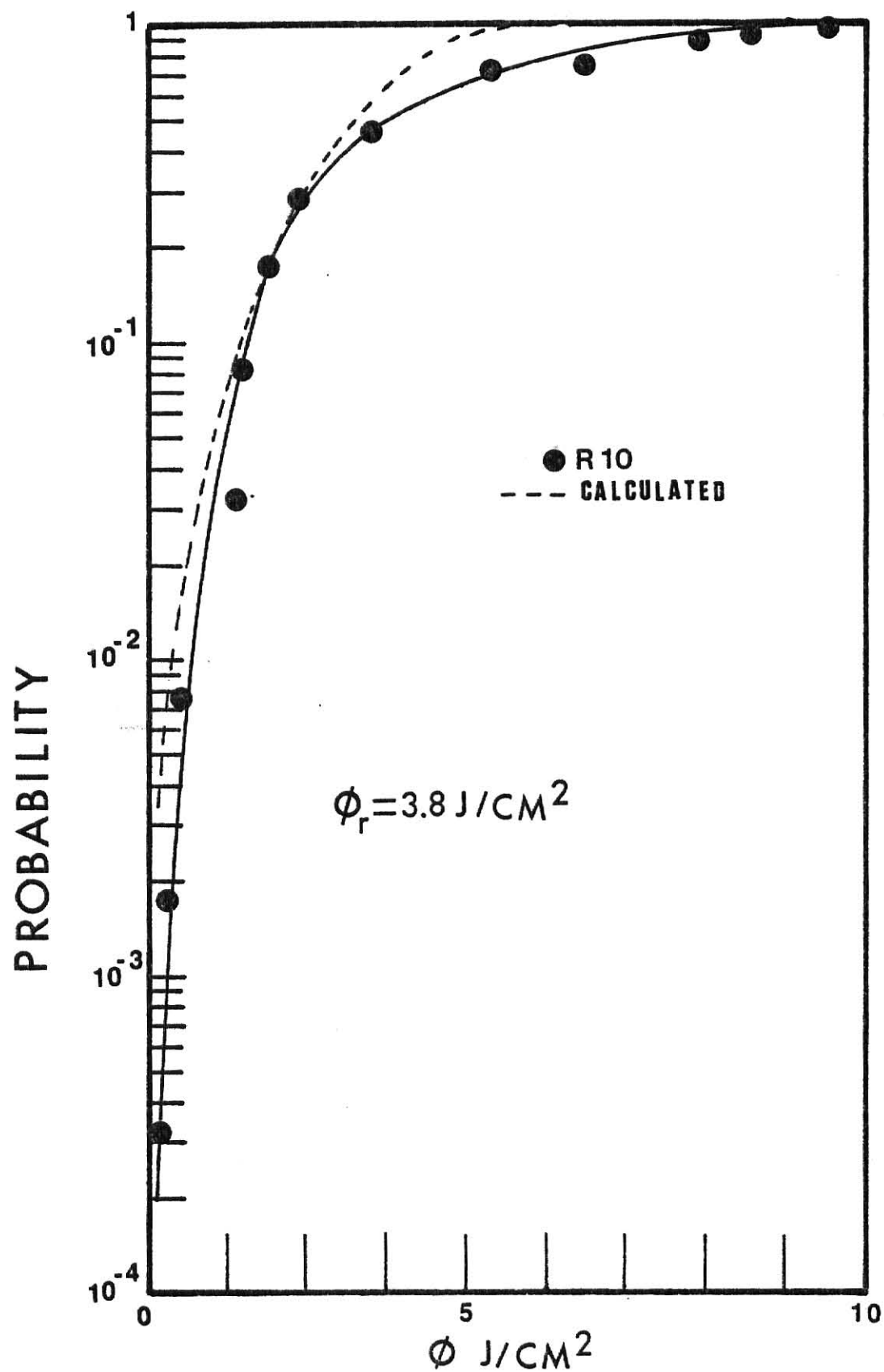


Fig. 37. Log $P(\phi)$ vs ϕ for Ethyl Acrylate

onset, can be cited. For our experimental measurements of $P(\emptyset)$ the energies at $P(\emptyset) = 10^{-4}$ are a good approximation to the threshold fluences. Experimental difficulties in measuring the yield become important and prevent the observation of $P(\emptyset)$ less than 10^{-4} .

In Table 44 are summarized the fluences, laser absorption cross sections, laser lines used and pressures used in the MPIUR of the esters that resulted in 50, 10, 1 and 0.1% reaction. Also included are the small signal cross sections, the thermal vibrational energies, the slopes, n , of the $\log P(\emptyset)$ vs $\log \emptyset$ plots, the threshold energies, and the \bar{n} and \bar{n}_r values. We are confident of the σ and σ_L data, as will be discussed in the next section. The $P(\emptyset)$ results are reliable but \emptyset itself is less certain.

From Table 44 a few general points can be noted: (i) The σ_L is the smallest for ethyl acrylate at 10, 1 and 0.1% reaction. The fluences required to achieve the specified $P(\emptyset)$ also are the highest for this molecule. (ii) Ethyl acetate and ethyl 2-bromopropionate have equal σ (within experimental error), and the \emptyset required to obtain the stated $P(\emptyset)$ are roughly the same for low $P(\emptyset)$ but differ by a factor of 2 at 50% reaction. The puzzling factor, however, is that, even though σ_L is lower for bromopropionate at high \emptyset , the required \emptyset is less than for ethyl acetate to give $P(\emptyset) = 0.5$ or 0.1. A plausible way to explain this behavior is for $E_0(\text{bromopropionate}) < E_0(\text{ethyl acetate})$. (iii) σ_L is larger for sec-butyl acetate than for n-butyl acetate and the corresponding \emptyset is lower for the same $P(\emptyset)$. However, the effect appears to be too large to explain by the σ_L differences alone and the measured \emptyset for sec-butyl acetate are thought to be in error. (iv) For $P(\emptyset) = 0.1$, σ_L (ethyl fluoroacetate) $\approx \sigma_L$ (ethyl acetate); but, the \emptyset is higher for ethyl acetate for same $P(\emptyset)$. The trend is the same for the four $P(\emptyset)$ values compared in Table 44. This trend may be explained by a lower E_0 (ethyl fluoroacetate) vs E_0 (ethyl acetate).

Table 44. Summary of $P(\emptyset)$, \emptyset , E_O , n , \bar{n} and \bar{n}_r for the MPIUR of Esters.

Ester	$P(\emptyset)$	\emptyset	σ	σ_L	\bar{n}	\bar{n}_r	line	n	P (torr)
Ethyl 2-Bromopropionate	0.5	2.7	3.4				R(14)	4.3	0.10
<u>sec</u> -Butyl Acetate	0.5	2.2	2.8				P(38)	5.5	0.07
Ethyl Fluoroacetate	0.5	2.5	2.3				R(20)	6.0	0.07
Ethyl Acetate	0.5	4.4	3.7				P(20)	4.2	0.05
<u>n</u> -Butyl Acetate	0.5	3.0	3.0				P(26)	6.0	0.10
Ethyl Acrylate	0.5	4.0	2.8				R(10)	6.6	0.05
Ethyl 2-Bromopropionate	10^{-1}	1.5		1.6	11.2	112			
<u>sec</u> -Butyl Acetate	10^{-1}	0.8		2.6	10.1	101			
Ethyl Fluoroacetate	10^{-1}	1.1		2.9	14.9	149			
Ethyl Acetate	10^{-1}	1.8		2.8	24.2	242			
<u>n</u> -Butyl Acetate	10^{-1}	1.8		2.0	17.4	174			
Ethyl Acrylate	10^{-1}	2.2		1.6	16.5	165			
Ethyl 2-Bromopropionate	10^{-2}	0.7		2.8	9.2	917			
<u>sec</u> -Butyl Acetate	10^{-2}	0.5		2.7	6.6	660			
Ethyl Fluoroacetate	10^{-2}	0.8		2.8	10.4	1045			
Ethyl Acetate	10^{-2}	0.9		3.2	13.8	1384			
<u>n</u> -Butyl Acetate	10^{-2}	1.3		2.5	15.7	1570			
Ethyl Acrylate	10^{-2}	1.6		1.9	14.2	1427			

Ethyl Fluoroacetate	10^{-3}	0.6	2.7	7.5	7556
Ethyl Acetate	10^{-3}	0.5	3.3	7.9	7933
<u>n</u> -Butyl Acetate	10^{-3}	0.9	2.7	11.7	11739
Ethyl Acrylate	10^{-3}	1.2	2.0	11.2	11268
Ethyl Acetate	10^{-4}	0.4	3.3	6.3	63443
Ethyl Acrylate	10^{-4}	1.0	2.0	9.3	93642

Energies are in kcal mole⁻¹ and cross sections are in 10⁻¹⁹ cm²/molecule. In order to obtain the total vibrational energy of the molecules the vibrational thermal contribution at 298 K must be added to the \bar{n} values, these being : 1.5, 1.3, 1.0, 1.0, 1.0, 1.3 and 1.3 photons for ethyl 2-bromopropionate, sec-butyl acetate, ethyl fluoroacetate, ethyl acetate, n-butyl acetate and ethyl acrylate, respectively.

Before more detailed examination of $P(\emptyset)$ vs \emptyset , σ_L , \bar{n} , \bar{n}_r , etc. can be made, some thought must be given to models.

4. Dependence of the Yield on Frequency.

The frequency of the laser line used to induce MPIUR had an effect on $P(\emptyset)$. This is more evident if $\log P(\emptyset)$ vs \emptyset plots are used instead of $\log P(\emptyset)$ vs $\log \emptyset$. Figs. 34 and 35 show these types of plots for ethyl acetate and ethyl fluoroacetate, respectively. One explanation of the dependence of $P(\emptyset)$ on frequency is that σ_L varies with frequency. In comparing σ is only a first approximation because of the strong red shift of the absorption band with laser fluence for MPA.

The magnitude of the red shift was proportional to the fluence. A red shift of 5 cm^{-1} at a fluence of 2 J/cm^2 was reported for ethyl acetate¹⁸. In general for two lines close together with similar σ , the one slightly to the red of the peak will be more effective in promoting reaction. As seen from Fig. 34 and 35, no marked dependence of the plots on the frequency of the line was observed unless the lines were far apart and with different σ . The least efficient lines were those lying to the blue of the absorption band because a red shift will only decrease the σ_L . On the red side of the band those lines lying far to the red, where the σ are small and a considerable red shift was necessary to increase σ_L , were also inefficient.

In order to remove the dependence of $P(\emptyset)$ upon σ_L , the yields should be compared on a plot of $P(\emptyset)$ vs absorbed energy. Unfortunately we were limited for such plots to the fluence range for which σ_L has been measured. Such plots will be examined in the conclusion section to as high a fluence as possible.

5. σ_L Dependence on Fluence.

The overall energy deposition cross section, σ_L , measured as described in section II.I were obtained for the esters investigated at some of the lines used to induce MPIUR. Our

absorption cross sections are compared to some obtained from other laboratories in Table 45. There is good agreement and we believe the σ_L are reliable. From results obtained in this work on the σ_L of the esters, the following was found: (i) A Beer's law type relationship where intensities have been replaced by fluences, was observed; this means that the σ_L values are pressure independent (from 0 to 5 torr). The lower limit was assumed because data were taken at 0.1 torr, which was sufficiently low that there are no collisions during the laser pulse. This independence of σ_L upon pressure simplified the consideration of energy absorption. For many small molecules the absorption cross section is pressure dependent. (ii) The σ_L extrapolated to a σ at low ϕ ($< 0.1 \text{ J/cm}^2$) in every case. (iii) There is significant dependence of σ_L on ϕ . (iv) The dependence of σ_L on ϕ varies with frequency. (v) The σ_L are power independent (for same $\phi < 1 \text{ J/cm}^2$) for pulses varying in length from 0.2 to 2 μs . This follows from the agreement of our σ_L with those from other laboratories which were done at 0.2 and 2 μs . while the pulse used in this work was 1.3 μs . No power dependence was also reported for SF_5NF_2 for pulses from ~ 200 to 1 ns. long³², this molecule can be considered a "large" molecule like the esters.

In order to find the cause of (iii), we did experiments with methyl acetate, a compound that does not undergo the characteristic six-centered elimination reaction. Methyl acetate was irradiated with the P(30), P(18) and R(14) lines, the infrared spectrum together with the σ_L vs ϕ plots are shown in Fig. 38. As seen from Fig. 38, this ester also showed a variation of σ_L with fluence. This indicated that the dependence of σ_L on ϕ did not result from product formation but must be explained by a red shift of the absorption at high fluence, power broadening, etc. For a red shift, the σ_L for P(30) could increase with ϕ ; however, up to a fluence of 0.90 J/cm^2 no change in σ_L occurred. It might be that in order for the red shift to cause an increase in the σ_L at this frequency, even higher fluence

Table 45. Laser Absorption Cross Sections.

Ester	ϕ J/cm ²	σ_L^*	$\bar{\nu}$	σ_L^{17}	$\bar{\nu}$	σ_L^{18}	$\bar{\nu}$
Ethyl Acetate	0.8	3.1 ± 0.3	P(20)	3.0 ± 1.0	P(18)	2.1 ± 0.2	P(22)
	0.2	3.3 ± 0.2	P(20)	3.5 ± 1.0	P(18)	3.5 ± 0.2	P(22)
Methyl Acetate	0.6	2.0 ± 0.3	P(18)	1.9 ± 1.0	P(16)		
	0.1	2.1 ± 0.2	P(18)	2.2 ± 1.0	P(16)		
Ethyl Fluoroacetate	0.7	3.2 ± 0.3	R(12)	3.1 ± 0.5	R(12)		
	0.1	2.3 ± 0.2	R(12)	2.3 ± 0.5	R(12)		
n-Butyl Acetate	0.7	2.7 ± 0.3	P(26)	2.6 ± 0.7	P(26)		
	0.2	2.9 ± 0.2	P(26)	2.7 ± 0.7	P(26)		
	0.6	2.0 ± 0.3	R(8)	2.0 ± 0.4	R(8)		
	0.4	2.2 ± 0.2	R(8)	2.1 ± 0.4	R(8)		
sec-Butyl Acetate	0.3	2.5 ± 0.3	P(38)	2.6 ± 0.6	P(38)		
	0.07	2.8 ± 0.2	P(38)	3.1 ± 0.6	P(38)		

σ_L must be multiplied by 10^{-19} cm²/molecule; the pulse durations were: 1300 ns. for σ_L^* measured in this thesis), 200 ns. for Ref. 17 and 2000 ns. for Ref. 18.

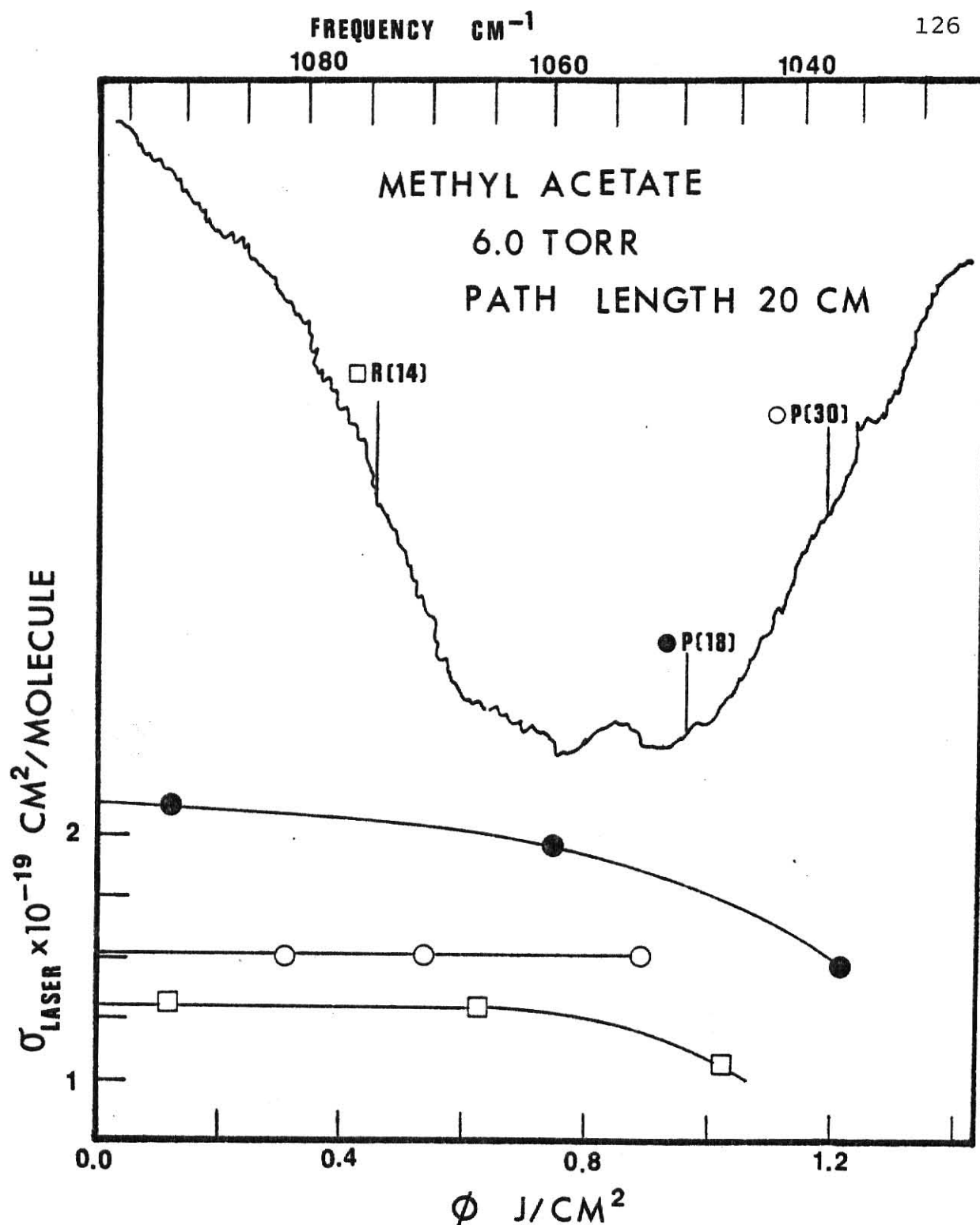


Fig. 38. Infrared Spectrum and σ_L vs ϕ pot for Methyl Acetate.

is required. On the other hand, the other two cross sections did decline. Therefore, on a relative basis, σ_L (P30) did increase. A decrease of σ_L with ϕ was observed for P(18) and R(14). The σ_L began to differ from σ at a fluence of $\sim 0.4 \text{ J/cm}^2$ for P(18) and $\sim 0.8 \text{ J/cm}^2$ for R(14). It is evident that one cannot predict the fluence for which σ_L start to change and how they will change with increasing ϕ .

An experiment was done to investigate the σ_L value at high ϕ with high pressure of buffer gas. A linear relationship was still observed between log transmittance vs pressure for a mixture of 4% ethyl 2-bromopropionate and 96% helium over the 1 to 8 torr pressure range. For this mixture, σ_L was independent of pressure. The observed constant σ_L was equal to σ , and did not decline with ϕ in the way that was observed in the absence of inert gas. The explanation may be that collisions of the excited ester molecules with helium atoms, which continually removed the vibrational energy, prevented the ester molecules from reaching high vibrational levels. Thus, the red shift never occurred. This experiment needs to be repeated with smaller amounts of helium to characterize the dependence of σ_L on added helium.

The variation of σ_L with ϕ remains difficult to explain with large molecules, as well as others. Work by Deutsch³³ on the dependence of optoacoustic signal (which is directly proportional to σ_L) on the fluence for SF_6 at 298 K and 145 K suggested that red shifts might be the explanation of the σ_L dependence on ϕ at low temperature where hot bands are essentially eliminated, whereas at 298 K the red shift did not account for the observed behavior of σ_L with fluence. Energy deposition measurements for vinyl chloride³⁴ showed that σ_L depended on laser power. Considerable power broadening was observed in going from a 180 ns. to a 45 ns. pulse. For this molecule adding helium increased σ_L . Both of these features are characteristic of molecules with bottlenecks in the low energy regime. Evidently the ester molecules do not have a low bottleneck. This is, at least, one simplifying feature of the large molecules.

C. A Simple Model for MPIUR.

Our objective was to develop a model that permits the estimation of the yield from laser induced reactions of ethyl acetate and butyl acetate for low to moderate extent of reaction. The objective was not realized because some of the basic assumptions proved to be inapplicable. The model is more appropriate for the case of MPIUR in an inert bath gas with the heat capacity of the bath gas larger than the heat capacity of the molecule absorbing the laser energy. However, the model does provide some insight into the MPIUR of neat samples. We assume that the pressure is sufficiently low that collisions during the laser pulse can be ignored. We also assume that the extent of reaction after the pulse ends is negligible. This assumption, which only applies at low percent reaction, is a consequence of the small rate constants for a big molecule near the threshold energy.

We assume that the distribution can be represented as a Boltzmann distribution with the average energy, $\bar{n}h\nu$, measured from the laser absorption cross sections, defining the temperature. Although a Boltzmann distribution may not be precisely correct³⁵, ladder climbing type computations with reasonable values for the individual cross sections give broad distributions closely resembling Boltzmann distributions³⁶. The assumption of a Boltzmann population as an initial vibrational energy distribution due to laser pumping is very convenient because the energy absorbed per molecule defines the distribution. If a parametrized form of the distribution is not assumed, then one needs to know the absorption cross sections for each level to solve the master equation and such data are difficult to obtain or even estimate reliably. Other types of distributions such as the Poisson, have been used but the ladder climbing calculations suggest that the breadth of the distribution is larger than the Poisson type. Boltzmann distributions for ethyl acetate and *n*-butyl acetate are shown in Figs. 39 and 40. These were calculated with accurate accounting for the density of states, N_E . As the final assumption, we consider that the degree of

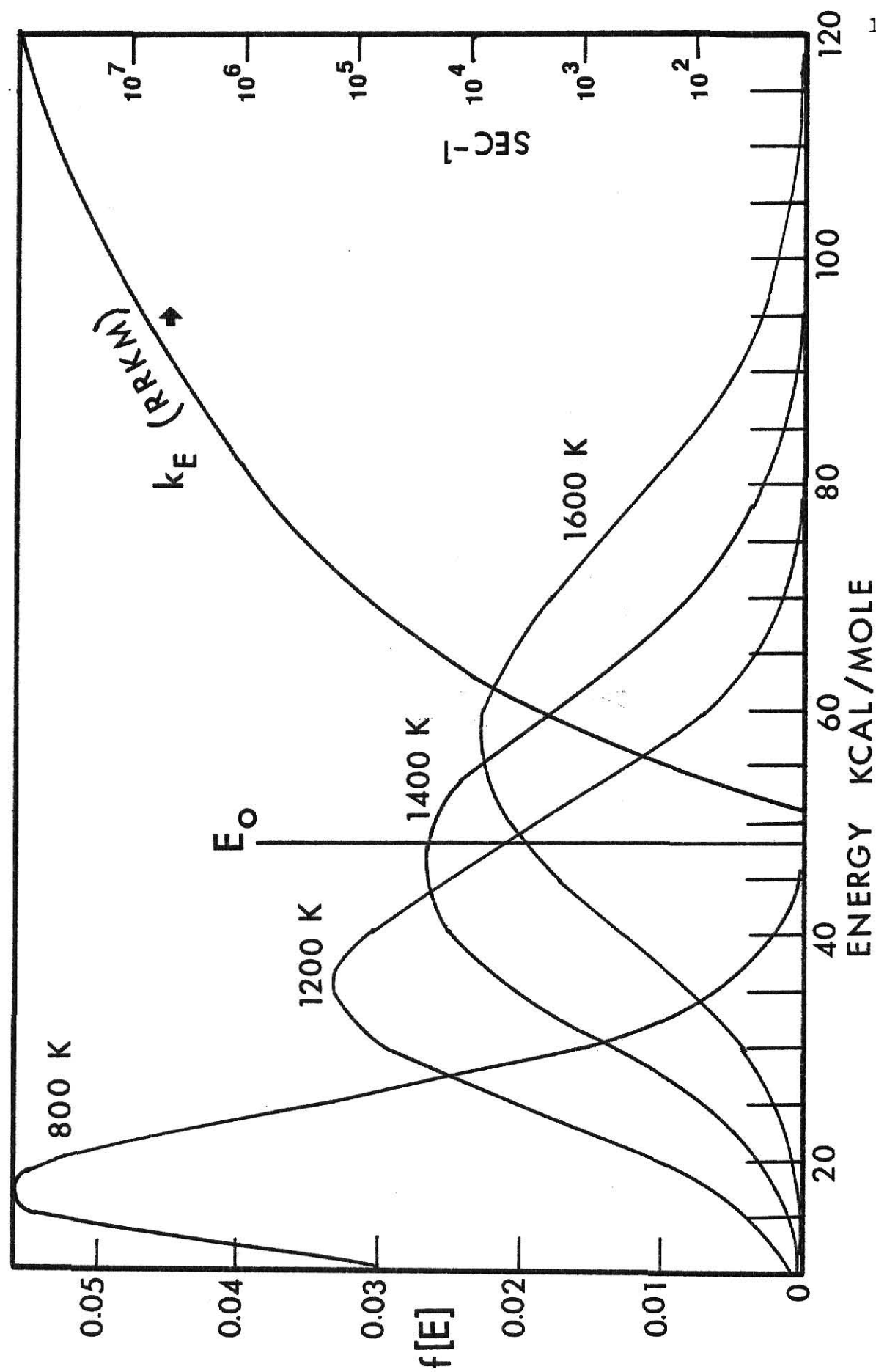


FIG.39 BOLTZMANN DISTRIBUTIONS FOR ETHYL ACETATE

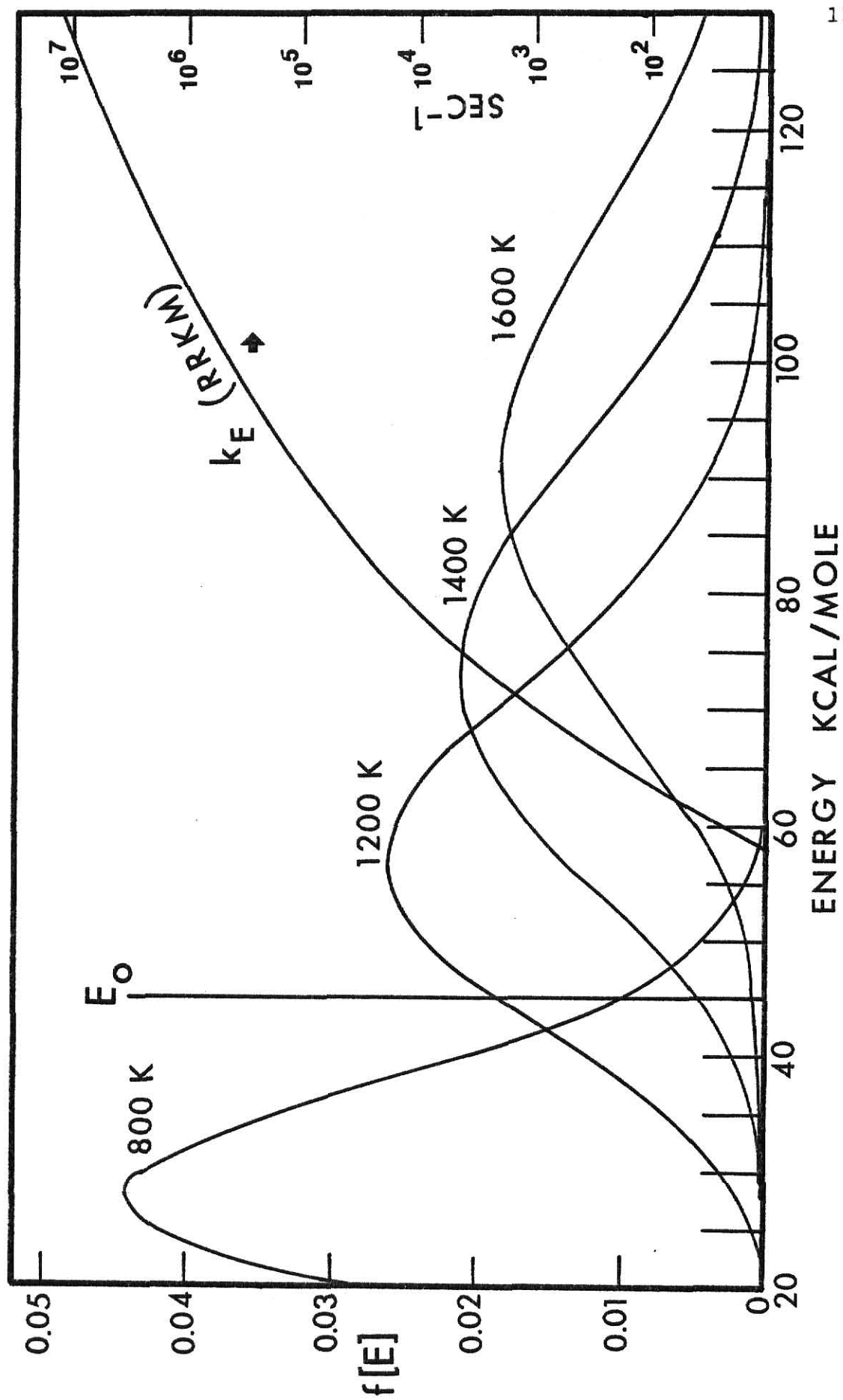


FIG.40 BOLTZMANN DISTRIBUTIONS FOR N-BUTYL ACETATE

reaction is governed by the competition between collision and reaction (with rate constant K_E) for each energy region of the distribution above E_0 . This assumption is what renders the model appropriate only for experiments with large amounts of cold, inert bath gas. According to this model, one must only compute the probability for reaction vs collisional deactivation for molecules of energy E_i .

We assume that the rate of vibrational redistribution is rapid relative to the rate of reaction allowing the use of the RRKM theory of unimolecular reactions to predict the rate constants vs vibrational energy. The RRKM rate constants are presented in appendix I. Under collision free conditions, all molecules above E_0 will react and these fractions are given in Figs. 41 and 42 for ethyl acetate and *n*-butyl acetate. Providing that these distributions govern the rate of reaction, the mean reaction rate constant is just the normal thermal unimolecular high pressure rate constant.

$$\int_{E_0}^{\infty} k_E f(E) dE = k_{\infty}(T).$$

These values, together with $\langle E \rangle$ and T are tabulated in Table 46.

For experiments performed in static cells one needs to account for the detrimental effect that collisions between excited ester molecules and quencher have on the reaction probability. In this section we will assume that the heat capacity of the reservoir gas is sufficiently high that no heating occurs. We also assume that diffusional effects, momentum transfer via shock wave, thermal conductivity, geometry etc. have no role. Thus, collisional deactivation is the only process competing with reaction. For large organic molecules like the esters considered here, which have relatively long lifetimes above the threshold energy for reaction, the collisional problem is severe. To apply a full master-equation treatment or even to follow the time

Table 46. $k_{\infty}(T)$, T , and $\langle E \rangle$ values for Ethyl Acetate and Butyl Acetate.

Ethyl Acetate			Butyl Acetate	
$k_{\infty}(T)$ sec ⁻¹	$\langle E \rangle$ kcal mole ⁻¹	T, K	$k_{\infty}(T)$ sec ⁻¹	$\langle E \rangle$ kcal mole ⁻¹
3.4×10^{-3}	14.6	700	1.4×10^{-2}	22.4
3.0×10^{-1}	18.7	800	9.0×10^{-1}	28.8
9.6×10^0	23.1	900	2.1×10^1	35.8
1.6×10^2	27.8	1000	3.2×10^2	43.2
1.5×10^3	32.8	1100	2.8×10^3	51.0
1.0×10^4	38.0	1200	1.6×10^4	59.1
5.3×10^4	43.5	1300	7.8×10^4	67.5
2.1×10^5	49.0	1400	2.9×10^5	76.1
7.3×10^5	54.8	1500	9.2×10^5	85.0
2.1×10^6	60.6	1600	2.5×10^6	94.0
5.5×10^6	66.6	1700	6.1×10^6	103.2
1.3×10^7	72.7	1800	1.4×10^7	112.5
2.8×10^7	78.9	1900	2.8×10^7	122.1
5.5×10^7	85.2	2000	5.3×10^7	131.5

evolution starting with a Boltzmann distribution, it is necessary to assume values for a large number of level-to-level energy transfer rate constants. Vibrational deactivation of highly excited polyatomic molecules has been studied using chemical and thermal activation experiments³⁷. From these experiments values of 4 to 8 kcal/mole for the average energy lost per collision of molecules ($E > E_0$) with cold polyatomic molecules seems appropriate. If the reservoir bath gas is appreciably "heated", then the mean energy lost per collision will have to be reconsidered. The simplest model is a step ladder model which assumes that each collision removes an average energy $\langle \Delta E_d \rangle$. The step-ladder model has the property that a particular average energy loss, $\langle \Delta E_d \rangle$, is much more probable than any other transition.

For a given vibrational energy level, i , the population is N_i and the fraction of this population that reacts is

$$f_R = N_i \frac{k_{E_i}}{k_{E_i} + w} .$$

The fraction of the population that is deactivated and transferred to a new level, $\langle \Delta E_d \rangle$ below the original level is

$$f_D = N_i \frac{w}{k_{E_i} + w} .$$

In these equations k_{E_i} is the rate constant for level i and w is the collisional frequency. The latter may be calculated as 5.18×10^5 and 1.64×10^6 collisions per second for ethyl acetate and *n*-butyl acetate at 0.05 and 0.1 torr, respectively.

As the molecules cascade down the energy ladder in increments of energy $\langle \Delta E_d \rangle$, the probability for successive reaction drops significantly because k_E declines exponentially with reduced E . When molecules are deactivated below E_0 , no reaction occurs.

The results of the calculations are shown in Figs. 41 and 42. The calculated yield vs \bar{n} are plotted for ethyl acetate and n-butyl acetate. The curves labeled "collision free" are the yields if all molecules above the threshold energy reacted. These can be compared with the curves calculated for the various assumed pressures and collisional deactivation models. The first point to note is that the computed curves especially for ethyl acetate, have the correct general shape, rising rapidly with energy and asymptotically approaching 100% reaction. The effect of collisions is to dramatically reduce the yield with the extent of reduction decreasing with higher average energy.

For 10 absorbed photons and $\langle \Delta E_d \rangle = 1500 \text{ cm}^{-1}$, the yields are reduced by factors of 50 to 120 for ethyl acetate and n-butyl acetate, respectively, to give yields of 0.1% and 0.05%. For $\bar{n} = 15$ photons, the reduction factors are 10 and 30, respectively. This model does serve to explain the dramatic reduction in yield when isopropyl bromide was used as a bath gas with ethyl acetate. It also explains why the extent of quenching was reduced for higher ϕ (higher \bar{n}).

The effect of variation of pressure and the $\langle \Delta E_d \rangle$ values were examined for ethyl acetate and n-butyl acetate. For both esters increasing $\langle \Delta E_d \rangle$, decreases the yield but the effect is more severe for n-butyl acetate. A few calculations were done for small $\langle \Delta E_d \rangle$. In the limit of $\langle \Delta E_d \rangle = 0$ the collisions have no effect. Even for $\langle \Delta E_d \rangle = 350 \text{ cm}^{-1}$ the effect is small and not very dependent on pressure i. e. essentially the same result was obtained at 0.1 and 0.01 torr. However, a much stronger effect was found at $\langle \Delta E_d \rangle = 1500 \text{ cm}^{-1}$, and $\bar{n} = 14$ photons the yield changed from 0.01 to 0.02 to 0.04 for a change from 0.2 to 0.05 to 0.005 torr of ethyl acetate, respectively. For the same $\langle \Delta E_d \rangle$ and \bar{n} values the yield changed from 0.0038 to 0.0042 to 0.0070 for a change from 0.1 to 0.05 to 0.01 torr of n-butyl acetate, respectively. The reason the small $\langle \Delta E_d \rangle$ are so ineffective has to do with the large breadth of the distribution functions

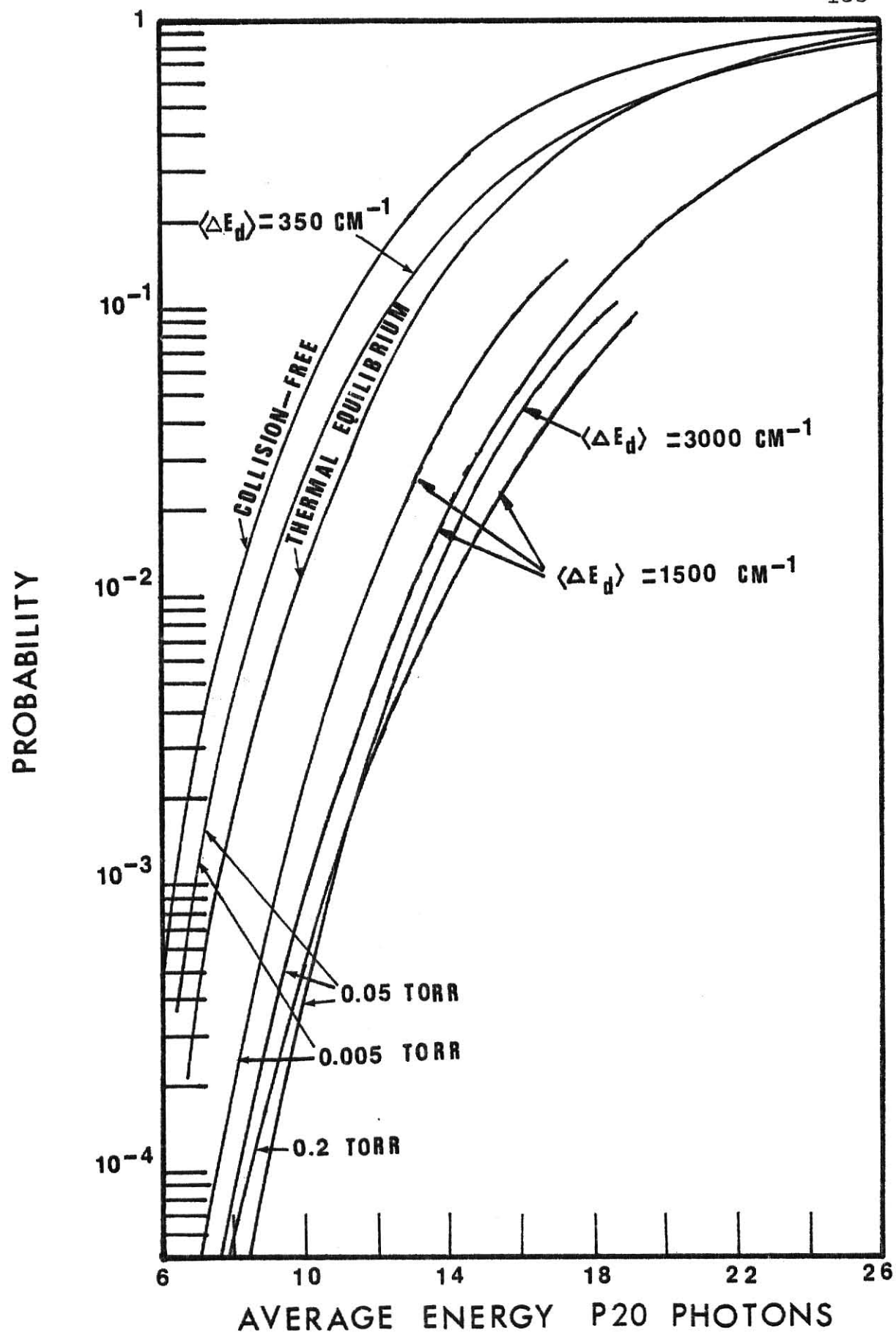


Fig. 41. Model Calculated Curves for Ethyl Acetate.

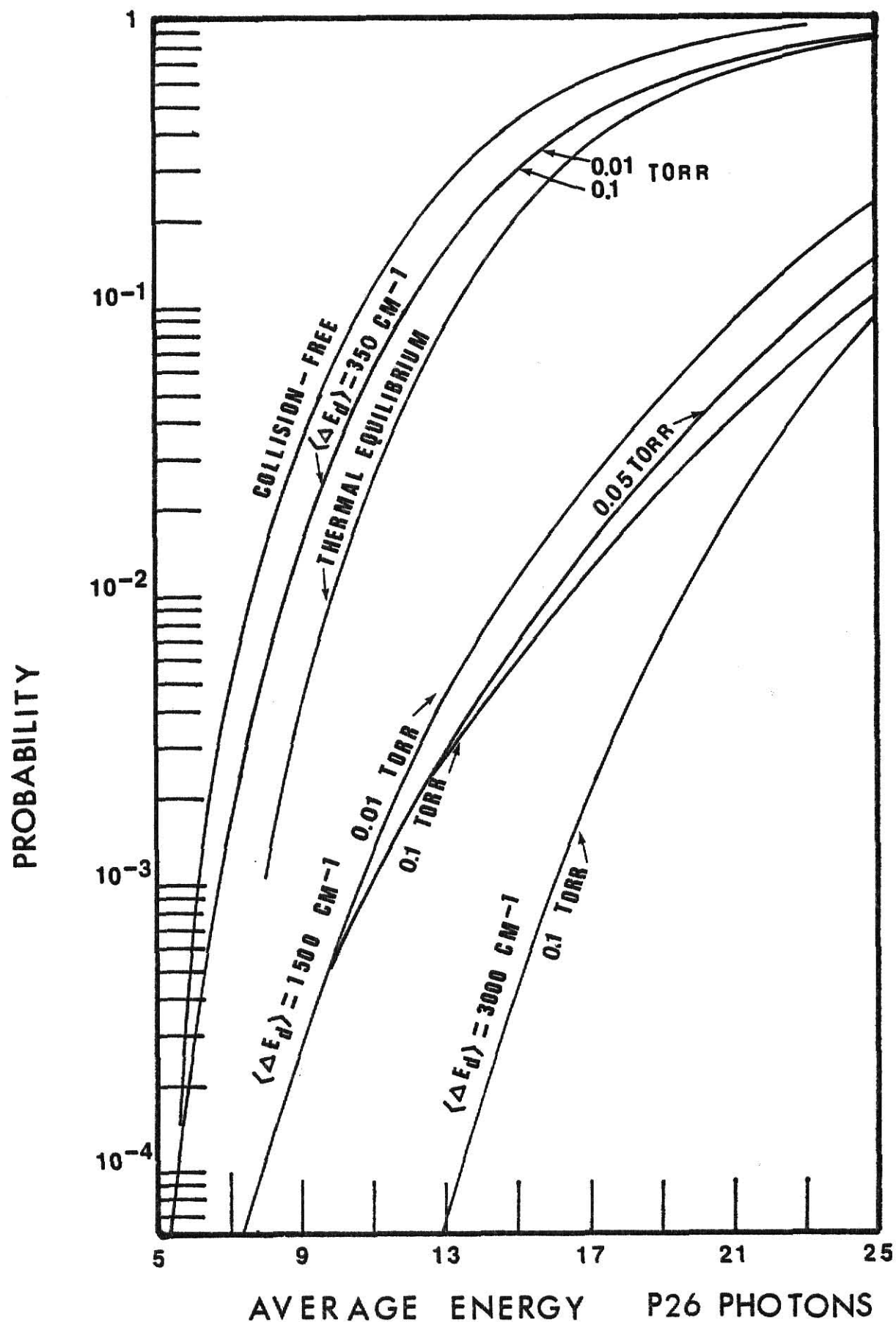


Fig. 42. Model Calculated Curves for *n*-Butyl Acetate.

the loss of 1-2 kcal/mole does not reduce the yield very much. The variation of the yield with pressure explains the non-linear shape of the Stern-Volmer plots. For n-butyl the pressure effect is noticed more at higher ϕ .

D. Deficiencies of Model for Neat Samples.

By assumption, the model ignored any contribution to the reaction yield during the laser pulse. To estimate when this assumption fails, one can examine the fraction of the molecules with lifetimes $< 5 \times 10^{-7}$ sec, which corresponds to one-half of the period of the laser pulse. Integration of the distribution from the energy giving this k_E to ∞ gives an estimate of the fraction of the distribution that will react during the pulse. This fraction is tabulated in Table 47 for various temperatures.

For low pressure ≤ 0.1 torr, this fraction also will not be collisionally stabilized since $k_E < w$. This fraction must be compared to the amount of post pulse reaction, which are the results presented in Figs. 41 and 42. This, of course, depends on the collision model and the results for $\langle \Delta E_d \rangle$ of 1500 and 3000 cm^{-1} which are also given in the Table for 0.05 and 0.10 torr of ethyl acetate and n-butyl acetate, respectively. From the Table it is seen that the contribution during the pulse becomes $\sim 10\%$ of the reaction at 1200 K ($\bar{n} = 13$) or $f_{\text{pulse}} = 0.0008$ and 1280 K ($\bar{n} = 22$) or $f_{\text{pulse}} = 0.006$ for ethyl acetate and n-butyl acetate, respectively at $\langle \Delta E_d \rangle = 1500 \text{ cm}^{-1}$. This difference in f_{pulse} is caused by the much more broad distributions of n-butyl acetate compared to ethyl acetate (see Figs. 39 and 40).

This calculation, of course, is for the cold bath gas case. In neat samples the reaction during the pulse will be the same but the total extent of reaction may be larger than given by the collision limited model. Thus, the yield should be dominated by post pulse behavior up to $\approx f = 0.01$ to 0.05.

Table 47. Fraction of Reaction Predicted by Model compared to Fraction of Reaction During the Laser Pulse.

Ethyl Acetate, 0.05 torr				n-Butyl Acetate, 0.10 torr			
$\langle E_d \rangle = 1500$		$\langle E_d \rangle = 3000$		$\langle E_d \rangle = 1500$		$\langle E_d \rangle = 3000$	
T	f_{model}	f_{model}	\bar{n}	f_{pulse}	f_{model}	f_{model}	f_{pulse}
600	1.2×10^{-9}	2.0×10^{-11}	3.7	4.0×10^{-16}	1.2×10^{-6}	4.3×10^{-9}	1.0×10^{-18}
800	3.6×10^{-6}	5.4×10^{-7}	6.2	2.1×10^{-9}	4.3×10^{-4}	2.0×10^{-6}	2.5×10^{-10}
1000	3.7×10^{-4}	1.8×10^{-4}	9.3	7.1×10^{-6}	5.5×10^{-3}	2.7×10^{-4}	5.7×10^{-6}
1200	8.3×10^{-3}	5.8×10^{-3}	12.7	8.4×10^{-4}	2.8×10^{-2}	9.6×10^{-3}	1.5×10^{-3}
1400	6.1×10^{-2}	5.0×10^{-2}	16.4	1.5×10^{-2}	1.3×10^{-1}	8.6×10^{-2}	3.5×10^{-2}
1600	2.1×10^{-1}	1.8×10^{-1}	20.3	8.7×10^{-2}	3.7×10^{-1}	3.0×10^{-1}	1.9×10^{-1}
1800	4.3×10^{-1}	3.9×10^{-1}	24.3	2.5×10^{-1}	6.6×10^{-1}	5.8×10^{-1}	4.9×10^{-1}
2000	6.5×10^{-1}	6.1×10^{-1}	28.4	4.7×10^{-1}	8.5×10^{-1}	8.0×10^{-1}	7.5×10^{-1}

The other serious assumption is that the heat capacity of the reservoir gas is sufficient to preclude "heating" of the irradiated volume. We must evaluate this assumption for irradiation of a pure sample where the irradiated molecules themselves provide the only reservoir bath gas. Providing that there is no significant cooling by diffusion, convection, or by thermal conductivity, the equilibrium energy, $\langle E \rangle$, of the irradiated volume is given by

$$\langle E \rangle = \int_{300}^T C_v(T) dT = \langle E_{\text{vib}} \rangle + E_{\text{rot}} + E_{\text{trans}} = \\ \langle E_{\text{vib}}^f \rangle + 3R (T-300).$$

Where $\langle E \rangle$ is the total absorbed energy and $\langle E_{\text{vib}}^f \rangle$ is the mean vibrational energy at temperature T . The average energy in units of \bar{n} will be raised by at least one more photon due to the contribution of $\langle E_{\text{vib}} \rangle$ at 300 K. These contributions (1 and 1.3 photons for ethyl acetate and *n*-butyl acetate, respectively) must be added to the \bar{n} values for Figs. 41 and 42. This extra amount of energy will raise the final temperature a small amount.

For ethyl acetate at high initial excitation, T_f is only 145° lower than the initial vibrational temperature because only 8-9 kcal/mole are lost. For 1000 K initial temperature, T_f is only 115 K lower. For *n*-butyl acetate, T_f is about 90 K lower than the initial Boltzmann temperature of 1400 K, while T_f is 75 K lower for a 1000 K initial temperature. Some of the T_i^V and T_f together with their respective $\langle E \rangle$ and $\langle E_{\text{vib}}^f \rangle$ are tabulated in Table 48.

Table 48. T_i^V , T_f , $\langle E \rangle$ and $\langle E_{vib}^f \rangle$ for Collisionless and Equilibrium Conditions for Ethyl Acetate and n-Butyl Acetate.

Ethyl Acetate				<u>n</u> -Butyl Acetate			
T_i^V	$\langle E \rangle$	T_f	$\langle E_{vib}^f \rangle$	T_i^V	$\langle E \rangle$	T_f	$\langle E_{vib}^f \rangle$
1600	60.6	1455	51.9	1400	76.1	1310	68.3
1400	49.0	1260	41.4	1200	59.1	1115	52.5
1200	38.0	1075	31.6	1000	43.2	925	37.7
1000	27.8	885	22.5	800	28.8	735	24.4
800	18.7	700	14.4	700	22.4	640	18.9

The results in Table 48 unequivocally show that the collisional model is inappropriate for irradiation of neat samples. Because of the small heat capacity of the translational and rotational degrees of freedom, relative to that of the internal degrees of freedom, collisions can only modestly reduce the mean vibrational energy rather than remove sufficient energy to cause all molecules to have $k_E < w$. This is demonstrated graphically in Figs. 41 and 42 by plotting the fraction of the distribution functions still remaining above E_0 after the energy has been equilibrated by collisions. Several collisions may be required to achieve the equilibrium; but, the important point is that collisions within the irradiated volume can not quench the reaction in irradiation of neat samples of large molecules.

After the equilibrium condition is reached, the irradiated sample will continue to react with depletion of molecules occurring by an ordinary thermal reaction:

$$[A] = [A]_0 e^{-k \Delta t}; \quad k = k_{\infty}(T).$$

The limitation to the time is provided by bulk transport processes that result in cooling. Unfortunately, this is difficult to define by our model. It is possible to get estimates of Δt by using the yields and the $k_{\infty}(T)$ values. The Table below gives estimates of Δt for these temperatures. At low temperatures, considerable deactivation may result during the collisional phase and the Δt has little significance. However, for $P(\phi) \approx 0.01$ the times are comparable to the laser pulse length. The cooling mechanism is difficult to envision. In fact, the thermal monitor experiments showed that the Δt are sufficiently small to make thermal reactions negligible and the times must be less than those shown in Table 49. Thus, one has a difficult situation at 0.05-0.1 torr pressure. The monitor experiments demonstrated no thermal reaction (i. e. no extensive intermolecular energy transfer). This means that cooling must occur faster than shown in Table 49 to prevent reaction.

At high $P(\phi)$ the thermal reaction will be augmented by reaction during the pulse and for $P(\phi) \geq 0.4$, one may expect much of the reaction to occur during the course of the laser pumping, as well as, by the reaction during the period governed by cooling. Again monitor experiments show no heating and some very efficient cooling mechanisms must be involved to explain why thermal reaction does not occur. Of course thermal reaction does occur if the pressure is raised slightly.

Table 49. Δt Estimates for Different T.

Ethyl Acetate			<u>n</u> -Butyl Acetate	
P(\emptyset)	t sec.	T K	P(\emptyset)	t sec.
1.2×10^{-4}	4.0×10^{-4}	800		
3.5×10^{-4}	3.6×10^{-5}	900	5×10^{-4}	2.4×10^{-5}
9.0×10^{-4}	5.6×10^{-6}	1000	6×10^{-3}	1.9×10^{-5}
4.5×10^{-3}	4.5×10^{-7}	1200	2×10^{-1}	1.4×10^{-5}
1.8×10^{-2}	8.6×10^{-5}	1400		
5.5×10^{-2}	2.7×10^{-8}	1600		

The t are obtained from the reciprocal of $k_{\infty}(T)$, these rate constants together with P(\emptyset) and T were given by the collisional model.

VI. CONCLUSIONS.

From this study of the MPA and MPIUR of organic esters, some general conclusions can be drawn. These conclusions are based on experiments done under conditions such that no thermal enhancement in the reaction occurs, as observed from thermal monitor experiments.

1) Initially, all the absorbed laser energy is deposited as vibrational energy. To measure the extent of the energy transfer from excited ester molecules to cold molecules by collisions, a small percent of a "thermal monitor" was added to ethyl acetate. Experiments done with a 3% isopropyl bromide, 97% ethyl acetate mixture at 0.05 torr indicated that the reaction probability of isopropyl bromide was much smaller than the reaction probability of ethyl acetate at all fluences studied. At 0.05 torr most of the dissociation undergone by ethyl acetate is laser induced, but at higher pressures (≥ 0.1 torr) an important fraction of the reaction occurs as a consequence of intermolecular energy transfer.

2) The $P(\emptyset)$ values measured in this work were not affected by the irradiation geometry. It was found that $P(\emptyset)$ was reduced if the irradiated cross section was less than $\sim 0.5 \text{ cm}^2$. All of our experiments were done with beams of cross sectional areas $> 0.7 \text{ cm}^2$. This effect of geometry may be due to a change in the rate of cooling of the irradiated volume, when the irradiated cross sectional area is reduced to such an extent that diffusion rate of cold and hot molecules becomes important.

3) The ester dissociation follows first order kinetics, with the number of pulses serving as time.

4) The reaction probability (defined as the number of molecules that react per pulse divided by the number of parent molecules in the irradiated volume) is independent of pressure (for neat samples), in the range from 0.002 to 0.5 torr.

5) Although the yield is independent of parent pressure, addition of a small amount of bath gas reduces the yield

significantly especially at low fluence, with large quencher molecules being more effective deactivators than diatomic molecules or monatomic gases.

6) For the six esters studied a plot of $\log P(\phi)$ vs $\log \phi$ showed an approximately linear behavior for $P(\phi)$ from 10^{-2} to 10^{-4} . At higher $P(\phi)$ the curve asymptotically approached a constant value; this typically occurs at $\phi > 4 \text{ J/cm}^2$. The high value of the slope of the linear portion of the $\log P(\phi)$ vs $\log \phi$ plots (from 4 to 6) reflects the strong dependence of the reaction probability on fluence.

7) The duration of the laser pulse could be varied from 1.3 to 0.13 microseconds, giving pulses of power differing by a factor of ten for a given fluence. Experiments done with ethyl acetate using low and high power pulses indicated that for $P(\phi) \leq 0.1$, no significant dependence of the yield on power results. However, the high power pulse may be more effective, by a factor of 2-3, in inducing reaction at high $P(\phi)$.

8) For sec-butyl acetate, the MPIUR gave the same product distribution as sensitized excitation. The MPIUR product distribution was independent of ester pressure from 0.05 to 1.0 torr and was also independent of fluence. Ethyl 2-bromopropionate also has two reaction channels. The MPIUR and sensitized excitation of this ester gave similar results. The ratio of ethylene to HBr elimination was 3 at $\phi < 1.5 \text{ J/cm}^2$ but it increased with fluence. One explanation is that the highly vibrationally excited ethyl acrylate molecules formed from the HBr elimination absorb photons during the laser pulse at high fluence and produce ethylene.

9) The absorption of laser energy as a function of ester pressure follows Beer's law from 0.01 to 5 torr giving laser absorption cross sections, σ_L , that are independent of pressure. The σ_L , however, depend on fluence. For low ϕ ($< 0.1 \text{ J/cm}^2$), the $\sigma_L \approx \sigma$. At higher ϕ , the σ_L increase if the line used to excite the ester is to the red of the maximum of the

absorption band, or they decrease if the laser line used is to the blue of the maximum of the absorption band. When the line used matches the maximum of the absorption band, the σ_L stay approximately constant with increasing fluence until, at high enough fluence, the red shift has moved the absorption band sufficiently, so that the line used no longer matches the maximum and σ_L declines. The dependence of σ_L on ν is not due to product formation, as was demonstrated by measuring some σ_L of methyl acetate, a compound that did not react at the fluence used.

The data reported in this thesis are fundamentally significant in the sense that they should be reproducible by an independent investigator if the restrictions imposed on the experiment are observed (constant fluence geometry, low pressure, low pulse repetition rate, etc.). The acquisition of reliable physical measurements is the first step toward understanding MPIUR.

The second step in understanding MPIUR is to develop simple (or complex is required) models to explain the fundamental physical data. One central idea is that the energy deposited in the molecule is rapidly (relative to the rate of reaction) redistributed within the internal degrees of freedom of the molecule. Based upon this general idea no dependence of $P(\nu)$ is expected on frequency provided that the same amount of energy is placed in the molecule. Therefore a plot of $P(\nu)$ vs E_{abs} is a better way of presenting the results than $P(\nu)$ vs ν . Such a plot is shown in Fig. 43 for all esters except ethyl 2-bromopropionate. The latter is omitted because the cross section data are not reliable. On such a plot the enhanced $P(\nu)$ at a given energy for a particular compound must be related to the intrinsic rate constants for unimolecular reaction. The very high rate of reaction for sec-butyl acetate may be related to the larger k_E values but it also may be experimental error related to the energy fluence measurements.

An important aspect for applications of MPIUR is the efficiency of the absorbed energy in promoting reaction.

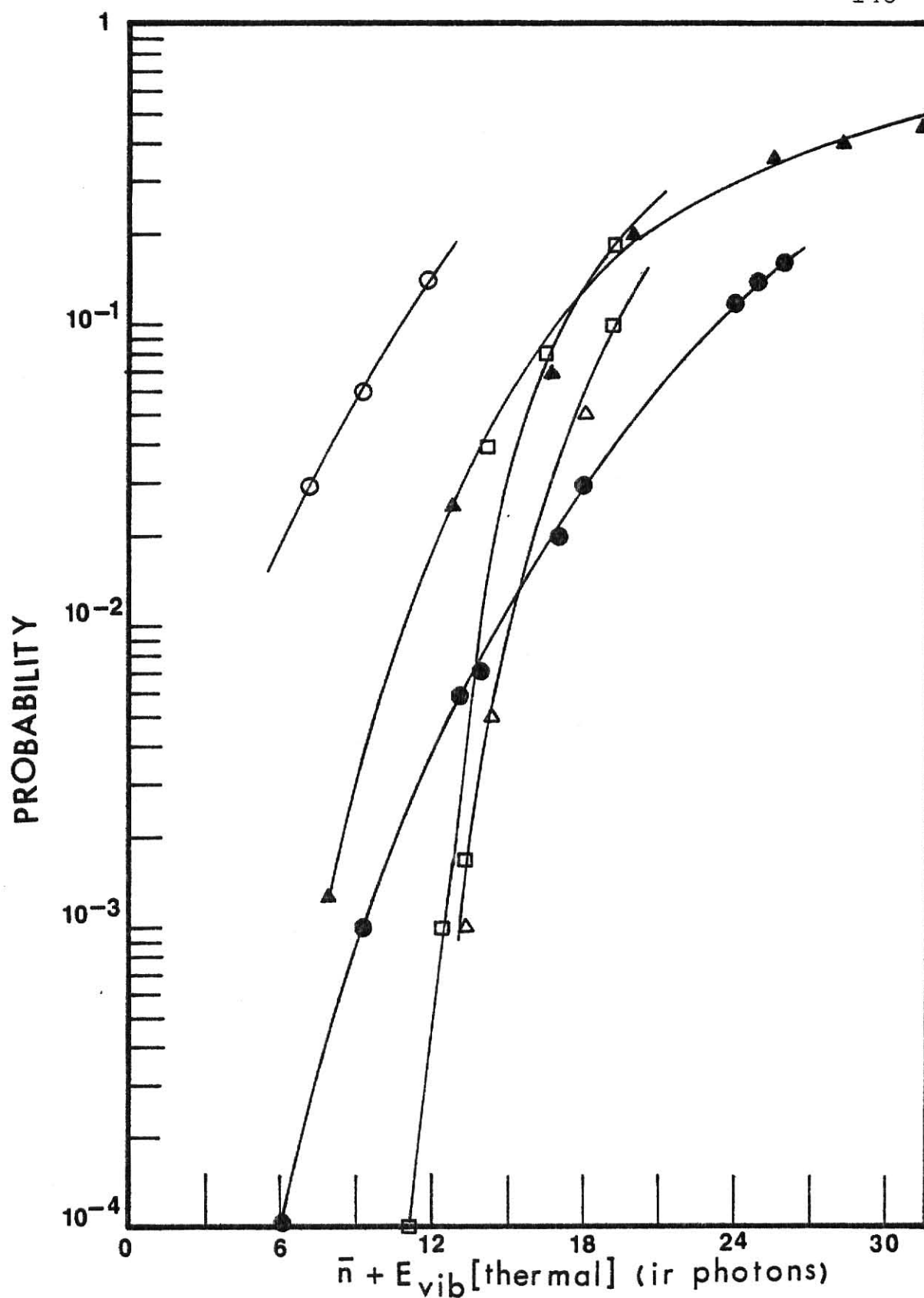


Fig. 43. Probability vs. mean energy of molecule. ● Ethyl Acetate, ▲ Ethyl Fluoroacetate, △ Ethyl Acrylate, □ *n*-Butyl Acetate, ○ *sec*-Butyl Acetate.

A useful plot is \bar{n}_r vs $P(\emptyset)$, see Fig. 44. The closeness of \bar{n}_r to the minimum number of photons required for the molecule to have energy $\geq E_0$ (16 photons for ethyl acetate) is a measure of the efficiency of the laser pumping. The results from Fig. 44 indicate that the laser induced reaction is inefficient at low $P(\emptyset)$ but becomes rather efficient for $P(\emptyset) \geq 0.1$. Qualitatively, the six esters show the same behavior. The σ_L at high fluence are needed to complete the curve at high $P(\emptyset)$. It should be emphasized again that the \bar{n}_r values were taken under conditions that excluded any reaction by "heating". If the pressure was increased to the extent that heating occurred, the \bar{n}_r values may even be larger.

To finalize this section a qualitative summary of the important points of the models that can be applied to the yield vs energy relation for different regions of fluence will be given for pure ester. The $P(\emptyset)$ vs \emptyset (or \bar{n}) curves can be divided into three regions. At low $P(\emptyset)$ 10^{-4} - 10^{-5} there are few molecules with $E > E_0$ and one or two collisions can deactivate the excited molecules below E_0 by $\langle \Delta E_d \rangle$ of 4 to 6 kcal/mole. The time scale for the deactivation by collision is much faster than the other cooling processes. Thus the model presented in the discussion section for a mixture of a small amount of absorber in a large amount of quencher approximately holds in this region of low $P(\emptyset)$. In this case the translational - rotational heat capacity is sufficient to accept the vibrational energy and quench the reaction. This region corresponds entirely to post pulse reaction.

For the region where $10^{-3} < P(\emptyset) < 10^{-1}$, the factors affecting the absolute yield are more complex. Although a small fraction of the reaction occurs during the pulse, most of the reaction is post-pulse. Thus the absorption measurements can be used to define approximate energy distributions. In this region, collisions are thought to be

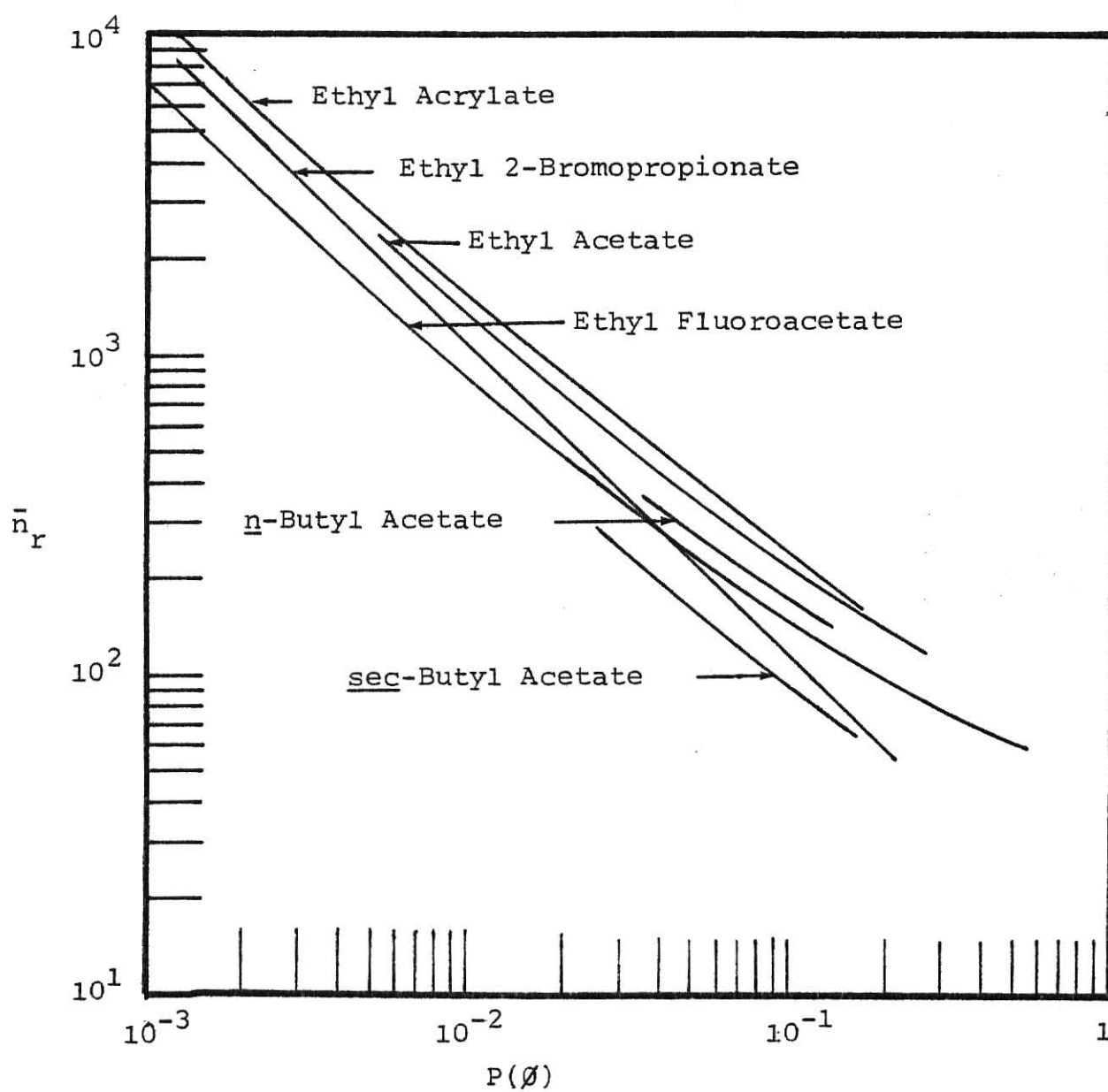


Fig. 44. \bar{n}_r vs $P(\phi)$ for the Esters.

inefficient in deactivating excited molecules because this range of $\bar{n}h\nu$, the Boltzmann initial temperature (vibrational) is high and collisions only cause the temperature to drop 50-100° less than the initial T_{vib} defined by the absorption measurements. No model to describe the behavior of the yield with absorbed energy is available for this region. However, it appears that the yield is limited by combined bulk and molecular phenomena which result in cooling on a 10 μs time scale. In this range increasing the pressure above 0.05 torr results in effects related to intermolecular energy transfer.

At high $P(\emptyset)$ (> 0.2), the fraction of the reaction that takes place during the pulse is significant, the kinetic equations then approach steady-state behavior. A steady-state results when the laser pumping rate is comparable to the rate of unimolecular reaction. Because the ester molecules are thought to have no bottleneck, a high power pulse can deposit the laser energy in the molecule in a short time, creating molecules in a high level of excitation that react before collisions occur. For this $P(\emptyset)$ region, a method to calculate $k_{\text{uni}}(\text{st})$ has been developed by Quack²⁷ that assumes that most of the reaction occurs under steady-state conditions. It should be noted that the steady-state implies that the rate of laser pumping (i.e. power) now becomes the rate controlling step i.e. increasing the power will drive the molecules to higher energy states before reaction occurs.

The values of the rate constants for ethyl acetate and ethyl acrylate at high $P(\emptyset)$ will be calculated using the method suggested by Quack²⁷. The unimolecular rate constant at steady-state is:

$$k_{\text{uni}}(\text{st}) = \langle k_{\text{I}}(\text{st}) \rangle \quad \text{I} .$$

Where $\langle k_T(st) \rangle$ in cm^2/J , is the slope of the linear portion of a plot of $\ln[1.0 - P(\emptyset)]^{-1}$ vs \emptyset , and "I" is the intensity obtained by dividing the fluence (in J/cm^2) by the pulse length (in sec.). The experimental data for ethyl acetate and ethyl acrylate have been used to obtain the plots from which the rate constants can be calculated, see Fig. 44. The slope $\langle k_T(st) \rangle$ is $0.483 \text{ cm}^2/\text{J}$ and is approximately the same for the two esters. The rate constants at a given \emptyset can be calculated by substituting for I in the above equation. In our case this results in :

$$k_{\text{uni}}(st) = 0.483 \text{ cm}^2/\text{J} \frac{\emptyset \text{ J}/\text{cm}^2}{1.3 \times 10^{-6} \text{ sec}} .$$

For ethyl acetate and ethyl acrylate the $k_{\text{uni}}(st)$ predicted by this method for $P(\emptyset)$ of 0.9, 0.75 and 0.5 are 3.0, 2.2 and $1.8 \times 10^6 \text{ sec}^{-1}$ and 2.7, 2.0 and $1.5 \times 10^6 \text{ sec}^{-1}$, respectively. These $k_{\text{uni}}(st)$ depend on the pumping rate of the laser pulse and for a shorter (higher power) pulse the $k_{\text{uni}}(st)$ will increase proportionally.

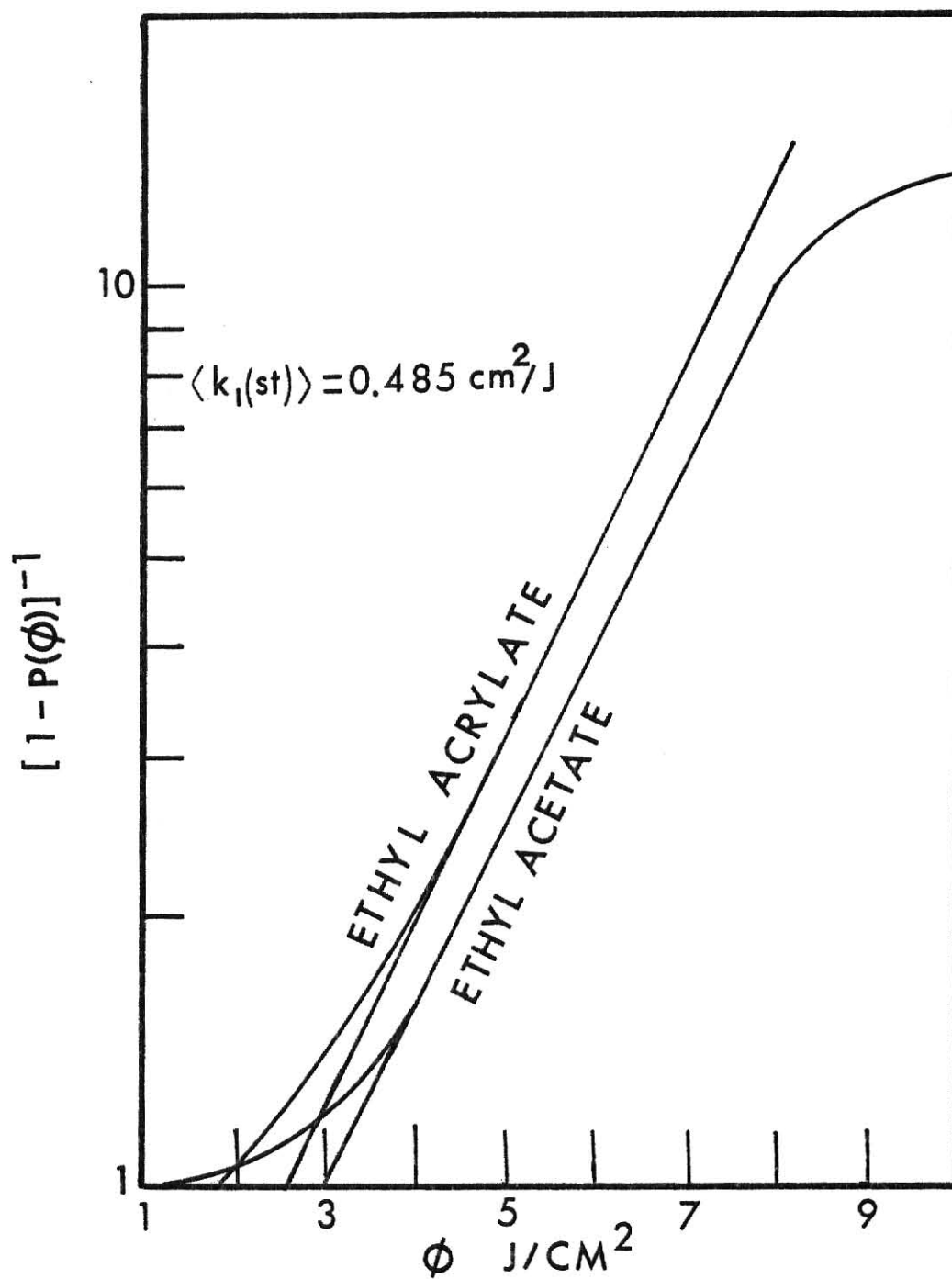


Fig. 44. $\text{Log}[1.0 - P(\phi)]^{-1}$ vs ϕ for Ethyl Acetate and Ethyl Acrylate.

. APPENDIX

The unimolecular rate constants as a function of energy for some of the esters investigated are calculated here using the RRKM theory¹¹ of unimolecular reactions. For this calculation one must have all of the vibrational frequencies of the molecule and of the transition state. It will be assumed that the moments of inertia of the molecule and transition state are the same.

Lack of information on the vibrational frequencies of the esters made necessary the use of approximate methods to estimate them. This was done by making reference to the vibrational analysis for methyl acetate³⁸. As an approximation all carbon-hydrogen stretches (symmetric or asymmetric) were taken as 2980 cm^{-1} and all hydrogen-carbon bendings (symmetric or asymmetric) were taken as 1430 cm^{-1} . This approximation is good in view of the fact that the contribution of the large frequencies to the entropy of the molecule or activated complex is small.

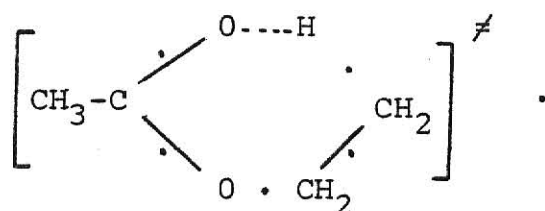
To obtain the 36 frequencies of ethyl acetate from those of methyl acetate a hydrogen was removed from methyl acetate, and a methyl group was attached in place of the hydrogen. To add the methyl one adds a carbon-carbon stretch (1250 cm^{-1}) in place of the carbon-hydrogen stretch, an oxygen-carbon-carbon bend (430 cm^{-1}) in place of one of the two hydrogen-carbon bends and a torsional motion about the new carbon-carbon bond (136 cm^{-1}). Next, the contribution of the methyl hydrogens are added to obtain the 36 vibrational frequencies of ethyl acetate, these being three H-C stretches (2980 cm^{-1}) and six C-H bends (1430 cm^{-1}).

Of the 36 frequencies estimated for ethyl acetate, the most important ones are those with values below 500 cm^{-1} . These are: two C-C torsions at 136 cm^{-1} , an oxygen-ethyl torsion at 100 cm^{-1} , a carbonyl-oxygen torsion at 187 cm^{-1} , a C-O-C deformation at 250 cm^{-1} , a carbon-carbonyl deformation at 430 cm^{-1} , and carbonyl in plane and out of plane bendings at 640 and 607 cm^{-1} , respectively.

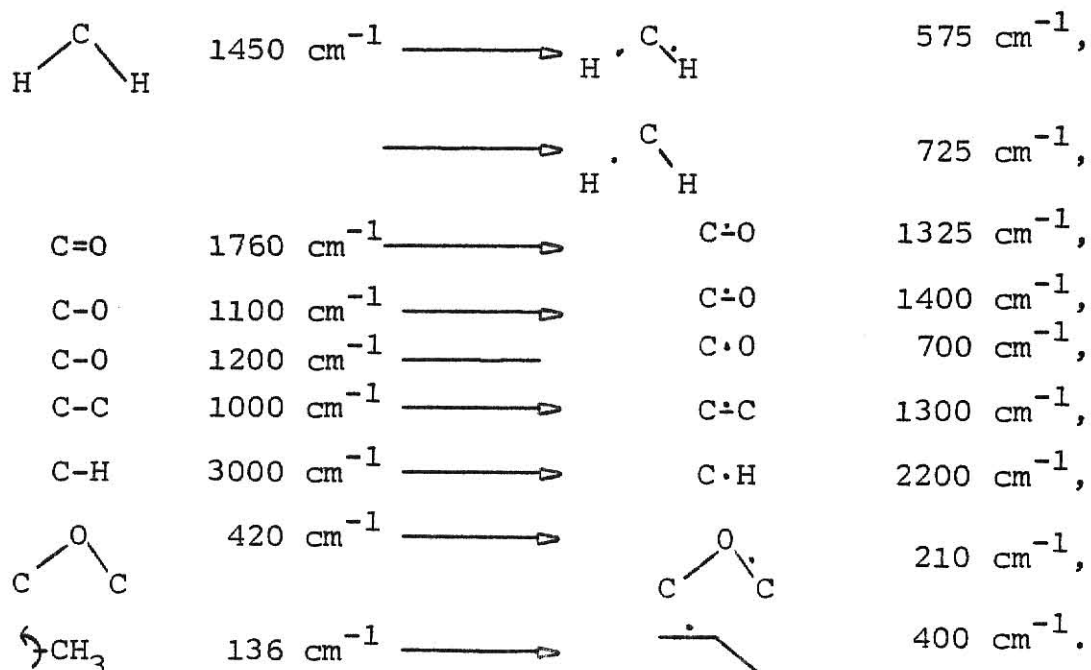
The same procedure was employed for the more complicated esters using ethyl acetate as the reference; i.e., appropriate hydrogen atoms were removed and other atoms or groups were attached in their place and frequencies were adjusted.

Once the 3N-6 vibrational frequencies were estimated, frequencies of similar magnitude were grouped into seven sets using the geometric mean; these frequencies were used to calculate the vibrational thermal energy and the density of states.

The approach used in Ref. 15 for ethyl acetate, was used to assign frequencies of the transition state. O'Neal and Benson modified some frequencies of the ethyl acetate molecule to take into account the change involved in forming the six-centered activated complex,



The following changes were made in constructing the activated complex frequencies:



Making the above structural changes provided a first estimate for the transition state model. Further refinement was obtained by matching calculated and experimental pre-exponential factors. A torsional motion (136 cm^{-1}) was taken as the reaction coordinate and eliminated to obtain $3N-7$ vibrational frequencies for the activated complex. Because of the greater restriction of motion in the six-centered activated complex (or because of higher frequencies), the change in entropy in going from molecule to activated complex is negative. Examination of several esters with statistical factors ranging from 1 to 9 gave a change in entropy per reaction channel close to -6.4 Gibbs/mole. This value for ΔS^\ddagger was used to obtain the best set of frequencies for the activated complex for cases in which the pre-exponential factors were not experimentally measured with high accuracy.

A computer program was used to calculate E_0 , ΔS^\ddagger , A_Q and A_{Arr} from the best set of frequencies of molecule and activated complex. The following input was necessary: frequencies of molecule and activated complex, the statistical factor for reaction (number of ways in which molecule can achieve the six-centered rearrangement in the activated complex), temperature (set equal to 600 K in all cases), the molecular weight and the moments of inertia of molecule and activated complex (these were taken as being equal, to make their ratio equal to one). The program calculated the threshold energy, E_0 , from the Arrhenius activation energy, E_a , as

$$E_0 = E_a - kT + [\langle E_{\text{th}} \rangle - \langle E_{\text{th}}^\ddagger \rangle]$$

where $\langle E_{\text{th}} \rangle$ and $\langle E_{\text{th}}^\ddagger \rangle$ are the mean thermal vibrational energy of the molecule and activated complex, respectively, as given by (22). Next the pre-exponential factor, A_Q , was calculated:

$$A_Q = kTL^\ddagger Q^\ddagger/hQ$$

where Q and Q^\ddagger are the partition functions of the molecule

and the activated complex respectively. Since it was assumed that the rotational contributions canceled, the pre-exponential factor in partition function form is

$$A_Q = \frac{kTL^\ddagger}{h} \frac{\prod_{i=1}^N [1 - \exp(-hv_i^\ddagger/kT)]^{-d_i^\ddagger}}{\prod_{j=1}^N [1 - \exp(-hv_j^\ddagger/kT)]^{-d_j}}$$

where v_i and v_j^\ddagger are the frequencies and d_i^\ddagger and d_j are the number of frequencies of the i^{th} and j^{th} groups for molecule and activated complex, respectively. The change in entropy was calculated by the program and employed in the calculation of A_{Arr} ,

$$A_{\text{Arr}} = [L^\ddagger ekT/h] \exp[-\Delta S_C^\ddagger/R] .$$

In this form the statistical factor, L^\ddagger , is written explicitly and S_C^\ddagger is the entropy of activation per channel. The total entropy of activation frequently include L^\ddagger , i.e.,

$$\Delta S^\ddagger = \Delta S^\ddagger (\text{per channel}) + R \ln(L^\ddagger) .$$

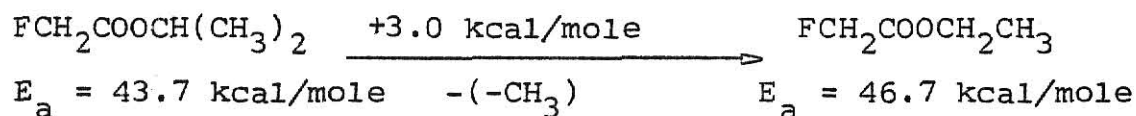
To obtain the A_{Arr} (per channel), ΔS^\ddagger (per channel) is used instead of ΔS_C^\ddagger in the above expression for A_{Arr} . When ΔS_C^\ddagger is set equal to -6.4 Gibb/mole, A_{Arr} (per channel) is $10^{12.13} \text{ sec}^{-1}$ at 600 K.

The A_{Arr} was calculated for several sets of frequencies until the literature value was obtained (in the case of n-butyl acetate and sec-butyl acetate, the literature values are thought to be low and high, respectively, and a ΔS_C^\ddagger of -6.4 Gibb/mole was used as a guide to obtain A_{Arr}). Thus $A_{\text{Arr}}^{\text{calc.}}$ are $10^{12.4}$ and $10^{12.8}$ rather than the literature values shown in Table 50.

Table 50. Values of Constants used in Calculating k_E .

Ester	$A_{Arr}^{lit.}$	$A_{Arr}^{calc.}$	$E_a^{lit.}$	$E_o^{calc.}$	L^*	S_C^*
Ethyl Acetate	$10^{12.6}$	$10^{12.6}$	48.0	48	3	-6.4
Ethyl Fluoroacetate	$10^{12.6}$	$10^{12.6}$	46.7	46	3	-6.4
<u>n</u> -Butyl Acetate	$10^{12.2}$	$10^{12.4}$	46.0	46	2	-6.4
<u>sec</u> -Butyl Acetate	$10^{13.3}$	$10^{12.8}$	46.6	46	5	-6.4

A_{Arr} are in sec^{-1} , energies are in kcal/mole and entropy is in Gibb/mole. The $A_{Arr}^{lit.}$ and $E_a^{lit.}$ in Table 50 were taken from reference 15, except those for ethyl fluoroacetate which were obtained by the following procedure:



The gain of 3 kcal/mole as isopropyl fluoroacetate³⁹ loses a methyl to become ethyl fluoroacetate was deduced by noting the difference in E_a for several halogenated and nonhalogenated isopropyl esters when losing a methyl to become ethyl esters. The pre-exponential factor of ethyl fluoroacetate was assumed to be the same as that for ethyl acetate since there is no structural reason to expect a change and since L^* is the same.

The frequencies in Table 51 and the E_o and L^* from Table 50 were used in a program that calculates k_E vs E for a given ester in one kcal interval using the RRKM theory.

$$k_E = \frac{L^* \sum_{E_o^*=0}^{E-E_o} P^*(E^*)}{h N_E^*} \quad \text{sec}^{-1}.$$

The sum of states for the transition state is given by

$P^{\ddagger}(E^{\ddagger})$. The sum runs from $E_O^{\ddagger} = 0$ to $E - E_O$. The density of states of the molecule at total energy E is given by N_E^* . The Haarhoff approximation was used for N_E^* at all energies. The direct sum was employed for $E_O^{\ddagger} = 0$ to 59 kcal/mole and the Haarhoff approximation above that.

Since E_O values are not known to better than ± 0.5 kcal/mole the E_O values were rounded for the k_E calculation. For ethyl acetate, ethyl fluoroacetate, *n*-butyl acetate and *sec*-butyl acetate E_O values = 48, 46, 45, and 46 respectively. Plots of k_E vs E for these esters are shown in Figs. 45 and 46.

An important general point to note is that the ethyl acetate and butyl acetate molecules must acquire energies of 85 and 105 kcal/mole respectively, before the lifetimes are as short as the laser pulse, i.e. 1×10^{-6} sec. For 15 kcal/mole of excess energy the lifetimes for the ethyl and butyl acetates are 1×10^{-4} and $10^{-1} - 10^{-2}$ sec. These lifetimes will not be changed by more than factors of 2-3 for rather extreme changes in one or two frequencies and these long lifetimes are an important aspect of the unimolecular reactions of large molecules. These are also important in any definition of collisionless behavior for these molecules.

The frequencies of the molecule and activated complex for the two elimination channels of ethyl 2-bromopropionate were estimated and used to calculate ΔS_C^{\ddagger} and A_{Arr} for the six-centered elimination of ethylene and the four-centered elimination of HBr. These frequencies and the E_O were used to calculate k_E vs E using the RRKM theory. The ethylene elimination channel was taken to have a ΔS_C^{\ddagger} equal to -6.4 Gibb/mole, as for the other esters and an E_a of 46 kcal/mole; this ΔS_C^{\ddagger} gives $A_{Arr} = 10^{12.6}$. This model gave the calculated k_E vs E curve of Fig. 47 for the C_2H_4 elimination. The HBr elimination was first assumed to have a $\Delta S_C^{\ddagger} = -2.2$ Gibb/mole, as suggested in Ref. 15 for four-centered HX eliminations. The activation energy was estimated as $E_a = 46$ kcal/mole, by analogy to that for HBr elimination of secondary bromine atoms next to a double bond capable of

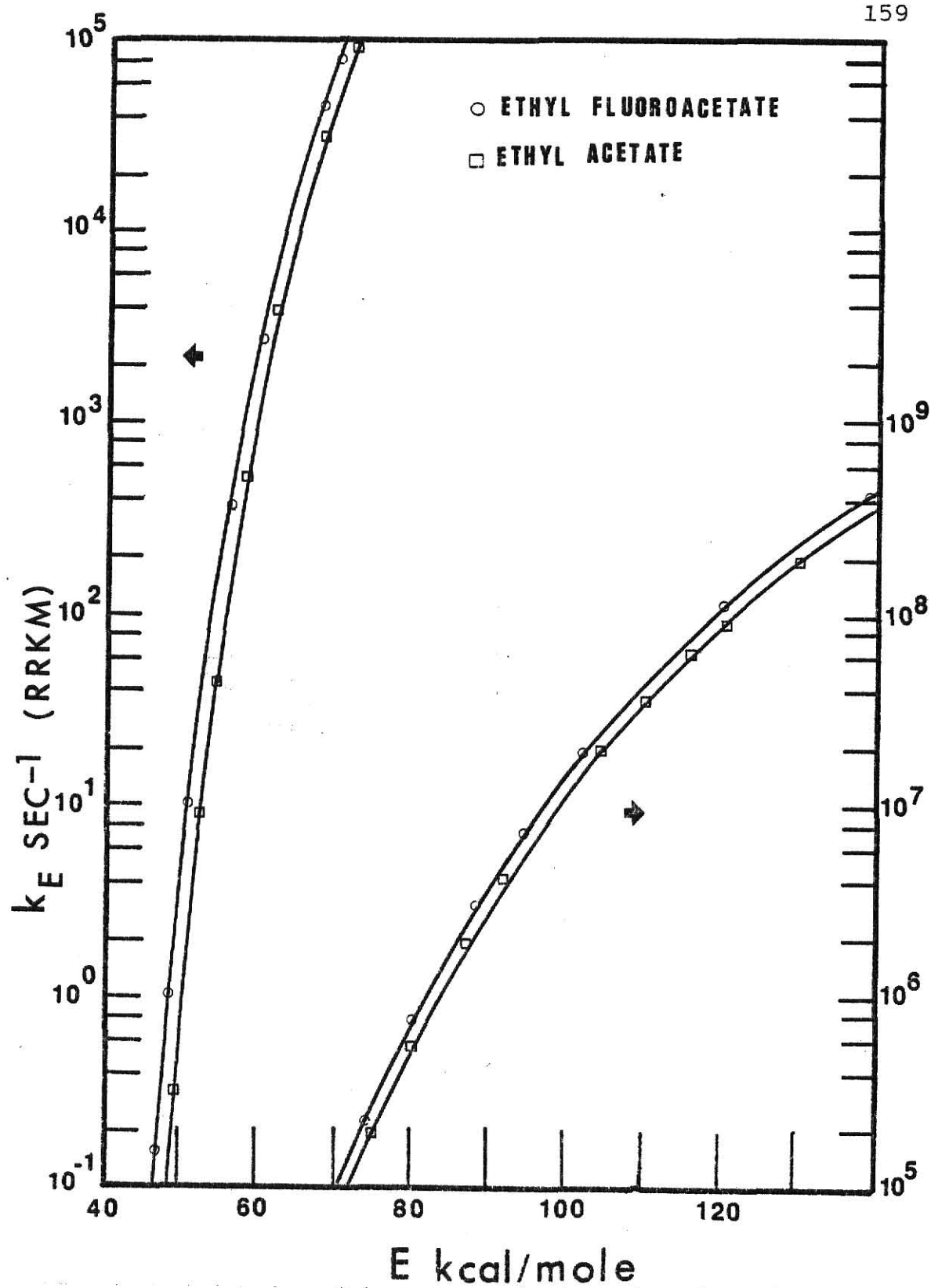


Fig. 45. k_E , $\text{sec}^{-1}(\text{RRKM})$ vs. E kcal/mole. □ Ethyl acetate, $E_0 = 48$ kcal/mole; $S_C^\ddagger = -6.4$ Gibb/mole. ○ Ethyl fluoroacetate, $E_0 = 46$ kcal/mole; $S_C^\ddagger = -6.4$ Gibb/mole.

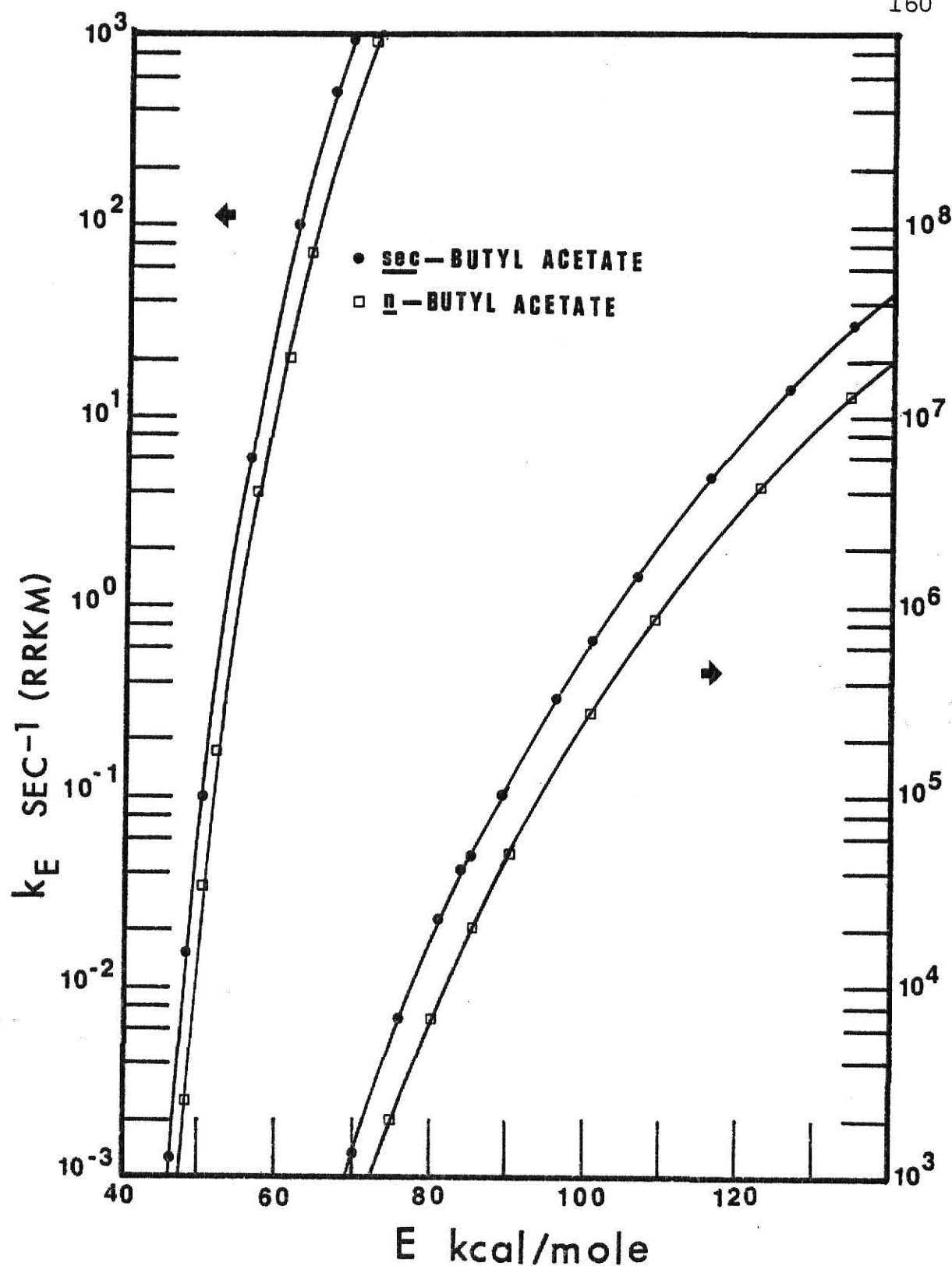


Fig. 46. k_E , $\text{sec}^{-1}(\text{RRKM})$ vs. E kcal/mole. • sec-Butyl acetate, $E_0 = 45$ kcal/mole; $S_C^\ddagger = -6.4$ Gibb/mole. □ n-Butyl acetate, $E_0 = 46$ kcal/mole; $S_C^\ddagger = -6.4$ Gibb/mole.

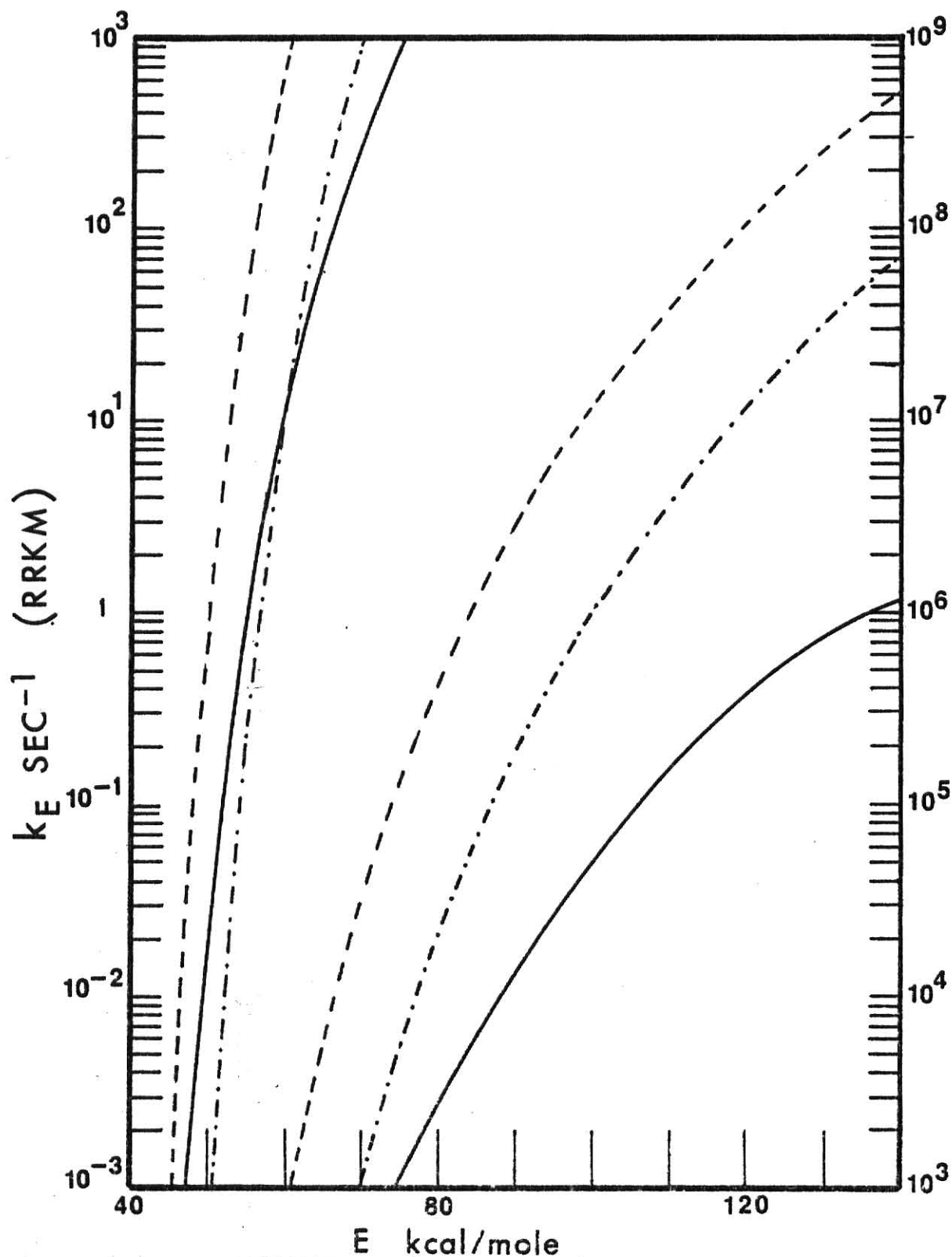
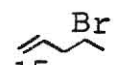
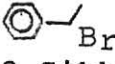


Fig. 47. k_E , sec^{-1} (RRKM) vs. E , kcal/mole for the two reaction channels of ethyl 2-bromopropionate.— Ethylene elimination, $E_0=46$ kcal/mole; $\Delta S_C^\ddagger=-6.4$ Gibb/mole. --- HBr elimination, $E_0=45$ kcal/mole; $\Delta S_C^\ddagger=-2$ Gibb/mole. HBr elimination, $E_0=49$ kcal/mole; $\Delta S_C^\ddagger=-4$ Gibb/mole.

conjugation in the transition state (, $E_a = 44.7$ kcal/mole, , $E_a = 38.8$ kcal/mole)¹⁵. For the model with $\Delta S_C^\ddagger = -2.2$ Gibb/mole and $E_o = 45$ kcal/mole, A_{Arr} was $10^{13.52}$ and the k_E values are two orders of magnitude larger than the k_E from the ethylene elimination, over most of the energy range. This contradicts the observed MPIUR and thermal excitation data where ethylene was produced in greater amounts than HBr. Therefore a model was developed which reduced the k_E of the HBr elimination as much as possible by assuming a conjugated effect with the carbonyl double bond in the transition state that could restrict a torsion and cause the change in entropy to be more negative, ΔS_C^\ddagger was estimated as equal to -4 Gibb/mole. The E_a was also increased to 50 kcal/mole. This model corresponds to $E_o = 49$ kcal/mole and $A_{Arr} = 10^{13.15}$. The resulting k_E were less than the k_E for C_2H_4 elimination for energies less than 60 kcal/mole but the k_E (HBr) increased rapidly with energy and became larger than $k_E(C_2H_4)$ for higher energies.

In order to match the observed C_2H_4 /HBr elimination ratio from ethyl 2-bromopropionate very unrealistic ΔS_C^\ddagger (< -7 Gibb/mole) and high E_o are required for the HBr channel. There is no evidence in the literature to support such a model for HBr elimination. Another approach that could explain the greater production of ethylene is to assume a E_a for the C_2H_4 elimination of ~ 40 kcal/mole by arguing that the Br atoms lower the E_a by an electron withdrawing effect during the transition state.

ACKNOWLEDGEMENTS

The author gratefully acknowledges all of the help and encouragement given to him by his major professor, Dr. D. W. Setser, without whom this thesis would not have been possible. He would also like to give special thanks to both Dr. W. C. Danen and Dr. R.M. Hammaker for their helpful comments along the way.

The author further wishes to express his gratitude to miss Clara Jang who prepared all of the computer programs used in this thesis.

Acknowledgment is made to the National Science Foundation (Grant CHE 77-22645) and the Petroleum Research Fund, administered by the American Chemical Society (Grant 9378-AC4) for financial support.

LITERATURE CITED

1. P. A. Schulz, Aa. Subdø, D. J. Krajnovich, H. S. Kwok, Y. R. Shene and Y. T. Lee, "Multiphoton Dissociation of Polyatomic Molecules", Submitted to the Annual Review of Physical Chemistry, (1979).
2. W. C. Danen, J. Am. Chem. Soc. 101, 1187 (1979).
3. D. M. Brenner, Chem. Phys. Lett. 57, 357 (1978).
4. V. S. Letokhov and A. Makarov, Opt. Commun. 17, 250 (1976). D. M. Larsen and N. Bloembergen, Opt. Commun. 17, 254 (1976).
5. C. D. Cantrell and H. W. Galbraith, Opt. Commun. 18, 513 (1976).
6. R. V. Ambartzumian, N. P. Furzikov, Y. A. Gorokhov, V. S. Letokhov, G. N. Makarov and A. A. Puretzky, Opt. Commun. 18, 517 (1976).
7. R. V. Ambartzumian, Y. A. Gorokhov, V. S. Letokhov, G. N. Makarov and A. A. Puretzky, JETP Lett. 23, 22 (1978).
8. J. L. Lyman, J. Chem. Phys. 67, 1868 (1977).
9. Aa. Subdø, P. A. Schulz, E. R. Grant, Y. R. Shen and Y. T. Lee, J. Chem. Phys. 68, 1306 (1978).
10. C. R. Quick Jr. and C. Wittig, Chem. Phys. Lett. 48, 420 (1977). C. R. Quick Jr. and C. Wittig, Chem. Phys. 32, 75 (1978).
11. P. J. Robinson and K. A. Holbrook, "Unimolecular Reactions", Wiley, New York, (1972).
12. J. D. Rynbrandt and B. S. Rabinovitch, J. Phys. Chem. 75, 2164 (1971).
13. J. L. Lyman, S. D. Rockwood and S. M. Freund, J. Chem. Phys. 67, 4545 (1977). 4188 (1978).
15. S. W. Benson and H. E. O'Neal, Report NSRDS-NBS 21, National Bureau of Standards, Washington, D. C. (1970).
16. W. C. Danen, W. D. Munslow and D. W. Setser, J. Am. Chem. Soc. 99, 6961 (1977).

17. G. P. Quigley, private communication.
18. R. B. Knott and A. W. Pryor, J. Chem. Phys. 71, 2946 (1979).
19. G. P. Quigley, Opt. Lett. 3, 106 (1978).
20. S. T. Lin, S. M. Lee and A. M. Ronn, Chem. Phys. Lett. 53, 260 (1978).
21. P. L. Houston and C. N. Plum, private communication.
22. J. C. Stephenson and D. S. King, Chem. Phys. Lett. 66, 33 (1979).
23. M. F. Goodman, J. Stone, J. C. Stephenson and D. S. King, J. Chem. Phys. 70, 4496 (1979).
24. D. Proch and H. Schroder, Chem. Phys. Lett. 61, 426 (1979).
25. C. R. Quick Jr. and C. Wittig, J. Chem. Phys. 69, 4201 (1978).
26. D. W. Setser and J. C. Jang, J. Phys. Chem. 83, 2809 (1979).
27. M. Quack, J. Chem. Phys. 70, 1069 (1979).
28. F. Brunner and D. Proch, J. Chem. Phys. 68, 4936 (1978).
29. P. Kolodner, C. Winterfeld and E. Yablonovitch, Opt. Commun. 20, 119 (1977).
30. M. C. Gower and K. W. Billman, Appl. Phys. Lett. 30, 514 (1977).
31. H. S. Kwok, "Picosecond CO₂ Laser Pulses and Intramolecular Relaxation in SF₆", Ph. D. Thesis Harvard University (1978).
32. J. L. Lyman, W. C. Danen, A. C. Nilsson and A. V. Nowak, J. Chem. Phys. 71, 1206 (1979).
33. T. F. Deutsch, Opt. Lett. 1, 25 (1977).
34. F. M. Lussier, J. I. Steinfeld and T. F. Deutsch, Chem. Phys. Lett. 58, 277 (1978).
35. C. C. Jensen, J. L. Steinfeld and R. D. Revine, J. Chem. Phys. 69, 1432 (1978). E. R. Grant, P. A. Schulz, Aa. Subdø, Y. R. Shen and Y. T. Lee, Phys. Rev. Lett. 40, 115 (1978).

36. C. Reiser, F. M. Lussier, C. C. Jensen and
J. I. Steinfeld, J. Am. Chem. Soc. 101, 350 (1979).
J. G. Black, E. Yablonovitch, N. Bloembergen and
S. Mukamel, Phys. Rev. Lett. 38, 1131 (1977).
37. D. C. Tardy and B. S. Ravinovitch, Chem. Rev. 77,
369 (1977).
38. T. Shimanouchi, "Tables of Molecular Vibrational
Frequencies Consolidated Volume I", NSRDS-NBS 39
U. S. Department of Commerce, Nat. Bureau of
Standards (1972).
39. G. Chuchani, J. A. Hernandez, M. Yepez and
M. E. Alonso, Int. J. Chem. Kinet. 9, 811 (1977).

INFRARED MULTIPHOTON INDUCED REACTIONS
OF ORGANIC ESTERS

BY

VALENTIN C. RIO
B.S., University of Texas at Austin, 1976

An Abstract of
A MASTER'S THESIS

Submitted in partial fulfillment of the
requirements for the degree

MASTER OF SCIENCE

Department of Chemistry

KANSAS STATE UNIVERSITY

Manhattan, Kansas

1980

ABSTRACT

The six-centered rearrangement reaction of organic esters was induced by infrared multiphoton absorption using a pulsed CO₂ laser. Esters generally have an absorption band in the frequency region of the 00⁰₁-02⁰₀ vibrational band of the CO₂ laser. Ethyl acetate, ethyl fluoroacetate, sec-butyl acetate, n-butyl acetate, ethyl 2-bromopropionate and ethyl acrylate were studied in the present work.

The first order behavior of the dissociation vs number of pulses was verified for ethyl acetate, ethyl-2-bromopropionate and sec-butyl acetate. Use of thermal monitors showed that there was no significant reaction resulting from collisional energy transfer at pressures below 0.05 torr, which means that laser induced reaction can be studied at low pressures. The reaction probability, defined as the number of molecules that react per pulse divided by the number of molecules occupying the irradiated volume, was measured for the six esters as a function of parent pressure, pressure of added bath gas, laser fluence, laser power, laser frequency and irradiation geometry.

The empirical relation, $P(\varnothing) = C(1.0 - (\varnothing/\varnothing_r)^n)$, generally reproduced the experimental behavior of $P(\varnothing)$ with \varnothing . There is little, if any, dependence of $P(\varnothing)$ on laser pulse length.

The sec-butyl acetate and ethyl 2-bromopropionate have two reaction channels. The ratio resulting from MPIUR was compared with that resulting from sensitized excitation experiments where a small fraction of ester in SiF₄ was irradiated with laser energy absorbed only by SiF₄. The ratio was the same for both types of experiments.

The small signal absorption cross sections, σ , were measured using conventional infrared absorption at the frequencies corresponding to the laser lines used for multiple photon induced unimolecular reactions. The laser absorption

cross sections, σ_L , also were measured from the net amount of energy deposited in the sample per pulse. The energy absorbed per pulse was independent of pressure and the σ_L were derived from Beer Lambert type plots. The σ_L were measured as a function of laser fluence from the small signal limit up to 3 J/cm^2 . The σ_L extrapolated to the σ at low fluence ($\phi < 0.1 \text{ J/cm}^2$) in all cases. However, the σ_L varied with fluence; this can be explained by a red shift of the absorbing band.

A model for considering $P(\phi)$ in MPIUR is presented which assumes that the distribution of the irradiated molecules at the end of the laser pulse can be approximated as a Boltzmann distribution with average energy, $\bar{n}h\nu$, calculated from the measured σ_L . For this model collisions of excited molecules with cold molecules are the only means of deactivation. This model is applicable to the case of a bath gas with heat capacity larger than the heat capacity of the molecule absorbing the laser energy for low $P(\phi)$. Some curves predicted by this model for ethyl acetate and *n*-butyl acetate are presented at several pressures. The implications of this model also are used to discuss the laser induced unimolecular reactions for the pure esters.